Ph.D Afhandling
Københavns Universitet

An Experimental Study of Electronic Shell Structure in Large Sodium Clusters

Klavs Hansen
The Niels Bohr Institute, University of Copenhagen,
DK-4000 Roskilde, Denmark

Roskilde, december 1990.

Foreword

Together with the four publications listed below, the present work is submitted to fulfill the requirements of the Ph.D. degree at the University of Copenhagen.

This thesis in conjunction with the publications summarizes three years of investigation of the quantum structure of metal clusters, emphazising the experimental study of electronic shell structure of large sodium clusters. The work was done at the Niels Bohr Institute's Tandem Accelerator Laboratory in Roskilde. It has resulted in demonstrating the existence of shell structure in sodium clusters composed of up to 600 atoms. Furthermore, application of theoretical work on the origin of shell structure and extension of this work to treat the influence of a finite cluster temperature has made possible an interpretation of the observed shell structure in abundance spectra. This interpretation relates to the position, the magnitude and the width of the observed abundance variations around the shell closings in spectra produced by adiabatic expansion. It includes a possible extension to even larger clusters as well as to clusters of other simple metals.

During the course of these three years I have enjoyed the guidance and inquisitive mind of my advisor, Sven Bjørnholm, to whom I address my sincere thanks. This work has only been possible because of his strong support and willingness to guide me into the field, completely new to me three years ago.

My experimental skills I owe mainly to Jørgen Pedersen who has taught me the value of common sense in a laboratory, and to Jørn Borggreen who has set an unreachable example by doing things with the proper care.

I would like to thank Hide Nishioka for the privilege of letting me work with him (at times long distance), Ben Mottelson for bestowing (some of) his impressive physical insight onto the local cluster community, and Matthias Brack for a fruitful collaboration that opened the road for an interpretation of the experimental results.

I have enjoyed the expertise of Olof Echt and Walter Knight who both chose to spend some time with the cluster group at the institute. Their long experience in the field has been invaluable, both in setting up the experimental apparatus and in setting some proportions to my work.

Contents

Introduction

One of the fascinating aspects of quantum mechanics is that when a small number of fermions are confined to a finite volume, the system will show systematic variations with particle number for a range of properties. Historically, this phenomenon was discovered in atoms. The electrons in a neutral atom, confined by the positive nucleus, are responsible for chemical reactivity. These reactivities depend on the number of electrons in a non-monotonous manner. This enableded Mendelejev to order the by then known elements into the periodic table according to their chemical properties.

Mendelejev did not, and could not, know the origin of this systematics. The tools to an understanding of the chemical properties became available only by the advent of quantum mechanics. The idea of discrete energies for the atom in connection with Pauli's Exclusion Principle set the stage for an interpretation of the periodic table in terms of these two concepts when they were applied to the electrons surrounding the atomic nucleus.

The nucleus, on the other hand, turned up to give another example of the phenomenon which became known as shell structure. Confined to a volume much smaller than the atom as a whole, the individual nucleons to some extent behave as if they move as independent particles in a potential which can be visualized as a spherical box with finite height and a smooth edge. (The validity of this picture is in no way trivial since the nucleons are strongly interacting particles). The quantization of independent particles in a spherical cavity has as a consequence the well known degeneracy of the states that differ only in magnetic and spin quantum numbers. A bunching of states, of which this degeneracy is an extreme example, is commonly referred to as a shell. In this case the word shell does not refer to the geometric structure of the system, but rather to the energetic structure.

In 1984 this small family of finite fermionic systems which exhibit shell structure was expanded by Knight and his collaborators in Berkeley [1]. The subject under study was clusters of alkali metals. In this context a cluster can be viewed as a lump of matter consisting of a countable number of atoms.

Working with an expansion source, the Berkeley group observed a very strong mass dependence in the abundances. The abundances showed very high values at the numbers 8,20,40,58 and 92, in each case followed by a sharp decrease for the clusters with one atom more than the numbers given. These strong abundance variations were interpreted in terms of the total energies of the electronic system of the clusters so that a large abundance correspond to a low energy of the electronic system and vice versa. It was soon noticed that the 'magic numbers' mentioned above coincide with the number of nucleons required to fill the shells in the nuclear spherical shell model of Jensen and Mayer [2]. The electronic energies of the clusters were then modelled in much the same way as the energies of the nucleons had been earlier, the essential ingredient being the delocalization of the fermions considered. Simultaneously with the Berkeley group, similar features were observed by Katakuse et al. in copper, silver and gold clusters produced by sputtering [3].

Although there are many similarities between the metal cluster and the electronic system of the atom and in particular the nucleus, they differ in some ways, of course. First of all, the sizes are different. A nucleon has a size of some cubic fermi $10^{-45}m^3$. Metal clusters are known from calculations and static polarizability measurements to have a volume per atom which is rather close to the bulk value (which is $9.0 \times 10^{-30}m^3$ for sodium). In combination with the electron mass, this dimension gives a fermi energy of a few electron volts.

But also the interactions are different in the two systems. In the cluster, the naked electron-electron interaction is a coulomb repulsion. In order to have bound clusters (and solids for that matter) this repulsion must be compensated by an attractive force. This force is supplied by the positive ions which donate the valence electrons when the cluster is formed. In addition to supplying the background positive charge, these ions will have a certain freedom to move around, thus giving the clusters new degrees of freedom present neither in the atom nor in the nuclei. These degrees of freedom are easily exited under experimental conditions.

Unlike the nucleus and therefore also the atom, the size of the cluster is not restricted by any intrinsic property. Indeed, clusters composed of several thousands of atoms have been observed. This fact allows the possibility of studying the nature of these systems from the very smallest through any size to the infinitely large.

Although the charge distribution of the ions is often successfully treated as a homogenous background, this cannot be completely correct. To some degree the electrons will feel the granularity of matter, too. The fact that the shell model seems to describe the behaviour of the electronic system in small clusters is no guarantee that this will also be true in larger clusters.

The purpose of my work has been to probe the shell structure in the large cluster region. I presents experimental evidence for electronic shells in sodium clusters with a size up to $N = 600$. In addition to the already known, shell closings at $N = 196, 260, 340, 440, 560$ have been observed. These agree well with predictions from a simple mean field potential. Furthermore, the strong attenuation of the observed signature of shell structure with cluster size is explained in terms of a finite temperature.

Shell Structure in Metal Clusters.

The experimental observation of a striking shell structure in metal clusters bears evidence on the validity of a single particle picture to describe the motion of the valence electrons in these systems. It is not a trivial fact that this picture is valid. Both electron-electron interaction and the interaction between electrons and the positive cores could have a magnitude which necessitated different and more complicated models for these objects. Presently it is not possible to evaluate the total magnitude of these perturbing effects in any realistic way. The experimental observation of e.g. strong intensity maxima at electron numbers corresponding exactly to the ones expected for shell closings in a spherical potential will be taken as evidence that a model of this kind describes the important features of the electronic structure. Implicit in this generally accepted conjecture is the assumption that the behaviour of the valence electrons to a large extent determine the properties of the whole cluster.

The starting point here will consequently be a model of the cluster where the valence electrons move freely in a smooth external potential created by the positive ions which donated the valence electrons. The potential will be smooth in the sense that the position of the ions are completely ignored. One example of these models is the jellium potential where the charge of the positive ions is averaged over a volume proportional to the number of ions and to which the electrons add a constant density with slightly larger radius to give the total single electron potential. More refined methods often keep the positive jellium background but treat the electrons with inclusion of selfconsistency constraints [4]. Whatever way the electrons are treated, the potential can be restricted to spherical symmetry or allow deviations from this. Deformations are inherent in the model because of the Jahn-Teller effect, which states that a degenerate electronic state cannot be the ground state but will deform at least until the degeneracy is lifted. By the properties of the spherical harmonic Y_{lm} functions, closed shell clusters are spherical in the ground state, whereas open shell clusters are not. Deformations have interesting consequences of their own, but will only be treated briefly here in relation to the effect they have on the experimentally observed shell structure.

Shell Structure

It is well known that spherical symmetry results in shell structure because of the degeneracy of states with different projections of angular momentum, m, but the same magnitude, l. This is true irrespective of the radial shape of the potential. There will furthermore be a spin degeneracy of two under normal conditions, i.e. where no spin-orbit coupling is present.

In a given potential, the energy levels can be labelled completely by the two quantum numbers n and l; l is the angular momentum and n is the radial quantum number (equal to the number of nodes in the radial part of the wavefunction). The exact value of the energy, $\epsilon_{n,l}$, is of course determined by the potential. Some conclusions can be reached concerning shell structure without reference to the specific potential, however. In the following it should be kept in mind that the terms 'shell structure' and 'single particle level density' are essentially equivalent for a fermionic system . A smooth level density corresponds to no shell structure, and a varying level density to the presence of shell structure. The considerations below are based mainly on [5] and are particularly useful in the limit of large quantum numbers. They do, however, apply to systems with surprisingly small average quantum numbers.

For a given external potential, the single particle energy, ϵ, will always increase with increasing n. In the special case of potentials that have a nearly constant value at the center and a smooth surface, it will increase with increasing l, too. In the limit of large quantum numbers, the single particle energy can be considered a continuous function of the quantum numbers. It is then possible to connect all points in the (n, l) plane that have the same single particle energy, ϵ, with a smooth curve. For the special class of potentials under consideration, this curve will have a negative slope (see fig 1). In the large quantum number limit it makes sense to expand this energy around a set of quantum numbers, n_0, l_0,

$$\epsilon_{n,l} = \epsilon_{n_0,l_0} + \frac{\partial \epsilon}{\partial n}(n - n_0) + \frac{\partial \epsilon}{\partial l}(l - l_0) + \ldots \tag{1}$$

The point (n_0, l_0) can be selected freely on the curve as long as the curvature is small, i.e. when the higher order terms left out in the expansion are small. If a piece of the $\epsilon = constant$ curve crosses a point corresponding to an integer value of both n and l, it will give a contribution to the single particle level density amounting to $2(2l+1)$ from that point, as mentioned above. But in addition to that degeneracy, the single particle energy will be invariant to first order in the quantum numbers under a simultaneous change in n, l provided the changes are related by

$$\frac{\partial \epsilon}{\partial n}\delta n = -\frac{\partial \epsilon}{\partial l}\delta l \tag{2}$$

($\delta n \equiv n - n_0, \delta l \equiv l - l_0$ and l, n are integers). If the ratio between $\frac{\partial \epsilon}{\partial n}$ and $\frac{\partial \epsilon}{\partial l}$ is a ratio of small integers, the relation (2) will be fulfilled for a number of different sets of integer increments $(\delta n, \delta l)$, differing only by a factor which is an integer number. Under these conditions, it will also cross points with different n, l, which will therefore also contribute to the level density, each by the amount $2(2l+1)$.

In the approximation that the second and higher derivatives of ϵ with respect to n and l are small, the slope of the curve will not change much if n or l is increased by a small amount. So locally the curve can be approximated by a straight line. An increase in ϵ then corresponds to a parallel displacement of the $\epsilon = constant$ curve. By increasing ϵ by a small amount, the line will no longer cross any simultaneously integer values of n, l. Consequently the contribution to the single particle level density from that line will be zero. When ϵ is increased further, however, the line will again cross sets of integer values of n, l and contribute to the level density with a non-zero value. A variation of the energy will then lead to an oscillation of the single particle level density. Both the period and the amplitude of this oscillation will be different from the values expected if the degeneracy of the different m-states of a single l-value was responsible for the level bunching.

The period can be evaluated by considering the typical values of the quantum numbers. Since the space is three dimensional, the typical quantum number n (or l) is $N^{1/3}$ (the last $N^{1/3}$ being carrier by the suppressed magnetic quantum number), and since the typical energy is ϵ_f, the first derivatives are of the order

$$\partial\epsilon/\partial n \approx \partial\epsilon/\partial l \approx \frac{\epsilon_f}{N^{1/3}}. \tag{3}$$

Thus increasing n or l by one will essentially reproduce the level density, but increase the energy by the value of this derivative. The periodicity in quantum numbers then means an approximate periodicity in the level density as a function of energy. The period is of the order

$$\hbar\omega_{shell}\epsilon_f/N^{1/3}. \tag{4}$$

The precise value of the period is determined by the slope of the $\epsilon =$ *constant* curve $-\frac{\partial\epsilon}{\partial l}/\frac{\partial\epsilon}{\partial n}$ Since these considerations do not explicitly depend on the value of the fermi energy, they will apply to the level density of a single cluster in the whole region (where the quantum numbers can be considered large and with a proper modification of the meaning of the fermi energy). It is not a priori obvious that they should also apply to the level density at the fermi energy when the cluster size is varied. If, however, the position of the levels depend on the size in a regular manner, they will apply. A suitable regular variation of single particle levels is seen in the example which will be discussed below, where the eigenvalues vary with N as $\epsilon_{n,l} = k_{n,l}N^{-2/3} + k_0$.

The period of $N^{1/3}$ should be contrasted with the expectations based solely on the angular momentum degeneracy, $2(2l + 1)$, where the shell spacing would vary like $\frac{\epsilon_f}{N^{2/3}}$.

It is interesting to note that a periodicity in shell spacing as a function of $N^{1/3}$ also arises if the clusters are ordered according to particle properties as contrasted to the wave properties considered to reach the above result.

Because the surface of a particle is proportional to $N^{2/3}$, adding a complete layer of atoms to a cluster will add a number of particles proportional to $N^{2/3}$. In differential form

$$\frac{\partial N}{\partial n_s} \propto N^{2/3} \Rightarrow n_s \propto N^{1/3} \tag{5}$$

where n_s is the shell number.

Since the N dependence is the same for geometrical particle packing and wave ordering, it is important to be able to distinguish between the two in some other way. This distinction can be made by calculating the two periods. For geometrical packing a new layer added will increase the radius by close to $2r_s$. In the wave case, the value with which the radius of the cluster has to increase to accommodate another electronic shell is essentially the wavelength of the electrons at the fermi level divided by 2π, i.e. $3.28r_s/(2\pi) = 0.52r_s$. Since the radius of the cluster is $r_N = r_s N^{1/3}$, $N^{1/3}$ will increase by around 0.52 if the if shells are quantal, and by almost 2 if they are due to packing of hard objects. An experimental verification of the quantal origin of the shell structure is thus possible without any detailed calculations of the single particle spectrum. Recently experiments on cold Cs and Na clusters have demonstrated the coexistence of electronic shells (in small clusters) and what is interpreted as hard sphere close packing of atoms (in large clusters)[6].

The observation that a shell closing involves states of different n and l is an important extension of the familiar, small N degeneracy due to the m quantum number. It means an extension of the regime where the electronic shells can be observed because of the slower decrease of the shell gap. Furthermore it emphazises the fact that shell structure is not a feature of a special potential such as the Coulomb potential or the three dimensional harmonic oscillator, but a more general phenomenon.

Supershells

There is another interesting consequence of this bunching. To understand this, consider fig 1 with the example of a constant ϵ-line sketched with the negative slope explained previously. In general it cannot be expected that the slope is constant along the $\epsilon = constant$ curve (this will be the case for e.g. the harmonic oscillator or the coulomb potential). Rather, the curve can be thought of as being composed of several pieces of straight lines with different slopes, patched together at the points of intersection. The periodicity of the density of states which appears if only one slope for the $\epsilon = constant$ is considered, still applies to different pieces of the curve with different slopes. In particular the order of magnitude of the period, $\epsilon_f/N^{1/3}$, is unchanged. The precise value of the period, however, will be different for parts of the curve with different slope, since the period depends on the value of the slope. The oscillating part of the single particle level density at a certain energy can then be expressed as a sum over contributions from different sections of the curve. These contributions will be periodic with different periods determined by the slope of the curve. In addition to the periodic contributions, the level density will contain a smooth part which will not be estimated here.

To see the physical meaning of a summation like this, consider the derivatives $\frac{\partial\epsilon}{\partial n}, \frac{\partial\epsilon}{\partial l}$. In the semiclassical limit, these derivatives are the frequencies (up to a factor of $\hbar$) of the classical motion connected to the quantum number in question, ie. $\frac{\partial\epsilon}{\partial n} = \hbar\omega_r, \frac{\partial\epsilon}{\partial l} = \hbar\omega_\theta$ if that motion is separable. If the ω's are in the ratio of integers, the corresponding classical orbit is closed and the ratio of the number of radial and angular turns is given by the ratio of the corresponding derivatives. Expressing the level density in terms of pieces of the $\epsilon = constant$ curve with different slopes can thus be understood as an expansion in terms of closed classical orbits.

The mathematical formalism for this expansion has been worked out in a very thorough way by Balian and Bloch [7]. Expressed in terms of the momentum, the result for the well behaved potentials considered here is

$$\rho(k) = \rho_0(k) + \sum_O A_O cos(I - \pi(M_r + M_l) + \frac{\pi}{4}) \tag{6}$$

where $I \equiv \frac{1}{\hbar}\oint \bar{p}(\bar{r})d\bar{r}$ is the action integral around the classical orbit with M_r radial and M_l angular turns and the sum is over these orbits (see [A] and references herein). ρ_0 is the Thomas-Fermi level density and constitutes the uniform value upon which the shell fluctuations reside.

The Woods-Saxon potential, which will be used as a model potential for sodium clusters, will have major contributions to the oscillating terms from the triangular and the square classical orbits. (The surface of this potential is diffuse and the orbits therefore are not strictly triangular or square, respectively, but no confusion actually arise). The $\frac{M_r}{M_l} = \frac{2}{1}$ pendulating orbit should contribute, too. But since it corresponds to orbits with no angular momentum, it is suppressed by the factor $2l + 1$ when compared to the two other major contributions.

The level density is then

$$\rho(k) \approx \rho_0(k) + A_\triangle cos(I_\triangle + \frac{17}{4}\pi) + A_\Box cos(I_\Box + \frac{21}{4}\pi) \tag{7}$$

An estimate of the $I_\Box, I_\triangle$ can be obtained with the fermi wave number and the length of the trajectories in the hard sphere potential;

$$I_\triangle \approx k_f 3\sqrt{3} r_N \tag{8}$$

$$I_\Box \approx k_f 4\sqrt{2} r_N \tag{9}$$

where r_N is the radius of the potential of cluster N, $r_N = r_s N^{1/3}$. The oscillating term is then simply a sum of two cosines with almost, but not completely equal frequencies. With approximately equal amplitudes for the two contributions ($A_\triangle \approx A_\Box \equiv A$), the sum is a product of two periodic functions:

$$\rho(k) \approx \rho_0 + 2A cos(\frac{I_\triangle + I_\Box}{2} + \frac{19\pi}{4}) \times cos(\frac{I_\triangle - I_\Box}{2} - \frac{\pi}{2}) \tag{10}$$

Consequently, the shell correction to the level density at the fermi level as a function of N will have a frequency equal to the average of the two frequencies. The spacing in N between shell is then determined by

$$\delta N^{1/3} k_f r_s \frac{1}{2}(4\sqrt{2} + 3\sqrt{3}) = 2\pi \Rightarrow \delta N^{1/3} = 0.58 \tag{11}$$

(with a fermi energy of 3 eV), in agreement with the estimate made when discussing quantal vs. geometrical shell structure.

The new feature arises because of the oscillating term in the second factor in (10). In addition to the shell structure periodic in $N^{1/3}$, the amplitude of these shell oscillations will be modified by a periodic function with period determined by

$$\delta N^{1/3} k_f r_s \frac{1}{2}(4\sqrt{2} - 3\sqrt{3}) = \pi \Rightarrow \delta N^{1/3} = 6.8 \tag{12}$$

i.e. about 12 shell periods (the value $r_N = r_s N^{1/3}$, and (8) and (9) have been used). This modulation of shell structure has been named supershells.

The Woods-Saxon Potential as Example

The above predictions of shell structure has been verified by an explicit calculation. For the Woods-Saxon potential

$$V(r) = \frac{-V_0}{1 + exp(-(r - r_s N^{1/3})/a)} \tag{13}$$

with parameters $V_0 = 6eV, r_s = 2.25\mathring{A}, a = 0.74\mathring{A}$, all bound states were calculated by solving the Schrödinger equation for all masses N from 1 to 5000. The total electronic energy for a cluster was then calculated according to the Pauli Aufbau Principle. The energy thus obtained is wrong due to terms left out and as well as terms counted double. The shell fluctuations around the smooth part of the energy is, however, expected to be represented right [8] (within the limitations of the model, of course). The shell fluctuations are extracted by fitting volume and surface terms in the functional form

$$E(N) = -dN + \sigma N^{2/3} + E_{shell}(N) \tag{14}$$

to the calculated total energies. Subtracting the first two smooth terms from the eigenvalue sum leaves $E_{shell}(N)$. This quantity is plotted in fig 6 in [A] vs. $N^{1/3}$. The shell closings can be seen as local minima in the shell energy, spaced about $\delta N^{1/3} \approx 0.6$. The supershell phenomenon is seen as a beat mode in the oscillation of the shell amplitude, showing two two periods, the first minimum occurring at $N \approx 1000$ and the second at $N \approx 4000$. One surprising feature is the the magnitude of the shell energy amplitude. For $N^{1/3} = 13$, the amplitude is 6 eV which, incidentally, is the same as the depth of the potential. Unfortunately this amplitude is not directly observable since it is distributed over the large number of electrons in the last, partly filled, shell.

The shape of the curve between two shell closings is parabola-like. This is readily understandable when it is realized that the energy of a level depends on cluster size according to $\epsilon_{n,l} \approx -V_0 + k_{n,l}N^{-2/3}$, which for large N can be approximated by a straight line across a shell. Since both the energy of the levels and the degree of filling vary linearly with N, the shell energy (which is essentially the total energy of the last filled level), will vary as a parabola.

Level densities for a single cluster can be calculated readily with the Woods-Saxon potential and examples are shown in ref [A]. These are observable (e.g. by ionization cross sections) and has been used to probe shell structure [9].

The method which will be presented in the following exploits the shell structure in the separation energies to provide the information. The separation energy is defined as

$$d(N) = -E(N) + E(N-1) + E(1) \tag{15}$$

and will therefore depend on the derivative of the shell energy. In addition it will include contributions from the volume and surface terms. To be able to compare experiments and theory, these terms have to be included. This is accomplished by adding the macroscopic, experimentally determined, volume and surface terms. For sodium they are [10]

$$d_\infty = 1.1eV, \sigma = 0.70eV \tag{16}$$

The resulting separation energies are sawtooth shaped. The smooth terms provide a scale against which the magnitude of the sawteeth must be measured. Since the surface term is smaller by $N^{1/3}$ than the volume term, this scale is essentially constant, $\approx 1.1 eV/atom$. The separation energies are shown in fig 2 vs. N and $N^{1/3}$. Conceptually these calculated separation energies form the basis for subsequent studies of shell structures in mass spectra formed by evaporation.

Experimental Procedure

Concept

Among the properties influenced by electronic shell structure are periodic variations in ionization thresholds, in total cluster stability and in the single electron level density [11]. In this project, the stability against evaporation was selected to probe the shell structure. As described earlier, the total energy of a metallic cluster can be decomposed into a smooth part and an oscillating part with mean value zero, the shell energy. The presence of an oscillating term implies that the energy per atom is lower for the closed shell clusters as compared to the non-closed shell clusters. This difference in stability will be reflected in the energy required to remove a single atom from the cluster, i.e. the separation energy [12]. Free clusters with non-zero internal excitation energy will manifest the stability as a time delay for breaking up (fragmentation, evaporation). Given the same excitation energy, the more stable clusters will on the average take a longer time than the less stable before evaporating an atom. When a particular initial cluster evaporates down through a chain of successively smaller N, it will reside for different times at different sizes. Thus an ensemble of free clusters from a broad mass distribution undergoing evaporation will produce intensity variations correlated to the variations in separation energy. This difference in abundances was illustrated in [14] where a collection of clusters was exposed to laser light ($h\nu = 3.68eV$) so intense that each cluster absorbed several photons, resulting in subsequent massive evaporation of atoms. After some microseconds, the clusters were accelerated and the abundances measured by a mass spectrometer. The abundances of the (singly charged) closed shell clusters $N = 9,21,41$ are strongly enhanced compared to the masses just above. The experimental concept that will be presented in the following can be viewed as an extension of this idea to large clusters.

The apparatus can be divided into two parts; the source and the mass spectrometer. The machinery is sketched in fig 3.

Cluster Material

The project aimed at demonstrating the existence of shell structure in large metal clusters and if possible the special features predicted in [A] regarding the periodic appearance and disappearance of shells.

The simple metals are expected to give the best agreement with the jellium approximation, which is an important prerequisite for the mean field (independent particle) model. Of the simple metals, sodium was selected for several reasons. The observed shell structure for the small alkali clusters increases with decreasing atomic number [11] and sodium is the second-lightest alkali metal. (In the following the term 'shell structure' will be used not only as a description of properties of the electronic energies of the cluster, but will also refer to the sharp abundance variations observed in the experimental spectra).

Using an expansion source the materials are limited to relatively high vapor pressure materials, a fact which excludes the lightest alkali metal, lithium. The best compromise between these restrictions is sodium. It furthermore has the advantage of being monoisotopic which is a convenient property when cluster size is determined by mass spectroscopy.

Source.

The clusters are produced in an adiabatic expansion source similar to the one used by the Berkeley group. A cross section of the source is shown in fig 4.

Sodium is filled through the gas inlet from the filling system which stores a few hundred ml of Na. The maximum sodium volume in the oven is $20ml$, about 1/3 of the total oven volume. The oven and the nozzle are heated to approximately 800^oC and 900^oC, respectively, by two tantalum wires running in groves in cylindrical ceramic heating elements. The two elements heat the stainless steel oven body and the nozzle, respectively, by radiation to avoid hot spots. Thin external stainless steel and molybdenum cylinders covering nozzle and oven completely act as heat shields. The rear end of the oven is the coldest part of the system. The whole arrangement is surrounded by a water cooled mantle (not shown). Temperatures are regulated by a servo system steered by two thermocouples. The temperatures are measured on the outside of the nozzle and in the rear end of the oven, respectively.

The nozzle, produced by spark drilling, can be made to a diameter down to $70\mu m$. The data are taken with three different sources with nozzle diameters from 70 to $100\mu m$. The inner shape of the nozzle is cylindrical with a length of about twice the diameter. In the production of the nozzle, the length is harder to control than the diameter and this might account for the different average size observed in experiments with otherwise identical conditions.

The cluster distribution is probably rather dependent on the details of the nozzle shape but since the desired mass range can be obtained with the relatively simple design presented above, no effort was made to elaborate the issue.

The Mass Spectrometer

After leaving the source and passing through two skimmers with differential pumping, the clusters fly for approximately 1 m before entering the mass spectrometer. The mass spectrometer works according to the time of flight principle (TOF). When the beam enters the spectrometer, it has a diameter of about $1cm$. The neutral clusters are ionized in a high potential, field free area a few cm long. UV light from a broad band xenon lamp operating continuously performs the ionization after being focused down to a diameter of about $2mm$. The light is filtered so that the photon energy is centered at $3.5eV$ with a FWHM of $1eV$. After ionization the clusters fly for $2cm$ before entering the accelerating stage, which is a $10cm$ long constant field tube consisting of 20 electrodes with teflon spacers, the voltage being divided evenly by a resistor chain. The zero field ionization region and the acceleration region are divided by a grid glued to a separating electrode. The exit electrode is grounded. As the light beam cone has a half angle of about 45°, three electrodes and four spacers have to be cut into two pieces each to make way for the light beam. This is necessary both to avoid surface charging by photo electrons and excessive heating of the teflon spacers. In order to keep the transverse electric field zero in spite of the proximity of grounded material (the chamber walls and the UV lens), thin heat resistant wires connect each pair of half-electrodes. A small longitudinal field in the ionization region (of the order of a few V/cm) saturates the count rate. A zero transverse field is needed because when ionized the clusters still move with thermal energies. These energies can be estimated to be around $0.1eVN$ where N is the number of atoms in the cluster. Minor changes of the ionization area were made during the experiments but the general idea was adhered to.

The ionization potential varies with cluster size, having local maxima at the closed shells. These variations have been measured by others [13] and the effect is $0.2eV$ or less. This should be compared to the spectral width of the ionizing lamp which is close to $2eV$. The suppression of the ionization of closed shell clusters will then be a less than 10 percent effect and this value is reached only in the case of the very strong effects at small shell numbers.

After leaving the acceleration region with an energy of typically $10keV$, the beam is collimated by a slit which can be varied in vertical extension between $0.05mm$ through $1mm$ to $2mm$. Immediately after the slit two $15cm$ long horizontal plates, spaced $2cm$ vertically apart, are located. The time definition for the time of flight mass spectrometer is obtained by applying a time dependent potential difference to the plates. If this potential is step function-like in time, only the ions which have traversed exactly half the length of the plates when the field flips will exit from the deflector plates with a zero vertical velocity. The trajectory of these ions will be vertically displaced, however. All other ions will appear under a non-zero angle. If all ions irrespective of mass have the same energy, the deflection will be mass independent. A second slit at the exit ensures that only the deflected ions will enter the flight tube after the deflection plates.

After a $1.6m$ long flight path with a horizontal adjustment the beam passes through a third slit with optional vertical dimensions $1, 2$ or $4mm$. This slit or the opening at the detector housing defines the resolution of the mass spectrometer.

After the slit, the ions enter a $50cm$ long, constant field reflectron which returns the ions after a near 180^o turn. The purpose of the reflectron is to improve the resolution of the TOF. It is made of 50 electrodes in the shape of aluminum cylinders with inner diameter $10cm$ and hight a little less than $1cm$. They are separated by $0.5mm$ thin rings of isolating material and connected by resistors located on the outside of the cylindrical frame. The entrance is covered by a grid. The high voltage far end contains a gridded aperture to a detector for the purpose of detection of non-reflected beam. This is necessary in order to be able to locate the beam during the first phases of an experiment.

Both detectors are channeltrons. To have a well defined terminating time the clusters hit an planar aluminum block acting as a conversion dynode. The conversion dynode works by liberating electrons upon impact of a cluster. The electrons are then guided by a strong field into the channeltron. In the channeltron secondary electron emission rapidly creates an avalanche which is detected and amplified before being routed to the data aquisition system. The voltage difference over the channeltron is kept at $2.4kV$ to insure amplification of the primary electrons. Since these must be guided from the conversion dynode to the channeltron in the first place, the potential at the dynode is more negative than the potential at the channeltron opening and usually $-3.1kV$. The whole arrangement is covered by a grounded housing. As a consequence the ions will get a post acceleration of around $3kV$. This helps to improve the detection efficiency.

The aquisition system consists of a TDC with a clock frequency of $50MHz$ and a channelwidth of $20 \times 2^m ns$, $m = 1$ to 4, and a PC. The TDC converts arrival time to a channel number. Count rates are 10^2 to $10^3 s^{-1}$, depending on the resolution (i.e. the slit size) and the average mass (i.e. the carrier gas pressure). The typical repetition rate is $10^3 Hz$. The dead time in the detector is thus immaterial as long as it does not exceed the present value of $100 - 200ns$, a number determined by the TDC.

Mass Resolution

The measured flight time of a ion is the time difference between the switching of the pulsing plates and the arrival of the signal to the TDC. This time is determined by the energy of the ions after acceleration, by the various fields the ion encounters on the way from the pulsing plates to the detector, and by the time delay from impact on the conversion dynode to the signal arrives at the TDC.

The delay introduced by the time from the release of the electron to the arrival at the bottom of the channeltron can be estimated to be approximately $10ns$. The variation is then expected to be less than that. The jitter in the time from arrival at the amplifier to the TDC is also less than that.

The energy of the ions after acceleration is a sum of the acceleration energy and the initial kinetic energy imparted to the clusters in the expansion process in the source.

The fields encountered by the ions after acceleration are the following:

1) pulsing field

2) free flight, zero field

3) reflectron field

4) detector field (post acceleration)

To get a good estimate of the mean flight time only the points 2) and 3) need be considered. If the free flight distance is L (equal to the sum of field free distance before and after the reflectron), and the field in the reflectron is $-E_r$, the total time is

$$t = \frac{L}{v} + \frac{2vm_1N}{eE_r} \quad (17)$$

(where v is the speed, $E_{tot} = \frac{1}{2}m_1 N v^2$). The purpose of the reflectron is to improve the resolution. This is achieved by selecting a field in the reflectron that minimizes the width of the distribution of arrival time as a function of speed. To first order, this minimization is achieved by setting

$$\partial t/\partial E_{tot} = 0 \Rightarrow E_r = \frac{4E_{tot}}{eL} \tag{18}$$

This value of E_r means that half the total flight time is spent in the reflectron. With the dimensions stated the flight time is

$$t = 50\mu s\sqrt{N}/\sqrt{V/1kV} \tag{19}$$

The limitation in the resolution due to a smeared ion energy is then

$$\frac{\delta t}{t} = \frac{1}{2t}\frac{\partial^2 t}{\partial E^2{}_{tot}}(\delta E_{tot})^2 = \frac{1}{8}(\frac{\delta E_{tot}}{E_{tot}})^2 \tag{20}$$

obtained by differentiating (16) twice and using the optimum reflectron field.

The energy smearing is caused partly by the variations in the velocity given to the clusters in the expansion in the source. This is at most equivalent to an energy of $T{\times}N{\approx}0.1eV{\times}N$ and probably much lower. (T is the temperature of the source). No direct measurements were made to observe the jet velocity nor the variations in that number. A substantial energy smearing from the recoil energy arising from evaporation can be ruled out. It would only influence the velocity distribution if the number of evaporated atoms is so large that in fact the cluster will be rejected from the beam before ionization because of the transverse momentum imparted in the same processes.

The time definition obtained with the pulsing system results in an energy smearing because the ions move between the pulsing plates with slightly different energies depending on the potential at the position of entry. The difference would cancel upon exit of the pulsing region if the field was kept constant because electrostatic fields are conservative. When pulsing, however, the field changes and a resulting energy difference emerges, the energy depending on the position of the ion in the beam. The maximum energy difference is $2d_{s,1}E_p$ where $d_{s,1}$ is the slit size (width of the beam) and E_p is the field between the pulsing plates. The deflection is typically $1cm$ and with lengths of the pulsing plates equal to $15cm$, the maximum energy difference relative to the total energy is

$$\delta E_{tot}/E_{tot} = 2d_{s,1}\frac{8}{l^2}cm \approx d_{s,1}\frac{1}{15}cm^{-1} = 1/300 \tag{21}$$

for the smallest slit. Without the reflectron the resolution would be limited by that value.

In addition to energy smearing, the resolution is limited by the finite width of the defining slit. The defining slit is either the one located in front of the reflectron or the one at the detector. Which one depends on the precise value of the slit size used in front of the reflectron. The finite size translates into a finite length of beam between the pulsing plates being accepted through the slit and consequently to a smeared starting time. By geometrical considerations it can be shown that

$$\delta t = \frac{d_{s,3}}{LeE_p}\sqrt{E_{tot}m/2} = \frac{d_{s,3}l^2}{8L}\sqrt{\frac{m}{2E_{tot}}}cm^{-1} \tag{22}$$

(for deflection 1 cm, L = 3 m , $d_{s,3}$ = 1,2 or 4 mm). Thus, for $l = 15cm$ and $d_{s,3} = 1mm$,

$$\delta t = \frac{d_{s,3}l^2}{8L^2}3tcm^{-1} = 9\times10^{-5}t \tag{23}$$

($L/3$ = distance from pulsing plates to slit $= 1m$).

This can not be compensated by the reflectron because it's not an energy smearing.

The limitation in the resolution is then the proper sum of the two terms

$$\delta t/t = 9\times10^{-5} \tag{24}$$

(due to the finite slit size), and

$$\frac{\delta t}{t} = \frac{1}{8}(\frac{\delta E_{tot}}{E_{tot}})^2 \tag{25}$$

(due to the energy smearing). Under the optimum conditions used in the examples the resolution $M/\Delta M$ should be better than at least 5×10^3 ($E_{tot} = 10keV$). This is not realized in the actual experiments where the resolution hardly exceeds 10^3. The explanation for this discrepancy is unknown. It might be related to the background which is observed to increase with cluster size. The background is correlated to the counted signal. A pronounced intensity increase e.g. at a shell closing is found to be accompanied by an increase in the background in the vicinity. Both background and the reduced resolution could be explained by fragmentation during and after the initial acceleration and before the ions enter the reflectron. Both ion optical effects of the pulsing plates and the divergence of the incoming beam were examined theoretically and found to contribute neither to the peak broadening nor to the background.

The flight time agrees extremely well with a square root dependence on mass provided an offset in time of the order of $0.5\mu s$ is assumed.

The Observed Spectra vs. the Produced

The observed spectra reflect the distribution of clusters that are ionized by the lamp and reach the detector within a time interval which allows assignment to a certain mass. This is not necessary the same distribution as the one produced by the source. In addition to the weak selection due to differences in ionization potential, the following processes will modify the primordial mass distribution:

1) Diffusion out of the beam will occur on the way from the nozzle to the ionization. The solid angle sampled is of the order 4×10^{-6} of 4π. The source gives a very directional beam by the nature of the expansion and this will counter the effect of the small acceptance angle. If the translational degrees of freedom are approximately equilibrated in the expansion, the lighter clusters will have higher thermal velocities than the heavier. Therefore the lighter species will have a higher tendency to diffuse out of the beam than the

heavier. The net result is an enrichment of the heavier species. No selection related to internal stability of the cluster should occur by this mechanism.

2) Evaporation will occur and is indeed expected to result in the local features of the spectra, i.e. the observed shell structure. It will shape a spectrum in two ways. Firstly by the effect that closed shells will have a longer decay time and consequently be enriched in the spectrum. Secondly by the rejection from the beam because of the recoil when a cluster evaporates an atom. This effect is size dependent. If the temperature of the cluster is $400K$ the energy released is $2T \approx 0.1eV$ [12] giving a velocity change of $\frac{1}{N}10^3 m/s$ in the center of mass reference frame. This should be compared to the speed reached in the expansion, which is of the order of $10^3 \frac{m}{s}$. As the opening angle is $1mm/1000mm = 10^{-3}$, evaporation from a cluster with mass up to several hundred sodium atoms will tend to eject that cluster from the beam. A comparison of own abundance spectra with spectra recorded under conditions where this selection is not in effect [14] shows no major differences in the magnitude of the shell effects for the small clusters which were examined. If this is true in general, it does not rule out evaporation and therefore depletion during the time it takes to fly from the nozzle to the ionization area. It does, however, indicate that evaporation occurs with roughly the same probability for any cluster, irrespective of shell structure.

3) The detection efficiency is expected to depend both on the velocity with which the ions collide with the conversion dynode and on the number of valence electrons of the ions but not on shell structure. The acceleration voltage was varied under constant source conditions in order to saturate the detection efficiency. Saturation was indeed achieved at low voltage judging from the total count rate variations.

Furthermore the pulsing of the deflection plates introduce a deformation of the spectrum (see below).

The Influence of Temperature and Pressure on the Spectra

The observed spectra exhibit features which depend on the source conditions and features which do not. The clarification of which features belong to which category was subject to a systematic experimental study.

The stagnation pressure of the carrier gas is by far the most important factor in determining the average cluster size, but also the oven temperature plays a role. Except for the spectra with a very small average mass, the overall shape of the distribution is quite similar to the one given in fig 5; the maximum gives a good estimate for the average size. In fig 6 the peak size, N_{peak}, is plotted vs. pressure at four different oven temperatures. These data are taken with the first oven and cannot be considered universal. Nevertheless they give a good idea of the variations. The pressure is thus a very convenient handle when the global shape needs adjustment. From the same figure it is seen that the oven temperature only has a significant influence on N_{peak} when the pressure is high. It does influence the count rate, though (see below).

The type of carrier gas influences N_{peak}, too. Since hot sodium is highly reactive, one is restricted to inert gasses, in practice the noble gasses. A systematic study of the influence of the gas type for small clusters has been published [15] and show an increase of average size with atomic mass of the carrier gas. A similar effect is seen for larger masses.

The intensity, or count rate, depends strongly on carrier gas pressure and oven temperature. In fig 7 are shown intensities vs. pressure from the same spectra. Since both intensities and average cluster size increase strongly with stagnation pressure, the total amount of counted atoms has a very strong pressure dependence. The sodium consumption is also found to increases with pressure. A priori this is not expected because the flow rate (measured as the volume of gas streaming through the nozzle) is independent of pressure and the sodium vapor pressure in the oven depends only on temperature.

Consequently the amount of sodium flowing out of the nozzle was expected to depend only on the oven temperature.

Another strongly determining factor for the intensity is the temperature of the nozzle. From high intensities at a nozzle temperature $70 - 80K$ above that of the oven, the intensity decreases several orders of magnitude when the temperature difference is increased a further $100K$. Lowering the nozzle temperature results in clogging of the nozzle. To avoid this, the temperature difference is kept at $100-110K$ at low stagnation pressures and around $150K$ for higher pressures.

Two properties of the spectra are remarkably invariant under changes of source conditions. The *shape* of the distribution depends only on the temperature and pressure through the average value, ie. $I_N = f(N, \bar{N})$ (to a multiplicative constant). All information concerning temperature and pressure seems to be contained in one parameter $\bar{N}(T, P)$. Even more remarkably, for $\bar{N} \geq 20$ the function depends only on the scaled cluster size $N/\bar{N}$ (if shell structure fluctuations are neglected);

$$I_N = f(N/\bar{N}). \tag{26}$$

This agrees well with expectations based on Schmolukowsky's equation for aggregation in the absence of evaporation. Fig. 8 illustrates this point. In addition to the scaling, one sees that the function is unsymmetric. Part of the asymmetry is due to the bias in the mass selection caused by the pulsing plates. When accelerated to constant energy, the density of mass N is reduced by a factor inversely proportional to the speed, giving a density biased by $N^{1/2}$. The universality is not changed by this correction and in the figure both values are seen to be proportional to $\bar{N}$ fairly well.

The second important feature of the spectra which is invariant under changes of source condition is *the abundance variations caused by shell structure* (the magnitude properly defined). Before being able to obtain an invariant measure of these very interesting variations, the intensities themselves have first to be extracted from the spectra.

From Mass Spectra to Shell Structure

To extract intensities, I_N, the raw spectra are fitted with a peak fitting program (developed by D.Radford). Assuming gaussian peak shapes and given approximate positions of the first two peaks in a spectrum, the first stage of the procedure locates peak positions all the way to the maximum mass still resolvable. In the second stage the peak positions are fitted to a third order polynomial in the mass followed by a fit of all intensities, widths and the background. In the third stage the width is fitted to a third order polynomial followed by an intensity and background fit.

The output after the second or third stage is the intensities, positions and widths of all peaks as well as the (mass dependent) background and the statistical uncertainties on the intensities. During the different fitting processes the validity of the fits are monitored by a χ^2 test. No assumption is made during the entire procedure concerning the integrated intensity of the peaks. Very little change in the peak positions and intensities is observed from the second to the third stage in the procedure.

Spectra taken with the reflectron show a very good agreement with a square root dependence of the flight time with mass. Thus the identification of masses can be made unambiguously. For the spectra produced without reflectron, the square root dependence is observed not to hold quite as good. This poses no problem with respect to identification of the masses since these spectra all deal with small masses where the extrapolation to zero mass can be made without problems. When this extrapolation is extended to the high mass side of the spectra it results in all cases in the identification of the local high intensity peaks with the expected shell closings for neutral clusters. This identification agrees with the spectra observed by Knight et al. Knight's identification is unambiguous because a quadrupole mass spectrometer was used. A convenient way of fixing the exact mass for the small clusters is then simply to spot two prominent shell closings and count the number of peaks between.

The spectrum shown in fig. 5 is shown in fig. 9 after fitting by the procedure described. Imposed on the envelope which gives the global shape of the intensities in the spectrum, the small mass region shows strong intensity enhancements at the shell closings followed by an abrupt drop for masses just beyond. The high mass region exhibit similar features with the important modification that the shell structure is much less pronounced, both with respect to amplitude and sharpness. Whereas the shell closings at eg. $N = 40$ is very sharp in the sense that the maximum at $N = 40$ is followed by a local abundance minimum, the drop from local maximum to local minimum around $N = 196$ takes place over a range of masses of the order of 5.

In order to extract the magnitude of the shell structure it is necessary to eliminate the envelope function from the quantity considered. As long as the envelope function, $f(N/\bar{N})$, is not known, this is not possible to do with mathematical rigor. Less will do however, and a convenient representation of the data was found to be the logarithmic difference or derivative

$$\Delta \log I_N = 2(I_{N+1} - I_N)/(I_{N+1} + I_N) \approx \partial \log I_N / \partial N \qquad (27)$$

if I_{N+1} and I_N are not too different. This derivative still contains some effects of the global shape. A further reduction could be obtained by considering the second or higher derivative. This is neither convenient nor physical appealing. The inconvenience has a technical but important reason; the higher the derivative one considers, the higher statistics is needed to see a given effect.

The physical reason to prefer the first derivative to the second is the observation that the topology of the abundance spectra around a shell closing has a close similarity to the derivative of shell energy or, in other words, with the shell structure present in the separation energy as found in calculations [A] and plotted in fig. 1. The close similarity between the first logarithmic derivative of the abundances and the second derivative of the shell energy is obvious from fig. 2 in [D] (left panels). This behaviour of the observed spectra is at variance with an equilibrium distribution. A distribution reached in chemical equilibrium will give rise to an spectrum in which the abundances vary similarly to the variations in the shell energy and not to the first derivative which is actually seen. In particular the abundances around a shell closing should show a degree of symmetry which is not observed. Consequently it can be ruled out that the abundance spectra sample quasieqilibrium distributions.

Generalization of the Logarithmic Derivative

A detailed comparison of the abundance derivatives and the shell energy will be made later. But in order to do that, it is necessary to improve the derivative. Due to the rapidly decreasing shell amplitude with cluster size, the requirements to the number of counted ions in a single peak increases rapidly, too, in order to have a clear signal in spite of statistical fluctuations. However otherwise annoying, the finite width of the shell closings for the larger shells can be useful when defining logarithmic derivatives in a way to partly circumvent this problem. A finite width of an intensity drop like eg. the one seen at mass 250 in fig 9, means that the derivative can be represented by $\Delta I_N = \frac{1}{3}(I_{N+2} - I_{N-1})$ equally well as by $\Delta I_N = I_{N+1} - I_N$. Taking statistical fluctuations into account, the former definition is even better because the uncertainty on each term is very nearly the same and the difference is 3 times larger in the first quantity as compared to the last. Neither should be preferred to the other, of course; a proper statistical weight should be assigned each. A suitable generalized derivative then takes the form

$$\Delta_1 I_N = \frac{\sum_{k=0}^{W}(I_{N+k} - I_{N-k-1})k^2}{\frac{1}{2}\sum_{k=0}^{W}(I_{N+k} + I_{N-k-1})}. \tag{28}$$

A smooth function could be introduced instead of the sharp cutoff in the sum. This was tried with a gaussian and found to have a negligible effect.

The derivatives thus defined have the important virtue of being independent of W as long as the second and higher derivatives of I_N with respect to N can be neglected. There is an upper limit to the value of W which can be used before the spectrum is distorted by this smoothing procedure. This limit is essentially the width of the shell closing in the raw data. These natural widths vary quite a lot (from 0 or 1 to more than 10), so a smoothing width W which is a function of N can be used. Fig. 1 in [D] (right panels) show the smoothed logarithmic derivatives of a sum of abundance spectra. with the width W equal to 8. Besides the shell structure which show up as strong and relatively sharp dips in the derivative, two other features should be mentioned. Very broad depressions are observed between the shell closings. These are interpreted as an effect of the increased stability caused by deformation of the cluster. They can be seen in some regions in the raw data, too. These features persist even at very large W. Secondly, the odd-even alternations which are seen seen from the smallest masses observed ($N = 3$) to $N = 70$ are clearly seen if $W = 1$. Not surprisingly, they are the first fluctuations to disappear with an increased W.

The oscillating features mentioned here all originate from a smoothly varying baseline which reflects the global shape of the original distribution. As the shape is unrelated to the electronic shell structure, it can be subtracted for a better visualization of the oscillations and for the purpose of obtaining a numerical estimate of the amplitude of the shell dips. By the same reasoning, different spectra can be added before differentiating (but after finding the peak intensities from the raw data). This procedure was followed in [B] in order to improve statistics.

Interpretation of Abundance Spectra

The close similarity between the local intensity variations in the experimental spectra and the first derivative of the shell energy is empirical. It can, however, be rationalized with a model for the observed cluster abundances in terms of evaporation. Based on [D], the fundamental assumptions underlying this rationalization can be stated as follows:

1) During the time (1ms) the clusters fly from the nozzle to the ionization region, a number of evaporations of single atoms from each cluster occur.

2) At the time they reach the ionization region all clusters have similar temperatures.

3) The evaporation of an atom is a statistical process, and the decay constant can be written as

$$k_N = \omega N^{2/3} e^{\Delta_1 F_{N-1}/T}. \tag{29}$$

where ω is of the same order of magnitude as the vibrational frequency which is about $10^{13} s^{-1}$. $\Delta_1 F_{N-1}$ is the free energy of evaporation, i.e. the difference in free energy between a cluster N and the cluster $N-1$ plus the monomer.

4) The cooling during evaporation occurs in such a way that the product of decay constant and abundance for a given cluster will be constant with respect to cluster size;

$$k_N I_N = constant. \tag{30}$$

It is fairly well established in the literature that if the first assumption holds, i.e. a reasonable amount of evaporation occurs, the second will also be true. The temperature of the clusters will be close to $\frac{d}{\log \omega N^{2/3} t}$. With a time $t = 1ms$ and a separation energy $d \approx 1eV$, the temperature is a little less than $400K$ [16].

The assumption of statistical decay is similarly standard. Is has been the subject of a rich chemical literature and has been widely applied to the study of clusters (see e.g. [17]). With this statistical decay, the probability of survival of a specific, isolated cluster with a sharp energy is then given by the well known exponential formula

$$P = e^{-kt} \tag{31}$$

The expression for the decay constant,

$$k_N = \omega N^{2/3} e^{\Delta_1 F_{N-1}/T} \tag{32}$$

is a modified version of Engelking's or the time honoured RRK or RRKM time constant [18] for unimolecular decay.

Two modifications are introduced into these time constants. Firstly, the energy dependence is written as an exponential function. Furthermore, the total excitation energy is expressed in terms of a temperature, T, defined as $E/(3N-6)$, where E is the total excitation energy, and $3N-6$ is the number of (vibrational) degrees of freedom. Although this terminology is an abuse of the word temperature, it is a convenient shorthand. The second and most important modification of the standard formula is the substitution of the ground state separation energy with the separation free energy. The free energy pertains only to the electronic degrees of freedom in this case. The free separation energy is defined similarly to the separation energy except that free energies are used instead of ground state energies:

$$\Delta_1 F_{N-1} \equiv F_N - F_{N-1} - F_1 \tag{33}$$

At $T = 0$ this expression reduces to the standard expression for the separation energy. At the temperatures under consideration, F_1 is always equal to E_1, i.e. no internal excitation occurs in the atom. The difference between the standard separation energy lies in the different free energies of the electronic systems of the mother and daughter cluster. This difference is absent in molecules because the level spacings in these are so much higher than the temperature that no electronic excitations occur in these species.

This is changed in the metal clusters. The energy gap between shells is of the order of $\epsilon_f/N^{1/3}$. Thus the larger the cluster, the more important the electronic excitations. In fact, a schematic analysis [5] has shown that at a temperature as low as 1/3 of the shell gap, no information is retained in the free energies of the shell structure which is present in the level density. For sodium at $500K$ the mass where this limit is reached at $N = 8000$. Any deviations from ideality reduces this number.

The inclusion of thermal effects on the electronic system is clearly needed for a reasonably realistic description of the magnitude of the shell effect. An evaluation along these lines was made in [C]. The effect of a finite ionic and therefore also electronic temperature was seen to be twofold.

Firstly, the amplitude of the fluctuating part of the free energy, the shell free energy, was reduced as compared to the zero Kelvin situation. The reduction is present even at temperatures where no electrons are exited, due to the zero temperature shell oscillations of the entropy. At higher temperatures, the electronic excitations will be the cause for the reduction in he shell free energy.

Secondly, the shape of the shell energy will change. At zero temperature the shape of the shell energy across a shell closing is parabola-like. In particular, the local minima will be sharp. The finite temperature will round these minima and ultimately turn the shell free energy curve into a curve best represented by a sinusoidal function with decreasing amplitude. In terms of separation energies it means that the sharp sawteeth at zero temperature will be rounded. Examples can be seen in [C].

In addition to these observations, the effect of thermal excitations on the single particle spectrum was monitored and found to be very small within the spherical jellium model employed. The significant reduction of shell structure observed can then be ascribed to the thermodynamics of electrons in a spectrum which is independent of temperature.

It should be noted that the inclusion of finite electronic temperature effects is not unique when applied to evaporation studies, even within the picture where the decay process is described by statistical methods. The correction to the zero temperature decay constant is only valid under the assumption that there is no barrier present when the atom leaves or approaches the cluster surface. This assumption is easily made but hard to prove. It will be made here without any further justification.

The last assumption stated, expresses a relation between abundances and decay constants;

$$k_N I_N = constant \tag{34}$$

or

$$I_N \propto {k_N}^{-1} \tag{35}$$

With the other assumptions made it seems inescapable if the shell energies are at least reasonable similar to the ones calculated in [A] and presented in the first section. The assumption relates observed abundances to differences in free energy by the formula (nummer).

On this background it is possible to compare not only the positions of the prominent shell closings but also their magnitude and widths. Since the position of the prominent shell closings are reproduced very well by the Woods-Saxon potential, the eigenvalues calculated from this potential were chosen also as a model for the clusters at finite temperatures.

The shell structure, as measured by the gap between two shells, is perturbed by the presence of a multitude of effects, alluded to previously. These are not accounted for in the model, and therefore the experimentally observed shell oscillation will in general be reduced when compared to the ideal case. The reduction inferred from small clusters is a factor of 2 or so. Partly justified by this reduction, a compression of the eigenvalue spectrum with a factor of 3 was made before calculating the free energies.

To facilitate the comparison with abundances, the second difference of the Helmholtz' free energies were calculated by the method described in [C]. The result is displayed in fig. 2 in [D] together with the first difference of the observed abundances. A smooth term has been subtracted from the latter curves. The most significant deviation from the zero temperature shell energy second difference is the substantially reduced amplitude, even at moderate cluster size. The observed decrease in amplitude is much faster with N than the $N^{-1/3}$ dependence predicted from general arguments and observed in the zero temperature calculation. The small and large cluster amplitudes differ by a factor of almost 10^3. It is most remarkable that an agreement over so large a range can be obtained with adjustment of a single parameter, that is, the factor of 3 introduced to compensate for the unknown smearing effects.

Besides the magnitude, the width of the shell closings are seen to be represented reasonably well by the calculation. With a calculation as the one presented, it is of course not possible to obtain an estimate of the significance of effects other than the electronic excitations. The agreement between observed and calculated widths is, however, encouraging.

Conclusion

Shell closings in sodium clusters have been observed in abundance spectra produced by an adiabatic expansion source. The shell closings are manifested through sharp changes in the abundance as a function of the mass of the cluster. Evidence for the quantal nature of this structure which has been observed in cluster consisting of up to 600 valence electrons, has been presented. The observed shell closings are located at $N = 8, 20, 40, 58, 92, 138, 196, 260 \pm 4, 344 \pm 4, 440 \pm 2, 558 \pm 8$, the first six being previously observed. The values observed agree with measurements of the photo-ionization thresholds of Cs clusters in [9]. These observed numbers agree surprisingly well with a model that describe the motion of the valence electrons as independent particles in an exterior potential.

The magnitude of the observed effect is observed to decrease rapidly with cluster size. This decrease, as well as the broadening of the shell closings can be explained as an effect of the finite temperature of the cluster.

Fig 1: Two $\epsilon = constant$ curves for a generic potential. The dots correspond to the states that are actually realized.

Fig 2: Separation energies for sodium calculated with the Woods-Saxon potential. The leftmost point is $N = 2$. Up to $N \approx 1400$ the points are connected with a thin line for visualization. The bulk volume and surface terms are added as described in the text.

Fig 3: Schematic diagram of the experimental apparatus:

A: Source, B: First skimmer, C: Ionizing Xenon lamp,

D: Ionization and acceleration region,

E: Slits. The pulsing plates are located between the first two slits,

F: Channeltron detectors, G: Reflectron.

Fig 4: The source. See text for details.

Fig 5: Abundances vs. flight time for a typical mass distribution. The mass where the distribution peaks is around $N = 170$.

Fig 6: The value of N for which the mass distribution has maximum value, for 12 different spectra plotted vs. stagnation pressure. In all cases Ar was used as carrier gas.

Fig 7: The count rate for all masses vs. stagnation pressure for four different temperatures. The spectra are the same as in fig. 5

Fig 8: The full width half maximum (FWHM) used as a simple for the scaling of the mass distribution. In the figure is shown FWHM vs. N_{peak} for the distributions of fig. 5 and 6. Besides the FWHM is shown the lower values for the half maximum point. Both quantities are seen to be proportional to N_{peak}.

Fig 9: Integrated peak intensities of the spectrum shown in fig. 5. The spectrum starts a little below $N = 40$ and ends just below $N = 400$. The position of the shell closings are seen clearly in spite of the statistical fluctuations of the individual peak intensities.

Fig 1

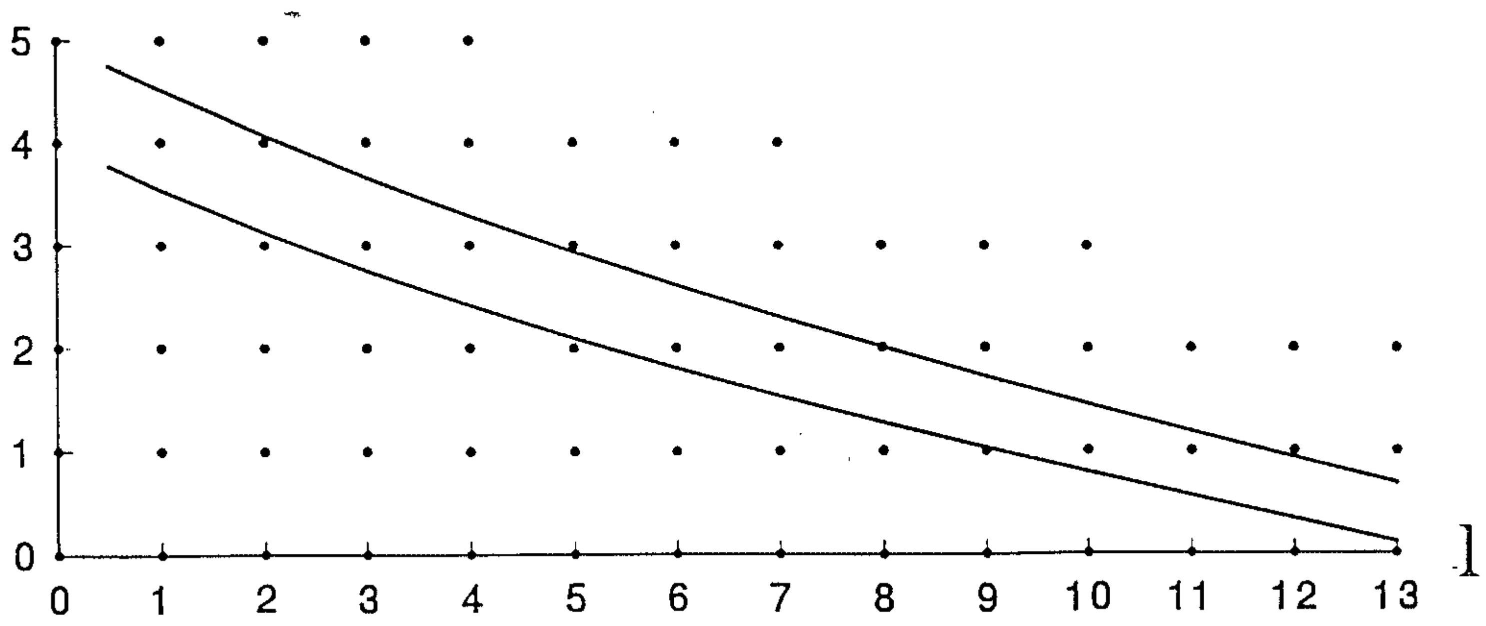

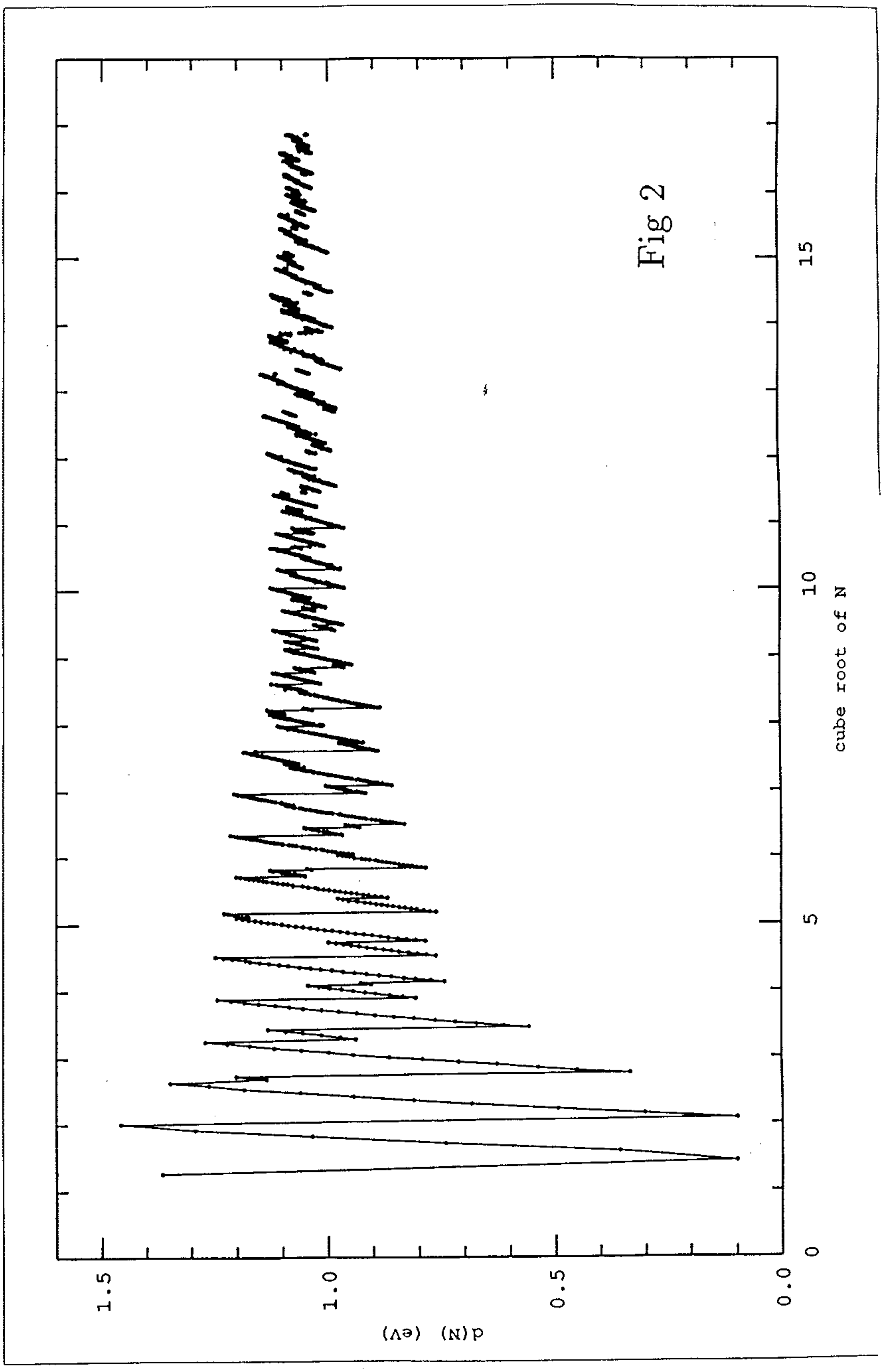

Fig 2

12-DEC-90:04:23:06, HBITAL, Roskilde, Denmark.
HBITAL$DUA2:[JP]PLOT.PLO;6

Fig 3

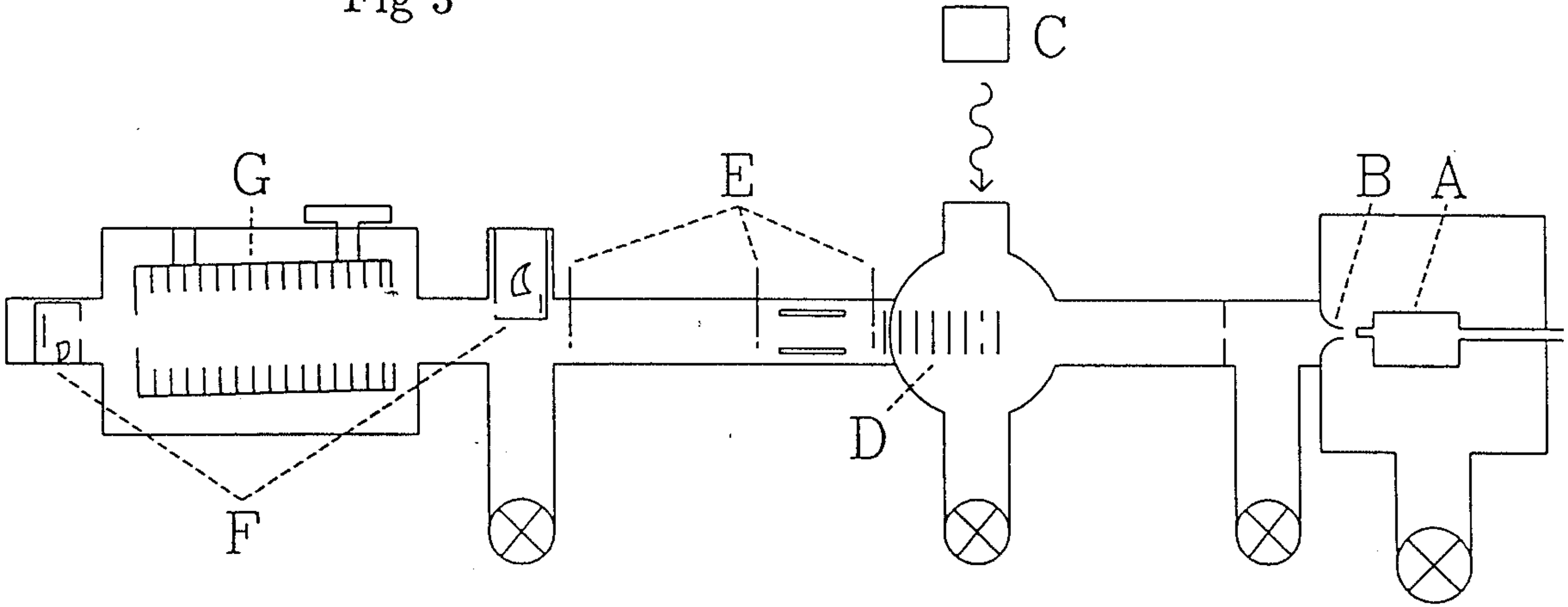

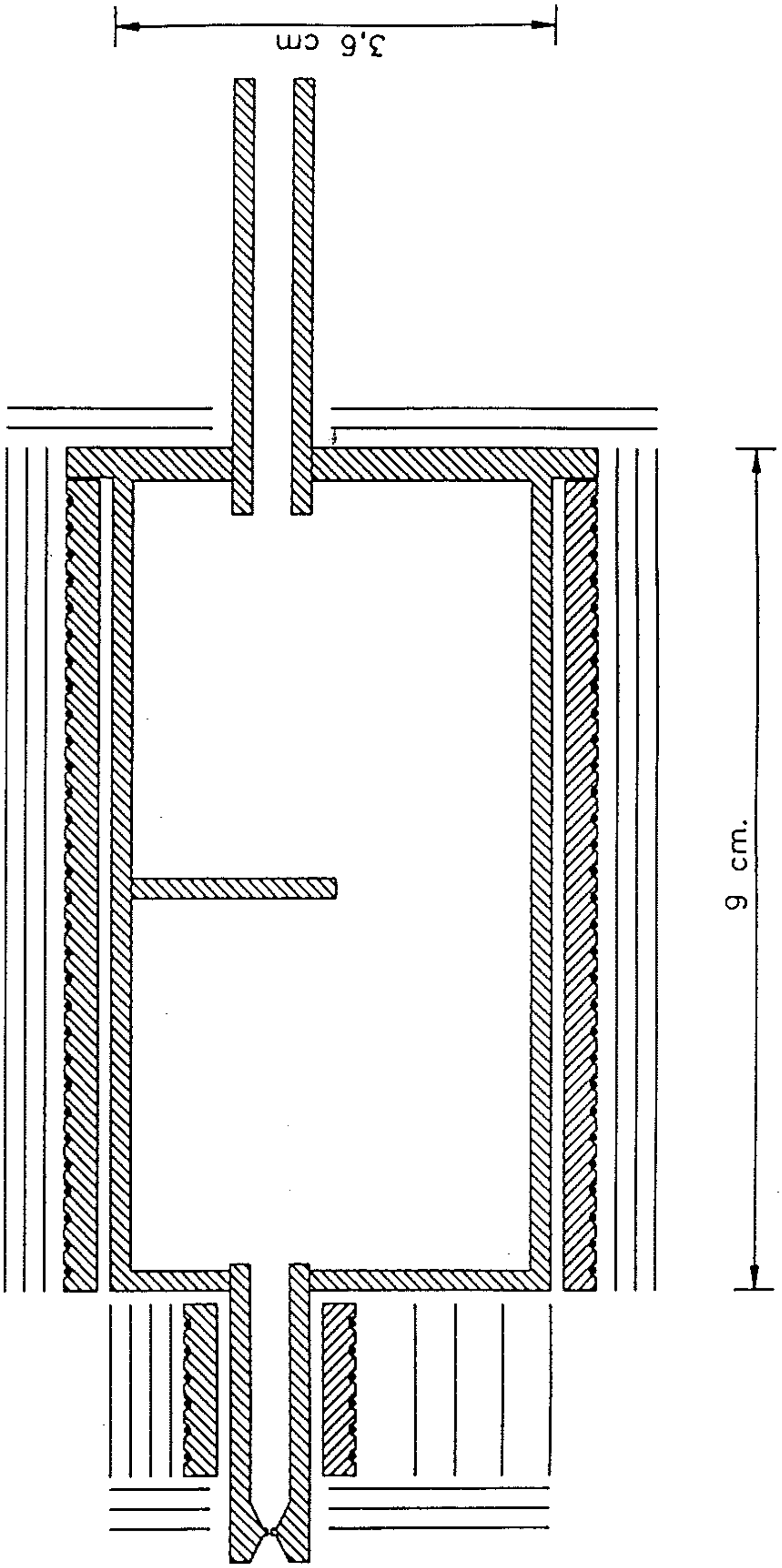

Fig 4

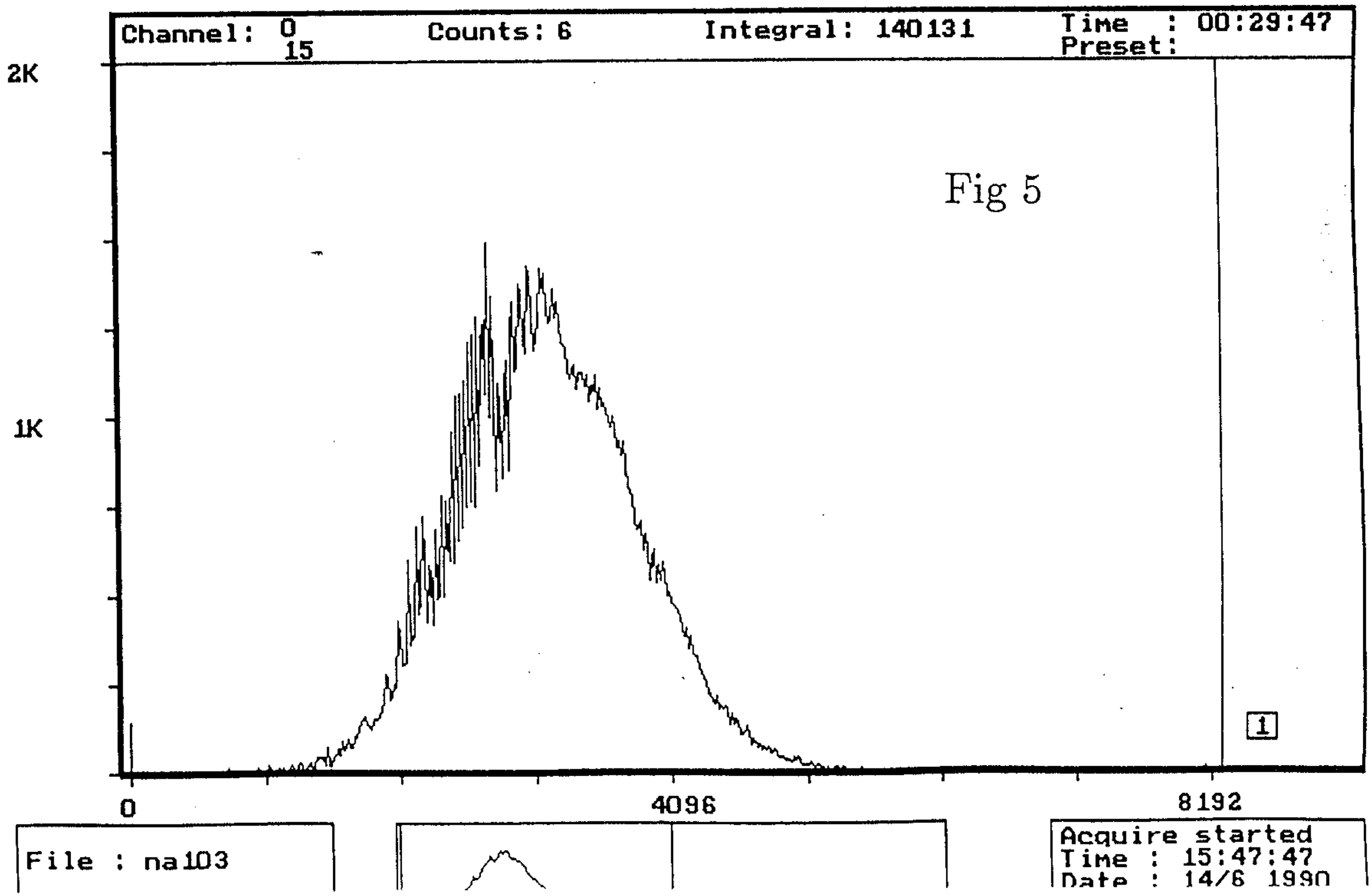
Fig 5

Channel: 0 15 Counts: 6 Integral: 140131 Time : 00:29:47 Preset:

File : na103

Acquire started
Time : 15:47:47
Date : 14/6 1990

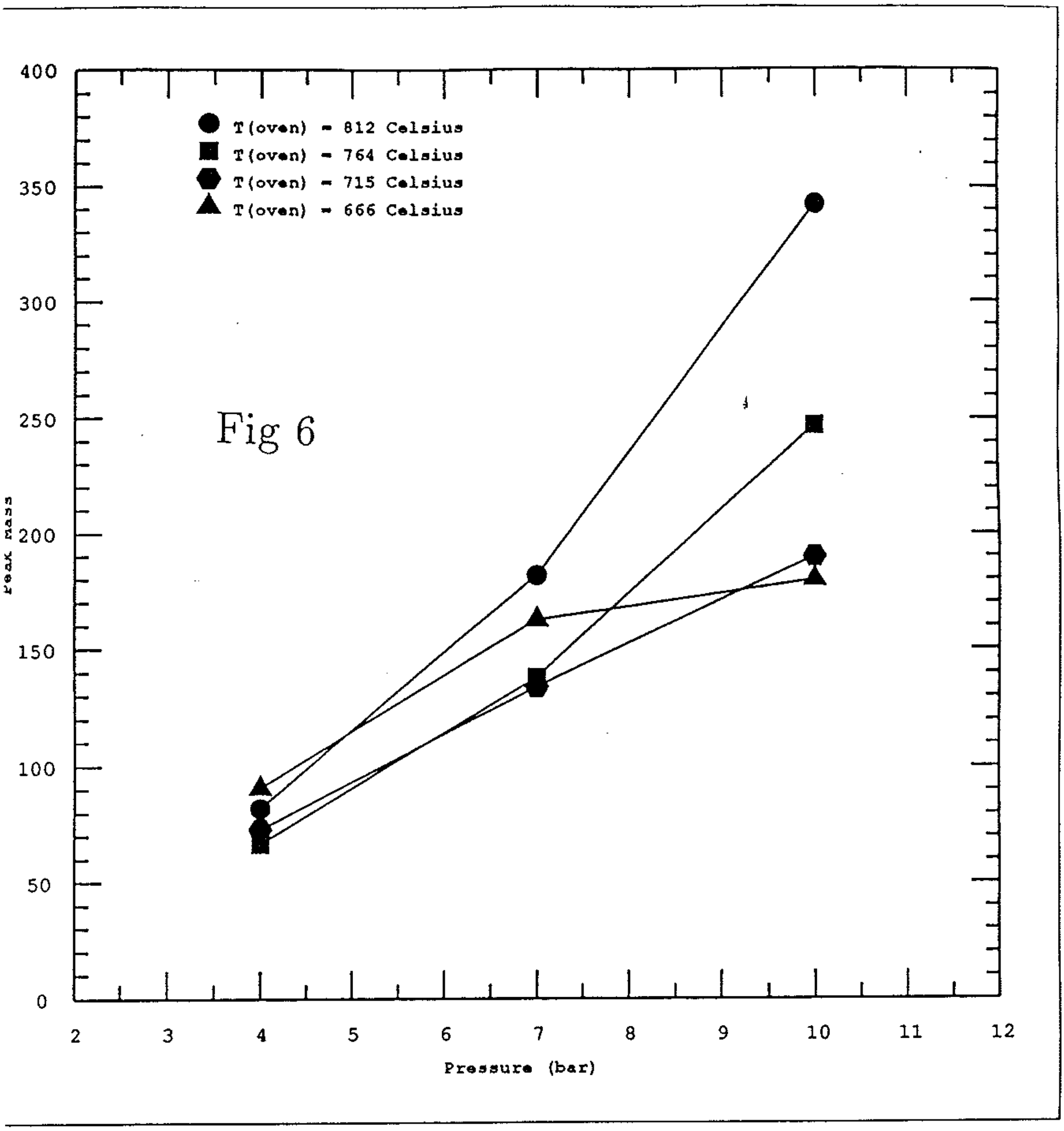

Fig 6

0:04:41:17, NBITAL, Roskilde, Denmark.
UA2:[KLH.TH]SPECTRA2.PLO;6

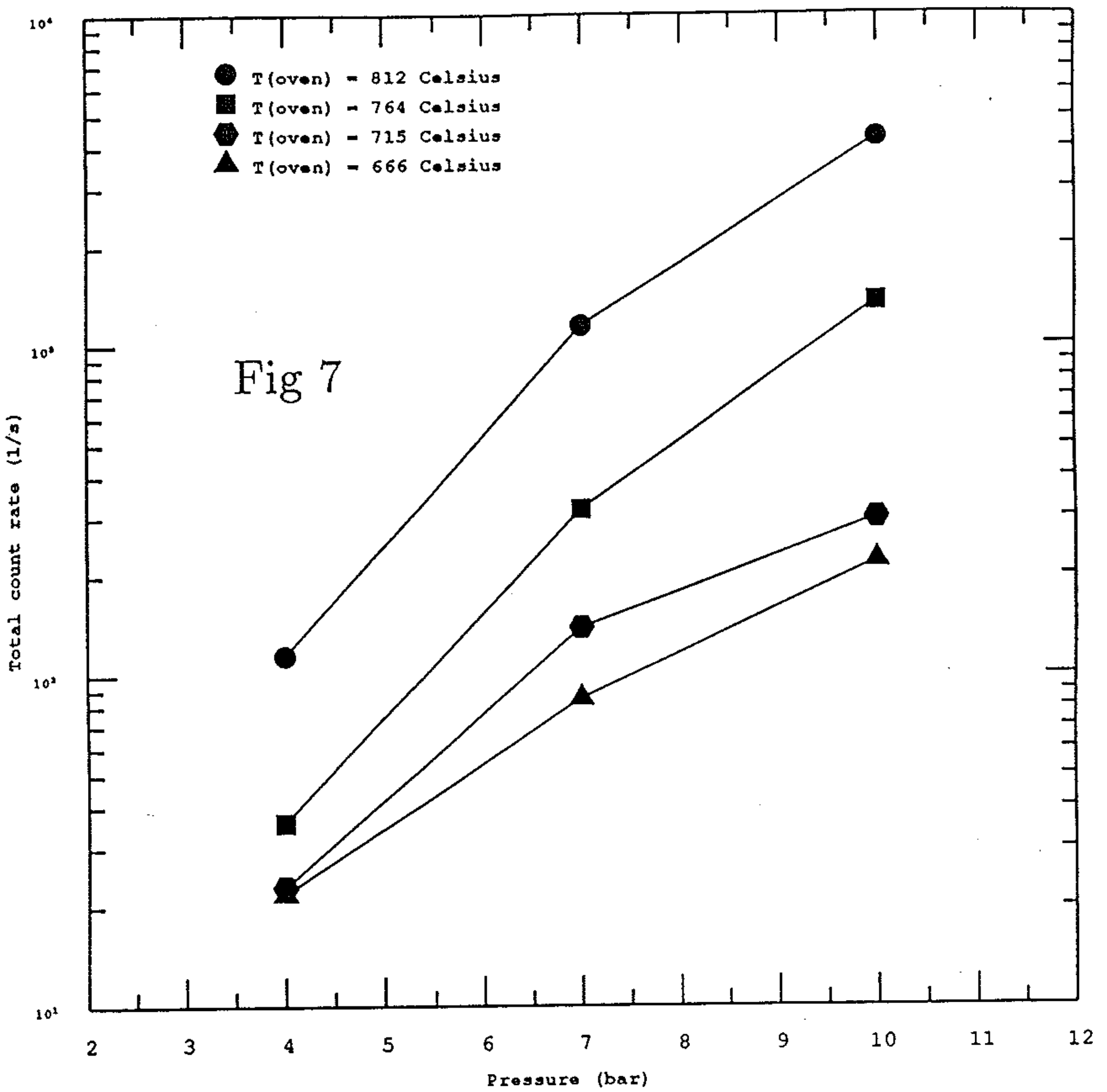

12-DEC-90:04:44:47, NBITAL, Roskilde, Denmark.

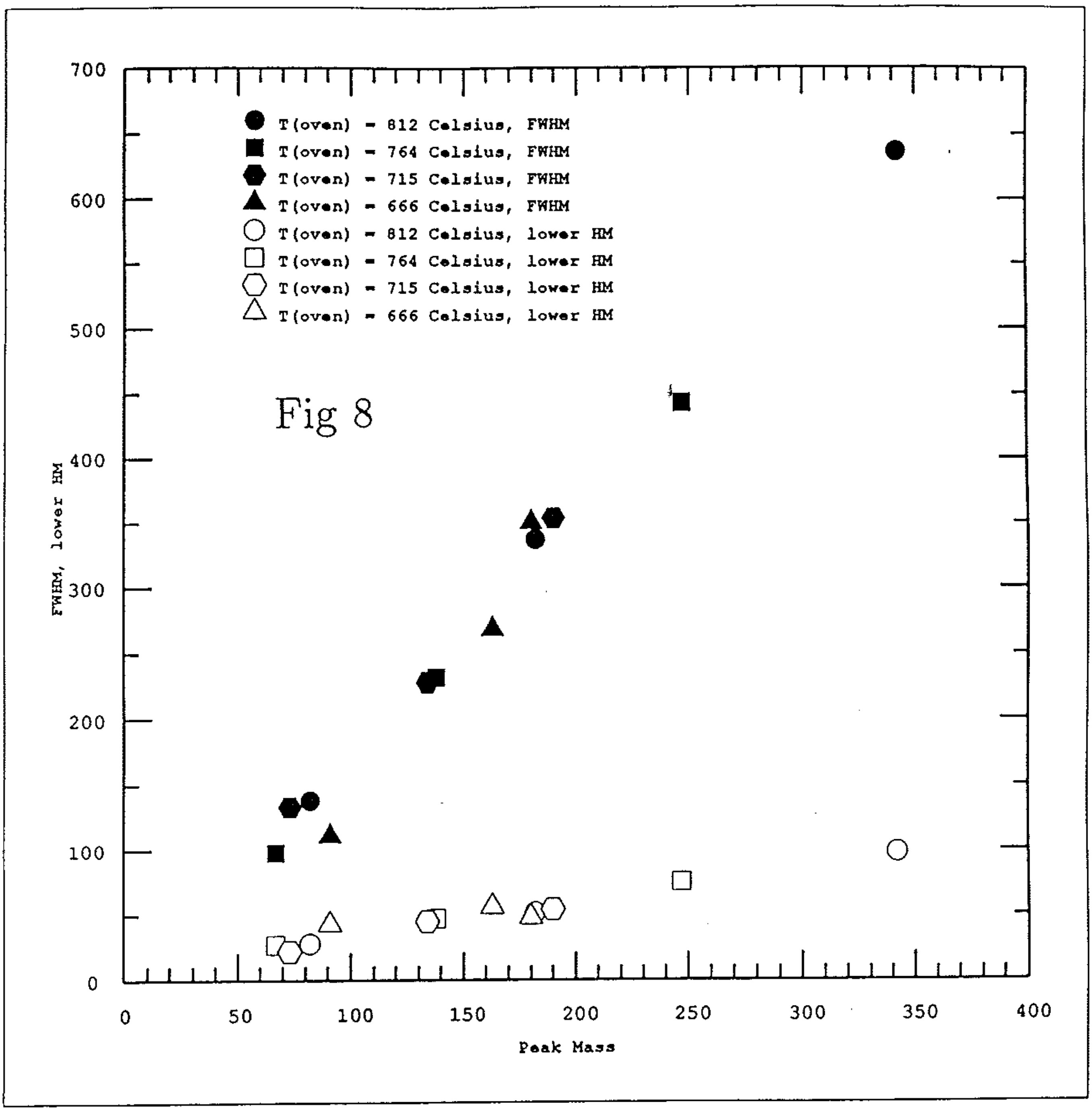

Fig 8

12-DEC-90:07:03:02, HBITAL, Roskilde, Denmark.
HBITAL$DUA2:[KLH.TH]SPECTRA3.PLO;7

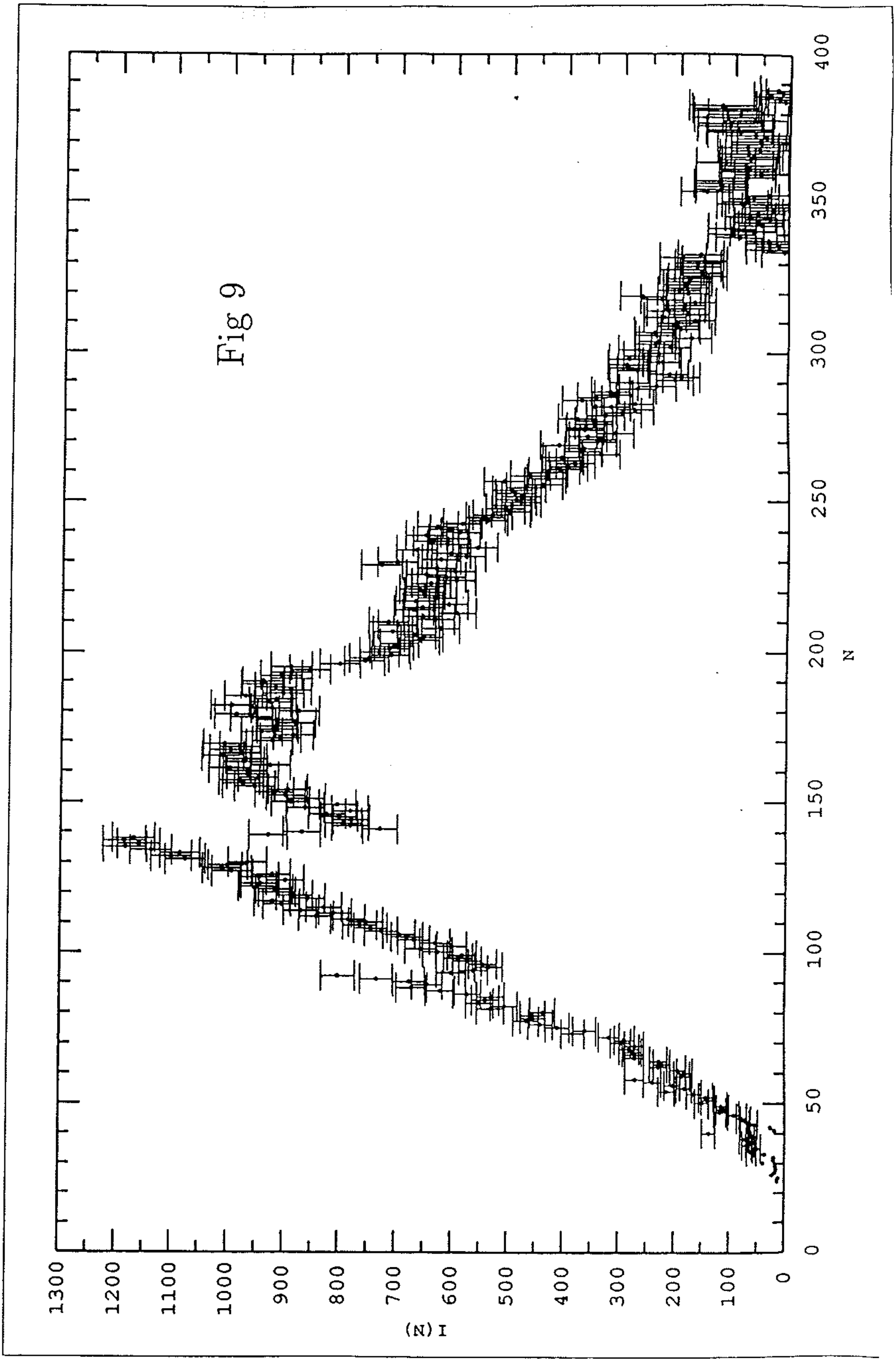

13-DEC-90:14:01:13, NBITAL, Roskilde, Denmark.
1DUA2:[KLH]PLOT.PLO;42

References

[1] Knight, W. D., Clemenger, K., de Heer, W. A., Saunders, W. A., Chou, M. Y., and Cohen, M. L., Phys. Rev. Lett. **52** (1984), 2141

[2] M.G.Mayer and J.H.D.Jensen, Elementary Theory of Nuclear Shell Structure, (Wiley, New York, 1955)

[3] Katakuse, I., Ichihara, T., Fujita, Y$_3$, Matsuo, T., Sakurai, T., and Matsuda, H., Int. J. Mass Spectrom. Ion Proc. **67** (1985), 229

[4] See e.g.: M.Y.Chou and M.Cohen, Physics Letters **113A** (1986), 420

[5] A.Bohr and B.Mottelson, Nuclear Structure, Vol. II, (Benjamin, Reading, Massachusetts,1975)

[6] T.P.Martin, T.Bergmann, H.Göhlich and T.Lange, Chem. Phys. Letters **172** (1990), 209

[7] R.Balian and C.Bloch, Ann. Phys. **69** (1972), 76

[8] V.M.Strutinsky, Nucl. Phys **A95** (1967), 420

[9] H.Göhlich, T.Lange, T.Bergmann and T.P.Martin, Phys. Rev. Lett. **65** (1990), 748

[10] C.Kittel, Introduction to Solid State Physics, (John Wiley, New York, 1986) and Handbook of Chemistry, (CRC Press, Florida, 1980)

[11] W.de Heer, W.D.Knight, M.Y.Chou and M.L.Cohen, Solid State Physics **40** (1987), 93

[12] P.C.Engelking, J.Chem.Phys. **87** (1987), 936

[13] M.M.Kappes, M.Schär, U.Röthlisberger, C.Yeretzian, E.Schumacher, Chem. Phys. Lett. **143** (1988), 251

[14] C.Bréchignac, Ph.Cahuzac, J.Leygnier and J.Weiner, J.Chem.Phys. **90** (1989), 1492

[15] M.M.Kappes, R.W.Kunz and E.Shumacher, Chem. Phys. Lett. **92** (1982), 413

[16] C.E.Klots, J. Chem. Phys. **83** (1985), 5854; C.E.Klots, Z. Phys. D **5** (1987), 83

[17] W.Forst, Theory of Unimolecular Reactions, (Academic Press, New York, 1973)

[18] M.F.Jarrold, U.Ray, J.E.Bower and K.M.Creegan, J. Chem. Soc. Faraday Trans. **86** (1990)

[19] P.G.J. van Dongen and M.H. Ernst, Phys. Rev. Lett. **54** (1985), 1396

[A]

PHYSICAL REVIEW B VOLUME 42, NUMBER 15 15 NOVEMBER 1990-II

Supershells in metal clusters

H. Nishioka
Department of Physics, Konan University, 8-9-1 Okamato, Higashinada-ku, Kobe 658, Japan
and The Niels Bohr Institute, University of Copenhagen, DK-2100 Copenhagen Ø, Denmark

Klavs Hansen
Tandem Accelerator Laboratory of The Niels Bohr Institute, DK-4000 Roskilde, Denmark

B. R. Mottelson
Nordisk Institut for Teoretisk Atomfysik (NORDITA), DK-2100 Copenhagen Ø, Denmark

(Received 5 April 1990)

Assuming a spherical mean field for electrons in metal clusters, single-particle level densities and electronic binding energies are calculated for clusters with up to 4000 valence electrons. Two phenomenological mean-field potentials, simulating microscopically calculated ones, are used. A global beating pattern, which envelopes individual shell oscillations, emerge from the calculations. The semiclassical interpretation of such a supershell structure, as proposed by Balian and Bloch in terms of interference of amplitudes associated with classical closed orbits, is found to be valid in the present case. Thermal effects, which tend to smear out shell and, therefore, supershell structures, are investigated qualitatively. Consequences of the shell structure are not obscured for cluster sizes up to several thousand atoms under the experimentally accessible temperature of 100–1000 K.

I. INTRODUCTION

For several years the properties of atomic and molecular clusters have attracted considerable interest. This is to a great extent due to the fact that the properties of clusters do not in general vary smoothly between the isolated atom or molecule and the bulk. One of the most striking manifestations of this nonuniform approach to the bulk is the variations in the abundance of clusters with different mass numbers, when produced, e.g., in a supersonic expansion or by sputtering.[1,2]

The abundance spectra show pronounced peaks for clusters composed of metal atoms as well as for nonmetal elements, albeit at different mass values for the two kinds of cluster. Whereas the peaks in the abundance spectra for clusters composed of nonmetal elements can be explained by reference to certain geometrical configurations of the atoms in the cluster, the explanation in the case of metal clusters is related to the quantized motion of the valence electrons within the entire cluster volume.

The "magic numbers" for metal clusters were first observed by Knight *et al.* (for sodium[3]) and by Katakuse *et al.* (for silver[4]) and were shown to be analogous to "magic numbers" for nuclei.[5] For the nuclei these numbers correspond to the numbers of neutrons and protons at which nuclei are particularly stable, and the investigation of stability versus particle number led to an understanding of the shell structure in nuclei.[6] It was realized that the "magic numbers" reflect shell closings arising from the quantization of the motion of delocalized fermions in a mean-field potential of high symmetry.

The mean-field potential of nuclei is observed to be almost constant ($\simeq -50$ MeV) in the interior and to vanish smoothly at the surface of the nuclei. Neglecting the spin-orbit coupling, which is very small in clusters of lighter elements, such a potential produces shell closings at particle numbers $N = 2,8,20,34,40,58,92$. These are precisely the number of electrons in the metal clusters for which the mass spectra exhibit local maxima.

The shell closings were found not only in the abundance spectra but also later for the static polarizability[7] and in the ionization potentials[8] (although the magnitude of the effect for the ionization potential is smaller than anticipated). There is, therefore, very little doubt that an important part of the ground-state energy of (alkali-metal) clusters with a number of atoms $N \lesssim 10^2$ is determined by the motion of the valence (or conduction) electrons and that these can be considered to move in a common mean-field potential similar to the potential experienced by a nucleon in a nucleus.

The discovery of quantal shells in metal clusters establishes illuminating connections between this field of research and the studies of atoms and nuclei which are also dominated by shell structure. In addition the discovery opens completely new possibilities for investigations of shell structure in systems with particle number N sufficiently large so as to reveal the characteristic structure expected in the semiclassical limit. With atoms and nuclei there is a natural upper limit of particle number N. With metal clusters there is no such upper limit. In principle N can be varied from 1 to ∞, so that investigation of changes in properties from atomic levels to bulk metals, characterized by band structure, should be possible. There are indeed current experimental efforts[9] to extend the measurements to large magic numbers.

The shell structure, or the quasiperiodic oscillation of the single-particle level density, tends to die out gradually as N becomes larger. In a spherical potential, however, the decrease in amplitude of the oscillation for a given value of N relative to the monotonous average level density is of the order $N^{-1/6}$ (Ref. 10). It is still 30% in the $N=10^3$ region, and does not exclude the possibility of observing shell effects for clusters up to, at least, this size range.

Balian and Bloch have shown[11] that the single-particle level density for a spherical cavity behaves in a very characteristic way. As a function of energy (or momentum) the level density shows a global long-wavelength oscillating pattern that envelopes short-wavelength periodic oscillations, each corresponding to an ordinary shell. We associate these long-range oscillations with "supershells." Balian and Bloch have clarified the origin of the supershells in a simple and beautiful way through a semiclassical treatment of the single-particle level density. The supershell is the beating pattern of two interfering waves associated in the semiclassical treatment with triangular and square closed orbits inside the cavity. The neighboring shell spacing in momentum is proportional to the inverse of the length of the shortest orbit (triangle), while the supershell spacing is proportional to the inverse of the length difference between the two orbits, which is ~ 11 times the shell spacing.

Despite its beauty Balian and Bloch's work has not received much attention in the 18 years that have elapsed since it appeared. This is because one period of the supershell encompasses a number of single-particle levels of the order of 10^3. As a consequence, this work was often considered to be a purely theoretical exercise of little relevance for the description of realistic quantum systems on the earth or elsewhere in the universe. The discovery of shell structure in metal clusters has brought new attention to their work, since now the supershell has become a phenomenon that can be investigated experimentally as well as theoretically.

The spherical cavity used by Balian and Bloch in order to illustrate the supershell is too simple to allow realistic predictions of the level densities in metal clusters. On the other hand, self-consistent calculations of the mean-field potentials for metal clusters using the spherical and homogeneous jellium model as an approximation to the distribution of the positively charged ions give an almost constant value for the potential inside the cluster and a smoothly and rapidly increasing surface part.[12,13] This leads us to expect that the results obtained with the spherical cavity are not entirely without relevance to metal clusters; we expect supershells to appear also with more realistic potentials.

In this paper we present the results of level-density and binding-energy calculations for electrons in potentials that simulate the self-consistent mean-field potentials derived by Ekardt for Na clusters.[12] The potentials are given in Sec. II. The results given in Secs. III–V show that there are indeed supershells in Na clusters, provided that the mean field is still a valid concept for clusters containing 1000 or more atoms. In these sections we also investigate the level densities semiclassically and prove that Balian and Bloch's interpretation of the supershells in terms of the closed orbits is valid for the metal clusters.

There are, however, several aspects to the cluster structure and their production processes that set limits to the observation of shell structure, and therefore, of the supershells. We shall make qualitative investigations of such finite-temperature effects in Sec. VI.

II. MEAN-FIELD POTENTIALS FOR VALENCE ELECTRONS

The Kohn-Sham density-functional method[14] is one of the most practical and also successful methods for calculating electronic properties of metals. Within the Kohn-Sham framework, the jellium approximation to the positively charged ionic background has given quantitative agreement not only with bulk properties, but also with the measured surface energies of alkali metals (except for lithium).[15] Recently this self-consistent jellium model has been applied to metal clusters, especially to Na clusters.[12,13]

Effective local mean-field potentials for the valence electrons were calculated assuming a spherical distribution of the ionic background with uniform density equal to that of bulk sodium metal. The measured magic numbers were verified by the calculated ionization potentials, displaying maxima at shell closings and thus indicating relatively high stability of clusters with closed shells.[16] Ekardt[12] also calculated the effective mean-field potentials for particle numbers corresponding to a complete filling of each orbit up to $N=198$. The general properties of these potentials are, first, almost uniform depth of the inner part, and second, a universal shape of the smoothly vanishing surface part. There are small deviations from the uniform depth of the inner part, which make the bottom of the potential wavy. These deviations show no systematic behavior except for a small dip near the surface, and become smaller as N increases. We shall assume that their effects on the shell and supershell structures are of minor importance so that they can be neglected.

Ekardt's potentials will here be approximated by a simple three-parameter analytic expression in terms of a spherical Woods-Saxon potential:

$$U(R)=\frac{V_0}{1+\exp[(R-R_0)/a_0]}\ , \tag{2.1}$$

with parameter values

$$\begin{aligned} &V_0=-6.0\ \text{eV}\ ,\\ &R_0=r_0N^{1/3},\quad r_0=2.25\ \text{Å}\ ,\\ &a_0=0.74\ \text{Å}\ . \end{aligned} \tag{2.2}$$

The quantity V_0 is the depth of the potential, R_0 is the radius, and a_0 is the surface thickness, whereas R is the radial coordinate. The potential (2.1) vanishes faster than Ekardt's as R exceeds R_0. Still, the Fermi energy is 3 eV (half of the total depth of the potential) as it should be, and the single-particle wave functions of the occupied states extend only slightly into the region $R>R_0$. Therefore the small difference at $R>R_0$ is not a serious problem for the calculation of the orbits occupied in the ground-state configuration. The value of r_0 in Eq. (2.2) is slightly larger than the Wigner-Seitz radius for bulk sodium (2.08 Å). This is due to the so-called "spill out" resulting from the extension of the electrons into the region outside the positive charge. As N increases r_0 should eventually approach the Wigner-Seitz radius. This slight dependence of r_0 on N is neglected in our calculations, because its effect should be of minor importance for the phenomena considered in the present work.

We also explore another type of potential, which was obtained through a semiclassical approximation[17] applying the Kohn-Sham density-functional method to a positive jellium background. In this approximation the density of the occupied electrons is expressed by a smooth three-parameter profile function which is determined variationally by requiring a minimum energy in the Kohn-Sham procedure. (For details see Ref. 17.) Figure 1 compares this potential (solid curve) with the Woods-Saxon potential (dotted curve) for $N=1000$. The inner part is slightly shallower and the outer part is deeper than the Woods-Saxon potential. A potential of this shape is called a "wine-bottle" potential in nuclear physics, and we will adopt this name in the following.

The "wine-bottle" potential has the advantage of reproducing the shallow minimum of Ekardt's potential in the surface region. On the other hand, the validity of the semiclassical approximation for metal clusters is still to be demonstrated.[18] All in all, it is difficult to know which of the two potentials is more realistic. In the following numerical studies we shall therefore use these two types of potential without any preference of one over the other. In doing so we are able to investigate effects on the shell and supershell structures coming from small differences in the potentials.

III. LEVEL DENSITIES IN THE WOODS-SAXON POTENTIAL

A. Quantum-mechanical calculation

The calculation of the single-particle level energies is performed by solving the radial wave equation numerically from the origin and identifying the solutions where the wave function vanishes smoothly, with the proper asymptotic form, for large distances.[19]

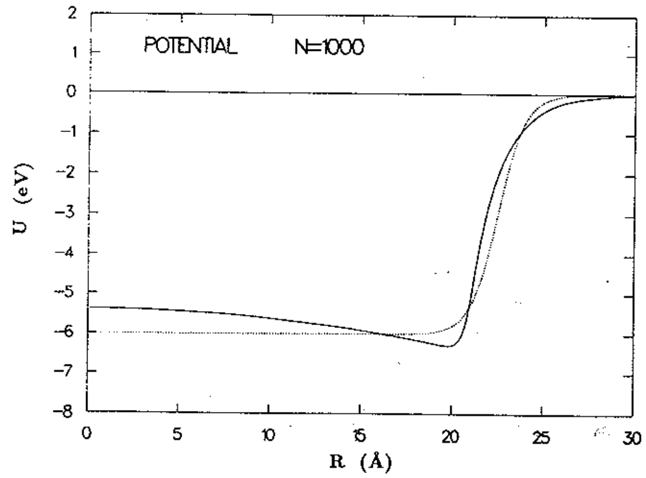

FIG. 1. Comparison of the Woods-Saxon potential (solid curve) and the wine-bottle potential (dotted curve) with $N=1000$.

As in the case of the spherical cavity,[11] we plot the level density as a function of the wave number k rather than of the energy. Then the shell peaks appear approximately equally spaced in k, with the separation $\Delta k=0.5N^{-1/3}$ Å^{-1}.

Since the Woods-Saxon potential has a flat bottom, the wave number k is defined in a natural way as

$$k=\frac{1}{\hbar}[2m(E-V_0)]^{1/2}\,, \qquad (3.1)$$

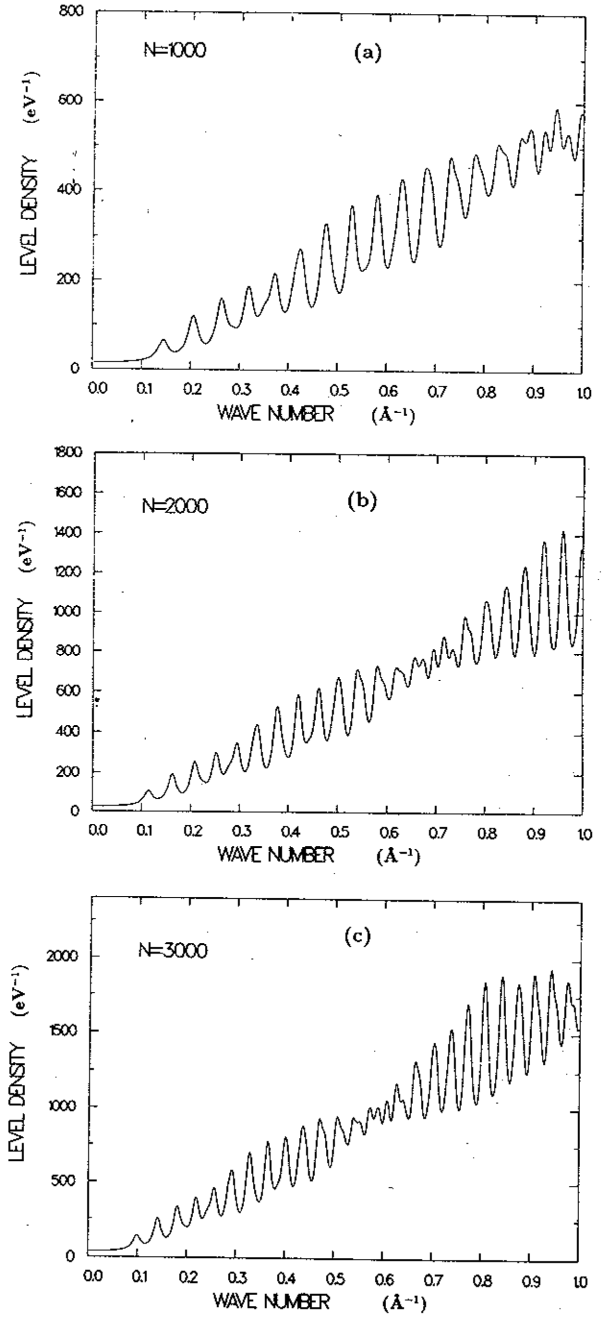

FIG. 2. Single-particle level densities in the Woods-Saxon potential with $N=1000$, 2000, and 3000 for (a), (b), and (c), respectively.

where m is the electron mass and V_0 is the depth of the potential ($V_0 = -6.0$ eV).

For each single-particle binding energy E_{nl} a wave number k_{nl} is defined by Eq. (3.1). In order to visualize the shell and supershell structures clearly, we use the formal method of adding an imaginary part k_i to each k_{nl}. Instead of a sequence of δ functions, the level density is then smeared out and is given by

$$\rho(E)=\frac{2m}{\hbar^2}\sum_{n,l}\frac{2(2l+1)}{\pi}\frac{2k_i k_{nl}}{(k^2-k_{nl}^2)^2+(2k_i k_{nl})^2}\ . \qquad (3.2)$$

The k_i is chosen to be $0.13N^{-1/3}$ Å^{-1}, which is a quarter of the spacing of successive shells.

In experimental situations the smearing width has actual physical significance in terms of a characteristic temperature of the system under investigation. For example, a proper treatment of the effect of shells on the abundance spectra requires the introduction of a width of the order of the temperature. We discuss this temperature effect in Sec. VI. In the present section the width is included merely to visualize the shell and supershell structures.

The calculated level densities $\rho(E)$ are shown in Figs. 2(a), 2(b), and 2(c) for $N=1000$, 2000, and 3000, respectively. The wave number k_f corresponding to the Fermi energy is 0.89 Å^{-1}. In addition to the equidistant shell minima, the supershell structure, which is an envelope of the shell peaks, is clearly seen in these figures. For $N=1000$ the first node of the supershell is located at the Fermi level k_f, and moves down gradually as N increases. For $2000 \lesssim N \lesssim 3000$ there is an antinode at k_f, indicating enhanced shell effects in this mass region.

Level densities at the Fermi energy have direct importance for a number of measurable quantities, and we have calculated $\rho(E_f)$ for each cluster number up to 4800. Figure 3 exhibits the values of $\rho(E_f)$ obtained by smearing the individual levels by 0.08 eV ($\simeq$900 K). The representation in Fig. 3 provides an alternative way of viewing the shells and supershells exhibited in Fig. 2.

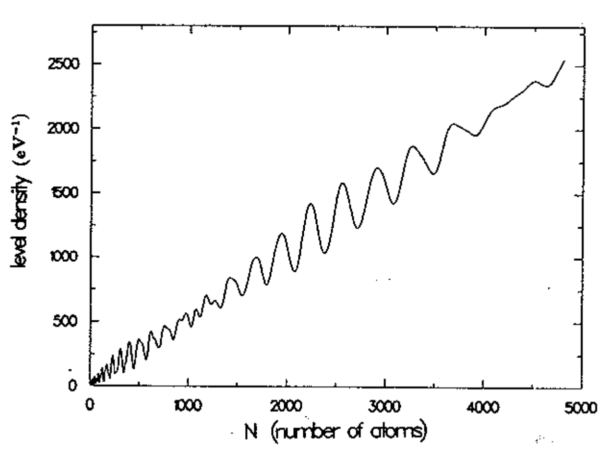

FIG. 3. Single-particle level densities at the Fermi energy in the Woods-Saxon potential. The smearing energy width is 0.08 eV. The Fermi energy is determined for each size N so that the integration of this level density up to the energy is equal to N.

In Sec. III B we shall compare these purely numerical results of the quantum calculations with the semiclassical theory of Balian and Bloch.

B. Semiclassical analysis

Deriving a semiclassical expression for the quantal level density in the spherical cavity in terms of a sum of contributions from different closed classical orbits, Balian and Bloch[11] were able to show that a supershell structure will emerge as a result of interference of amplitudes associated with classical triangular and square orbits. We investigate whether their interpretation of the supershells is also valid in the case of a Woods-Saxon potential.

There are several differences in the semiclassical expression for the level density between the cases of the spherical cavity with an infinitely high wall and of the smooth Woods-Saxon potential.[20] A convenient expression was derived for smooth spherical potentials by Berry and Tabor.[21] For the Woods-Saxon potential their expression reduces to

$$\rho(E)=\rho_{\mathrm{TF}}(E)+\sum_{\mathbf{M}}A_{\mathbf{M}}\cos\left[2\pi\mathbf{M}\cdot\left[\frac{\mathbf{I}_{\mathbf{M}}}{\hbar}-\frac{\alpha_{\mathbf{M}}}{4}\right]+\frac{\pi}{4}\right]\ , \qquad (3.3)$$

where the $\mathbf{M}$ is a vector of two positive (nonzero) integer components, M_l and M_s. Each set of M_l and M_s represents a classical closed orbit with M_l turns in the angular direction and M_s oscillations in the radial direction. The quantity $\mathbf{I}_{\mathbf{M}}$ is a set of two actions of the corresponding invariant torus with the frequency ratio $\omega_l/\omega_s = M_l/M_s$. The $\alpha_{\mathbf{M}}$ denotes the Maslov index associated with the closed orbit $\mathbf{M}$ [see Eq. (3.6)]. The amplitude $A_{\mathbf{M}}$ is positive for all values of M_l and M_s. The first term in Eq. (3.3) is the Thomas-Fermi average level density, which does not contribute to the shell structure.

The action term in the exponential is given as

$$2\pi\mathbf{M}\cdot\mathbf{I}_{\mathbf{M}}=\oint \mathbf{p}(\mathbf{r})\cdot d\mathbf{r}\ , \qquad (3.4)$$

where the $\mathbf{p}(\mathbf{r})$ is the classical momentum of the particle which moves along a closed orbit, and the usual relation $\mathbf{p}=\hbar\mathbf{k}$ with the quantal wave vector is assumed. The magnitude of the momentum is given by

$$|\mathbf{p}(\mathbf{r})|=\{2m[E-U(r)]\}^{1/2}\ . \qquad (3.5)$$

The integration in Eq. (3.4) is over one period of the closed orbit.

Equivalent to the smearing of the level energies, the $|\mathbf{k}(\mathbf{r})|$ is replaced by $|\mathbf{k}(\mathbf{r})|+ik_i$. When included in Eq. (3.3) this imaginary part of the wave number produces a suppression factor $e^{-k_i L_{\mathbf{M}}}$, where $L_{\mathbf{M}}$ is the trajectory length of the corresponding closed orbit.

A typical length of orbits turning around M_l times in the angular direction before they close is $2\pi M_l R_0 = 4.50\pi M_l N^{1/3}$ Å. As already stated, the value of k_i used in the quantum-mechanical calculation shown in Fig. 2 is $0.13N^{-1/3}$ Å^{-1}, and the suppression factor thus becomes $e^{-1.8M_l}$, which is a rapidly decreasing function of M_l. In the level-density calculation at the Fermi

TABLE I. Existing single-turn closed orbits in the Woods-Saxon potential. The calculation was made for $N=100,200,300,\ldots,$ up to 3000. The orbits are denoted by M_s, where the $M_s=2$ corresponds to a straight-line orbit through the center, and the $M_s=\infty$ orbit corresponds to the circle.

Number of atoms	M_s
$N<300$	$2,3,\infty$
$300\le N<800$	$2,3,4,\infty$
$800\le N<2200$	$2,3,4,5,\infty$
$2200\le N$	$2,3,4,5,6,\infty$

level shown in Fig. 3, the suppression factor is similar to the one stated above in the mass region $N\simeq 10^3$. We therefore consider only closed orbits with one turn ($M_l=1$) in the following.

Although all orbits are rounded off in a smooth potential, the single-turn orbits can still be identified by the numbers M_s. As a consequence we shall still denote the $M_s=3$ and 4 orbits by the triangular and square orbits, respectively, in analogy to the spherical cavity case.

Unlike the spherical cavity, there are only a finite number of single-turn orbits in the Woods-Saxon potential. The number increases as $\propto N^{1/6}$. The single-turn orbits near the Fermi energy, where the shell and supershell structures have the largest effects on observables, are listed in Table I for different intervals of N. Among the closed orbits in Table I the pendulating and circular orbits ($M_s=2$ and ∞, respectively) contribute to the level density only to higher order in $\hbar^{1/2}$. They have negligible contributions in the $\hbar\to 0$ limit.

Following Balian and Bloch we view the triangular ($M_s=3$) and square ($M_s=4$) orbits as responsible for the supershell structure in moderate-size clusters $N\lesssim 3000$.

The Maslov index in the smooth potential case is

$$\alpha_{\mathbf{M}}\cdot\mathbf{M}=2M_s+2M_l\ . \tag{3.6}$$

Defining

$$W_{M_s}=\frac{1}{\hbar}\mathbf{M}\cdot\mathbf{I}_{\mathbf{M}},\quad \text{where } \mathbf{M}=(1,M_s)\ , \tag{3.7}$$

the difference of the phase in Eq. (3.3) between the contributions of the triangular and square orbits is

$$\Delta\varphi=2\pi(W_3-W_4)-\pi\ . \tag{3.8}$$

When $\Delta\varphi=2n\pi$ (n is an integer) the two contributions add constructively, and when $\Delta\varphi=(2n+1)\pi$ they add destructively.

The difference $\Delta W=W_3-W_4$ was calculated at the Fermi energy for $100\le N\le 3000$. The result is shown in Fig. 4 where it can be seen that $\Delta W=1.0$ at $N\simeq 900$, indicating destructive interference and therefore a node of the supershell at the Fermi energy. The value of ΔW is 1.5 at $N\simeq 2200$, indicating a constructive sum of the amplitudes. The slope of the ΔW curve is less steep in the region $2000<N\lesssim 3000$, and therefore the antinode of the supershell will persist in a wide range of N. All the results of the semiclassical estimates are paralleled in the quantum-mechanical calculations as shown in Figs. 2 and 3.

For completeness we Fourier transformed the quantum-mechanical spectrum shown in Fig. 2 in order to confirm the dominance of the two closed orbits:

$$f(L)=\left|\sum_{nl}2(2l+1)k_{nl}^{-3/2}e^{ik_{nl}L}\right|\ . \tag{3.9}$$

We included single-particle levels from the lowest energy up to $E_{nl}<-2.5$ eV, slightly higher than the Fermi energy. We also transformed the smeared level density of Eq. (3.2) in order to show the effect of the smearing. For the convenience of display the absolute values are taken.

Figure 5 shows the results for $N=3000$. The solid and dashed curves are with and without the smearing, respectively. In both curves there are two prominent peaks, at lengths $L=171.2$ and 184.1 Å. In the Woods-Saxon potential they cannot be expected to exactly equal the trajectory lengths, but they should be very near to them. The corresponding triangular and square trajectory lengths in a spherical cavity with the radius $r_0N^{1/3}$ Å are 168.6 and 183.6 Å, respectively. The positions of the two peaks are thus very close to the lengths of triangular and

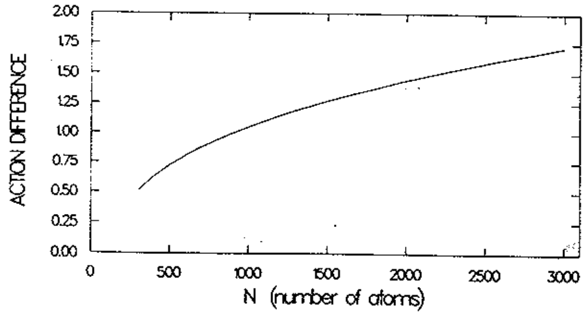

FIG. 4. The action difference ΔW between the triangular and square orbits in the Woods-Saxon potential.

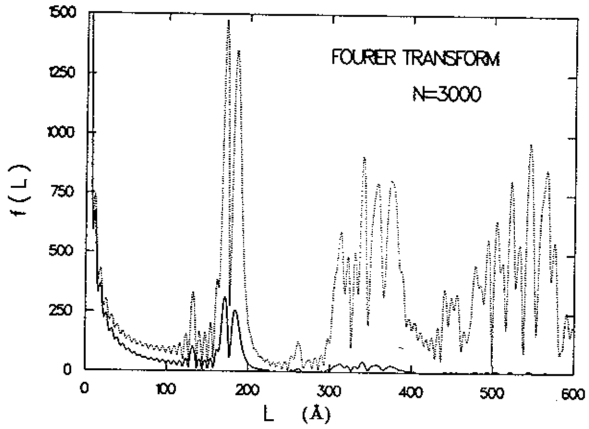

FIG. 5. Absolute values of Fourier components of the level energies in the Woods-Saxon potential with $N=3000$. The solid and dashed curves are with and without the smearing, respectively.

square orbits in the spherical cavity. This confirms that the interference of the two amplitudes associated with the two closed orbits is indeed the source of the supershell structure also for the case of the Woods-Saxon potential.

The difference of the phases of Eq. (3.9) between the two peaks at the Fermi energy is $(1/2\pi)k_{nl}(\Delta L)=(1/2\pi)0.89(184.1-171.2)=1.83$, which agrees within a reasonable accuracy with the semiclassical calculation of the phase difference ΔW, as shown in Fig. 4.

There are other smaller peaks in Fig. 5. They can all be identified with closed orbits. The peaks with larger L contribute to fine structures in the level density and are strongly suppressed in the solid curve for the smeared level density. The small peak at $L \simeq 130$ Å comes from the pendulating orbit.

IV. BINDING ENERGIES

The most direct experimental verification of the calculated electron eigenenergies would be based on spectroscopic experiments. At present such experiments are missing, except for quite small clusters. The mass spectroscopic measurements of cluster abundances, on the other hand, hinge on variations in separation energies of evaporated neutral atoms, and these variations also reflect the electronic shell effects. In the following we therefore calculate the shell oscillation part of the total binding energy of valence electrons in each cluster using the Woods-Saxon potential. We subsequently identify this part with the oscillating contribution to the total binding energy of the metal clusters.[22] The peaks in the abundance spectra correspond to particularly stable clusters, namely, to clusters which have larger binding energies than the clusters with neighboring masses.

We proceed as follows. For each N all single-electron energies E_j of the occupied states in the ground-state configuration are summed up. This sum is then divided into a smooth average part $E_{\rm av}$ and a shell part $E_{\rm shell}$:

$$E(N)=\sum_{j=1}^{N} E_j = E_{\rm av}(N)+E_{\rm shell}(N)\ . \tag{4.1}$$

The $E_{\rm av}$ is parametrized as consisting of a volume term ($\propto N$) plus a surface term ($\propto N^{2/3}$). The coefficients are obtained through a χ^2 fit to all $E(N)$ between 1 and 4800 leading to the result $E_{\rm av}=-4.34N+2.96N^{2/3}$ eV. When this is subtracted from the energy sum (4.1), the resulting $E_{\rm shell}$ is obtained as shown in Fig. 6. We note that the abscissa is not N itself but $N^{1/3}$. With this choice of scale the oscillations are equally spaced. The number of

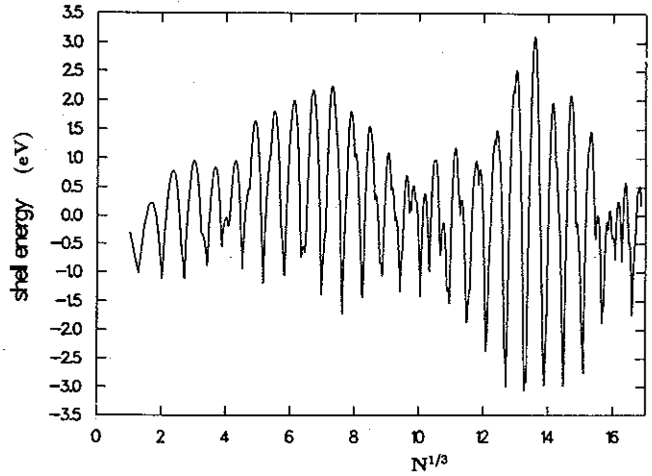

FIG. 6. The shell part of the total electronic binding energies of clusters as a function of $N^{1/3}$.

TABLE II. Minimum points of the shell energy as a function of the electron number. The pairs included in parentheses denote double minima which are close to each other.

Electron number N	$N^{1/3}$	Shell energy (eV)	Electron number N	$N^{1/3}$	Shell energy (eV)
2	1.26	−1.02	832	9.41	−1.35
8	2.00	−1.11	1012	10.04	−1.43
20	2.71	−1.12	1100	10.32	−1.00
40	3.42	−0.90	1216	10.67	−0.70
⎡58	3.87	−0.56⎤	1314	10.95	−1.54
⎣68	4.08	−0.19⎦	1516	11.49	−1.87
92	4.51	−0.94	1760	12.07	−2.38
138	5.17	−1.19	2048	12.70	−3.00
198	5.83	−1.07	⎡2334	13.26	−3.08⎤
⎡254	6.33	−0.74⎤	⎣2368	13.33	−2.92⎦
⎣268	6.45	−0.67⎦	2672	13.88	−2.99
338	6.97	−1.40	3028	14.47	−2.99
440	7.61	−1.74	3438	15.09	−2.77
562	8.25	−1.44	3848	15.67	−1.87
694	8.85	−1.07	4154	16.08	−0.78

different mass numbers included in one oscillation increases proportionally to $N^{2/3}$.

The minimum points in Fig. 6 represent the most stable spherical clusters, which are tabulated in Table II. The predicted stable clusters from 2 up to 138 were all observed in the measured abundance spectra. The magnitude of the E_{shell} is related to the quantity $\hbar\omega_{\text{sh}}\Omega$, where $\hbar\omega_{\text{sh}}$ is the energy distance between neighboring shells in the Fermi-energy region, and Ω is the effective number of degenerate levels in a shell.[10] In a spherical potential $\hbar\omega_{\text{sh}} \propto N^{-1/3}$ and $\Omega \propto N^{1/2}$. Therefore the magnitude of E_{shell} should increase as $N^{1/6}$. This roughly agrees with the overall tendency seen in Fig. 6.

There is however a very strong deviation from this overall dependence of $N^{1/6}$. It is due to the supershell structure. The envelope of E_{shell} has minima at $N \simeq 1000$ and 4000, maxima at $N \simeq 500$ and 2500. These mass numbers of diminished or enhanced E_{shell} exactly coincide with those at which the supershell structure in the level density has a node and an antinode, respectively, at the Fermi level. When E_{shell} is suppressed we do not expect to detect enhanced peaks in the abundance mass spectrum, and when E_{shell} is enhanced we do expect enhanced peaks. In this way the supershell structure is expected to reflect itself in experiment.

V. LEVEL DENSITIES IN THE "WINE-BOTTLE" POTENTIAL

The quantum-mechanical calculations of the level densities have also been made for a "wine-bottle" potential. As shown in Fig. 1, the potential is not entirely flat inside the surface, and the definition of the corresponding wave number by Eq. (3.1) is therefore not quite unambiguous. In order to compare with the case of the Woods-Saxon potential, we nevertheless use Eq. (3.1); with the value of V_0 chosen to be -5.95 eV. The magnitude of the imaginary momentum k_i is the same as before ($0.13N^{-1/3}$ Å^{-1}).

The results are shown in Figs. 7(a), 7(b), and 7(c) for $N=1000$, 2000, and 3000, respectively. At $N=1000$ the shell structure is enhanced compared to the Woods-Saxon case. At the Fermi level ($k_f=0.89$ Å^{-1}) there is an antinode of the supershell structure. At the $N=2000$ the shell structure is suppressed all over. There seems to be a node of the supershell structure near $k=0.6$–0.7 Å^{-1}, but it is not so clear as in the Woods-Saxon case. At $N=3000$ the supershell structure is clearly seen with a node at $k \simeq 0.75$ Å^{-1}.

We examine these variations of the level densities semiclassically. The semiclassical expression (3.3) is still valid provided that the eigenenergy is higher than the central ($R=0$) point of the potential ($\simeq -5.4$ eV). In the following we focus on the Fermi-energy region ($=-3.0$ eV).

The number of single-turn classical closed orbits is larger than in the Woods-Saxon case, as shown in Table III. This will make the interference of amplitudes associated with closed orbits more complicated. We therefore take into account three orbits ($M_s=3,4,5$) instead of two. The action W_{M_s} is defined by Eq. (3.7), and the

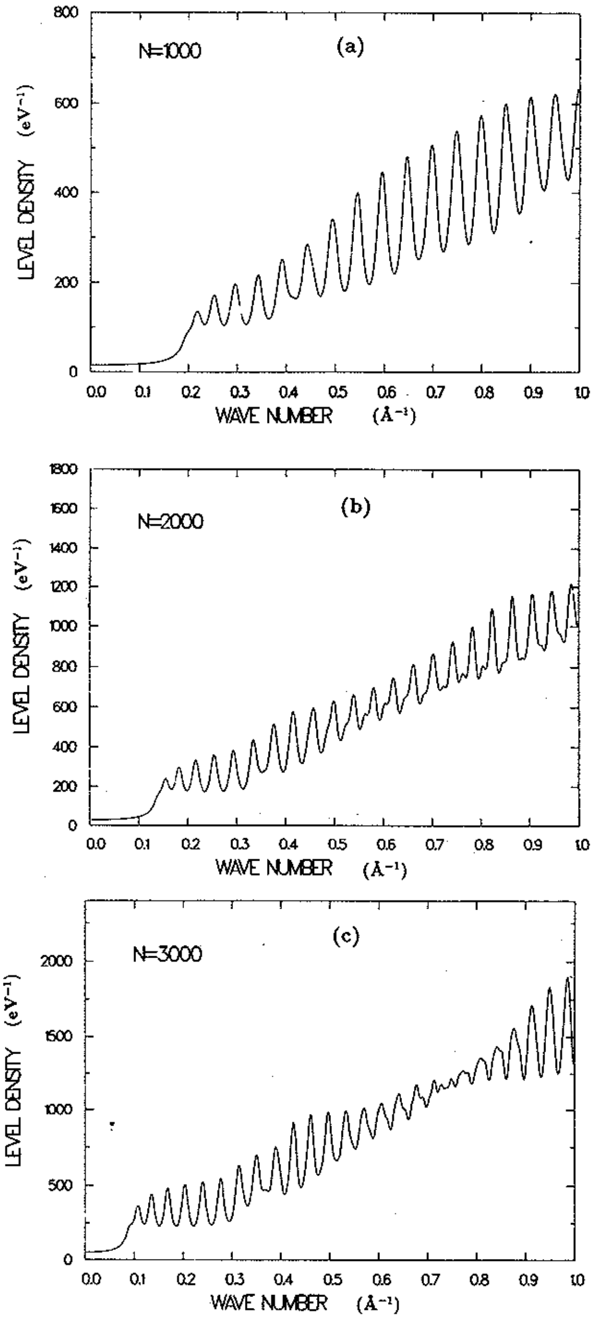

FIG. 7. Single-particle level densities in the wine-bottle potential with $N=1000$, 2000, and 3000 for (a), (b), and (c), respectively.

TABLE III. Existing single-turn closed orbits in the wine-bottle potential. See caption of Table I.

Number of atoms	M_s
$N<200$	2,3,4,5,∞
$200 \le N < 300$	2,3,4,5,6,∞
$300 \le N < 600$	2,3,4,5,6,7,∞
$600 \le N < 900$	2,3,4,5,6,7,8,∞
$900 \le N < 1500$	2,3,4,5,6,7,8,9,∞
$1500 \le N < 2500$	2,3,4,5,6,7,8,9,10,∞
$2500 \le N$	2,3,4,5,6,7,8,9,10,11,∞

presence of static deformations particle orbits that were degenerate at $\beta=0$ are spread out over an energy interval of order

$$\Delta E \sim (\Delta\beta)E_f \sim \left[\frac{TE_f}{N}\right]^{1/2} . \tag{6.8}$$

The effect of the energy shifts (6.8) will be more important in smearing out the shell structure than the thermal damping effects discussed above if

$$\Delta E > T , \tag{6.9}$$

which gives a crossover at

$$N^* \sim \frac{E_f}{T} . \tag{6.10}$$

It appears that most studies of metal clusters carried out so far have involved temperatures of order a few hundred K and thus the crossover in these experiments would be at $N^* \sim 10^2$.

VII. SUMMARY

We have investigated shell and supershell structures in Na clusters. We assume a mean field for the valence electrons and simulate the mean field by two types of potentials (Woods-Saxon and wine-bottle potentials). In the Woods-Saxon potential the supershell structure is clearly recognized in the calculated level density of each cluster. Semiclassical consideration supports the interpretation of the supershell structure as coming from interference of amplitudes associated with triangular and square orbits. The shell part of the total binding energy for each cluster is also calculated as a function of the atom number N. The supershell structure is clearly reflected in the binding energy.

For the wine-bottle potential the supershell structure is also recognized in the level densities. But the nodes of the supershells appear at different wave numbers compared to the Woods-Saxon case. Moreover, the supershell pattern is not always a simple beating pattern of two waves. The reason for this complexity was investigated semiclassically, and it was found that other classical orbits (especially the pentagon orbit) have non-negligible contributions to the level densities in addition to the two most important orbits.

Although the Woods-Saxon and the wine-bottle potentials are similar to each other in shape, they produce level densities which contain different supershell structures. This means that the supershells are very sensitive to the details of the potential shape. The exact shell closings (magic numbers) are also sensitive to the potential shape.

We have also briefly considered thermal effects which tend to smooth out the shell-structure phenomenon. At the present time it does not appear that these effects will obscure the consequences of shell structure for cluster sizes up to several thousand atoms. There is an interesting crossover in the dominant mechanism for damping of single particle motion that is expected to occur for cluster sizes of order 100 atoms.

ACKNOWLEDGMENTS

We would like to express our sincere thanks to Sven Bjørnholm for stimulating discussions and encouragement through this work and also for reading through the manuscript and giving us useful comments and suggestions. We are grateful to Thomas Døssing, Matthias Brack, and Michael Hansen for discussions and assistance in computation. This work was supported by the Danish National Science Foundation.

---

[1] Proceedings of the Fourth International Meeting on Small Particles and Inorganic Clusters, Aix-en-Provence, 1988 [Z. Phys. D **12** (1989)].

[2] W. A. de Heer, W. D. Knight, M. Y. Chou, and M. L. Cohen, in *Solid State Physics*, edited by H. Ehrenreich, F. Seitz, and D. Turnbull (Academic, New York, 1987), Vol. 40, p. 93.

[3] W. D. Knight, W. A. de Heer, W. A. Saunders, M. Y. Chou, and M. L. Cohen, Phys. Rev. Lett. **52**, 2141 (1984).

[4] I. Katakuse, T. Ichihara, Y. Fujita, T. Matsuo, T. Sakurai, and H. Matsuda, Int. J. Mass Spectrom. Ion Phys. **67**, 229 (1985).

[5] Independently W. Ekardt had predicted the magic numbers theoretically by calculating the ionization potential and the mean binding energy per electron in Ref. 12.

[6] M. G. Mayer and J. H. D. Jensen, *Elementary Theory of Nuclear Shell Structure* (Wiley, New York, 1955).

[7] W. D. Knight, K. Clemenger, W. A. de Heer, and W. A. Saunders, Phys. Rev. B **31**, 2539 (1985).

[8] W. A. Saunders, K. Clemenger, W. A. de Heer, and W. D. Knight, Phys. Rev. B **32**, 1366 (1985).

[9] T. P. Martin (private communication); S. Bjørnholm (private communication).

[10] A. Bohr and B. R. Mottelson, *Nuclear Structure II* (Benjamin, New York, 1975), p. 578.

[11] R. Balian and C. Bloch, Ann. Phys. (N.Y.) **69**, 76 (1971).

[12] W. Ekardt, Phys. Rev. B **29**, 1558 (1984).

[13] D. E. Beck, Solid State Commun. **49**, (1984) 381.

[14] W. Kohn and L. J. Sham, Phys. Rev. **140**, A1133 (1965).

[15] N. D. Lang and W. Kohn, Phys. Rev. B **3**, 1215 (1971).

[16] W. Ekardt, Surf. Sci. **152**, 180 (1985).

[17] M. Brack, C. Guet, and H. Håkansson, Phys. Rep. **123**, 275 (1985); M. Brack, Phys. Rev. B **39**, 3533 (1989).

[18] This semiclassical approximation was tested for nuclei in Ref. 17 and was found to be valid for bulk properties of nuclei.

[19] Three parameters determine the numerical precision of the eigenvalues; the step size, the cutoff length, and the maximum accepted difference between the logarithmic derivative of the wave functions calculated outwards from $R=0$ and inwards from $R=R_{\max}$. With increments in N of 100 all three parameters were varied in order to check the convergence as well as the orthogonality of the wave functions. The values 0.05 Å and R_0+12 Å for the two lengths, and 10^{-6} for the third parameter gave precision of better than 10^{-3} eV.

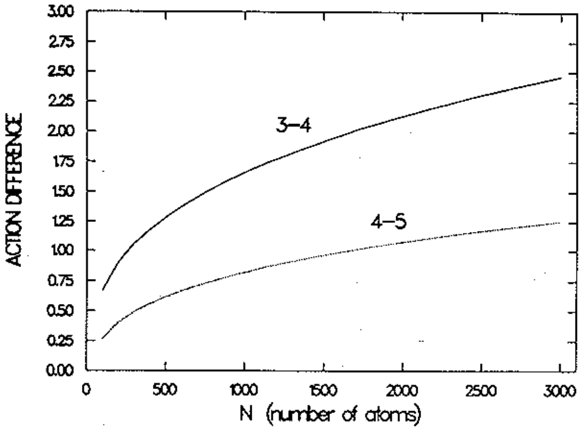

FIG. 8. The action differences in the wine-bottle potential; ΔW_{34} between the triangular and square orbits (upper solid curve), and ΔW_{45} between the square and pentagon orbits (lower dotted curve).

differences are defined as $\Delta W_{34}=W_3-W_4$ and $\Delta W_{45}=W_4-W_5$. As explained in Sec. III, when ΔW is an integer the interference is destructive, when ΔW is a half-integer it is constructive.

The action differences are shown in Fig. 8. The upper curve is for ΔW_{34}. It should have the dominant effect on the supershells. The quantity ΔW_{34} is 1.5 at $N\simeq 800$ and 2.5 at $N\simeq 3100$, at which mass numbers the interference is thus expected to be constructive. This prediction agrees with the quantum-mechanical results. [cf. Figs. 7(a) and 7(c)]. The value of ΔW_{34} is, on the other hand, 2.0 at $N\simeq 1600$ suggesting destructive interference. The lower curve in Fig. 8 shows ΔW_{45}, which also becomes 1.0 at $N\simeq 1600$. Since the curve of ΔW_{45} is very flat, the destructive interference of the square and pentagon orbits extends into the region $1000\lesssim N\lesssim 2500$. At $N\simeq 1600$ both of the interferences of the $M_s=3$ and 4 orbits and $M_s=4$ and 5 orbits are destructive, but this also means that the interference of the $M_s=3$ and 5 orbits is constructive. This complicated situation may be responsible for the obscuration of the supershell structure at $N=2000$ [cf. Fig. 7(b)].

VI. EFFECT OF FINITE TEMPERATURE ON SHELL STRUCTURE

In the molecular beam investigations of metal clusters it appears that the clusters are being studied at temperatures in the range of order 100 to 1000 K. In this range there are a number of different effects that will attenuate the energetic consequences of electronic shell structure. We shall in the following briefly consider (a) the thermal distribution of occupation probabilities for the electronic levels, (b) the scattering of electrons on the fluctuations of the positive ions, and (c) the effect of the thermal distribution of cluster shapes on the spectrum of electronic eigenvalues.

(a) The diffuseness of the Fermi distribution at $T\neq 0$ implies an evening out of the shell structure effect of electronic binding energies. This effect has been extensively discussed in connection with the studies of shell structure in excited nuclei (see, for example, Ref. 10, p. 607). The shell structure is associated with a "bunching" of electronic eigenvalues on an energy scale of order[23] $\hbar\omega_{\rm sh}\sim E_f/N^{1/3}$ (see Fig. 2). Thus, at temperature T the shell effect will be significantly reduced for cluster sizes exceeding

$$N^*\sim\left[\frac{E_f}{T}\right]^3 . \tag{6.1}$$

(b) A simple estimate of the electronic scattering on the fluctuations in the distribution of the positive ions can be based on the observed electrical resistivity ρ of the bulk metal. From the Drude formula we obtain the scattering lifetime

$$\tau=\frac{m}{e^2n\rho} , \tag{6.2}$$

where m, e, and n are the mass, charge, and number density, respectively, for the electrons. Since the high-temperature resistivity of the metal (in both the liquid and solid forms) varies approximately linearly with the temperature the smoothing of shell structure due to scattering has a similar temperature dependence as that resulting from the distribution of occupation probabilities. Taking, for example, the observed high-temperature resistivity[24] of Na we have

$$\rho\simeq 3.0\times 10^{-8}T\ \Omega\,{\rm cm} , \tag{6.3}$$

which implies a damping width Γ_ρ for each electronic level

$$\Gamma_\rho=\frac{\hbar}{\tau}\simeq 1.5T . \tag{6.4}$$

Thus the scattering of the electrons on the positive ions implies smoothing out of the electronic shell structure effects and limitation on cluster size that is numerically very close to the values (6.1) resulting from the distribution of occupation probabilities.

(c) For small clusters and low temperatures it is necessary to consider the effect on the shell structure resulting from the thermal fluctuations in the shape of the clusters. For small amplitude deviations from spherical shape we can expand the total energy of the electronic system in a power series in deformation parameters β,

$$V=\tfrac{1}{2}C\beta^2 , \tag{6.5}$$

with

$$C\sim NE_f \tag{6.6}$$

for configurations in the neighborhood of closed shells.[25] Thus at finite temperature we expect fluctuations in β of order

$$\Delta\beta\sim\left[\frac{T}{C}\right]^{1/2} . \tag{6.7}$$

These fluctuations are essentially static as compared with the characteristic periods in the electronic motion. In the

[20] The semiclassical formulation of the level density in general form of potentials was first given by M. C. Gutzwiller in J. Math. Phys. **8**, 1979 (1967); **10**, 1004 (1969); **11**, 1791 (1970); **12**, 343 (1971).

[21] M. V. Berry and M. Tabor, Proc. R. Soc. London Ser. A **356**, 375 (1977).

[22] V. M. Strutinsky, Nucl. Phys. A **95**, 420 (1967).

[23] It should be emphasized that the characteristic energy spacing of the shells is much greater than the spacing E_f/N of the individual quantum levels. The recognition of important thermodynamic effects resulting from the discreteness of electronic levels on the latter energy scale was an early example of a "quantum size effect" in metal clusters (R. Kubo, J. Phys. Soc. Jpn. **17**, 975 (1962); L. P. Gor'kov and G. M. Eliashberg, Zh. Eksp. Teor. Fiz. **48**, 1407 (1965) [Sov. Phys.—JETP **21**, 940 (1965)]). But the experimental identification of these effects has proven illusive [W. P. Halperin, Rev. Mod. Phys. **58**, 533 (1986)].

[24] *Metals Reference Book,* 5th ed., edited by C. Smithells (Butterworths, London, 1976), p. 949.

[25] The estimate (6.7) assumes that the deformations are so small that the energy shifts (6.8) due to these deformations are small compared with the energy spacings of the shells, $\hbar\omega_{\mathrm{sh}} \simeq E_f N^{-1/3}$, which demands, for closed-shell configurations, $T \ll E_f N^{1/3}$, a condition that will always be well satisfied.

[B]

Mean-Field Quantization of Several Hundred Electrons in Sodium Metal Clusters

S. Bjørnholm, J. Borggreen, O. Echt,[a] K. Hansen, J. Pedersen, and H. D. Rasmussen
The Niels Bohr Institute, University of Copenhagen, DK-2100 Copenhagen Ø, Denmark

(Received 22 June 1990)

Measurements of the mass-abundance spectra of sodium clusters from supersonic expansions are presented. The spectra show evidence of a regular spherical shell structure with magic numbers N_0 scaling approximately with the cube root of the number of sodium atoms N, and hence the number of delocalized (valence) electrons in the cluster. Altogether twelve shell closings are observed, adding to the previously known shell closings, $N_0=2$, 8, 20, 40, 58, 92, and 138, the 8–12th magic numbers $N_0=196$, 260, 344, 440, and 558. The implications of shell structure in such large systems are discussed.

PACS numbers: 71.25.Lf, 03.65.−w, 35.20.Wg, 36.40.+d

The discovery by Knight *et al.* in 1984 of quantal shell structure in small droplets of sodium metal, with characteristic magic numbers, has opened new perspectives in the study of shell structure in many-fermion systems.[1] Previously these were confined to atoms and atomic nuclei. The perspective is widened by subsequent discoveries of similar shell structures in clusters of potassium,[2] cesium,[3] copper, silver, gold,[4] and other simple metals.

In a parallel development, mean-field theories[5–7] based on methods borrowed from the description of simple metals in bulk form (jellium model) have led to a picture of the binding field of the valence electrons much like the nuclear mean field,[8] except that the nuclear spin-orbit interaction is missing. Thus, the simple picture of conduction electrons moving freely and independently inside a metal, bounded only by the surface, seems to be valid down to the smallest sizes comprising less than one hundred atoms.

This Letter addresses the question of the extension of shell structure to larger sizes. Our approach is experimental. It gives substance to a recent theoretical study[9] of the same problem.

The extension to sizes exceeding one hundred particles is interesting for several reasons. Viewing metal clusters as samples of bulk matter in embryonic form,[10] the shell structure reflects a very special situation where the electron quantization is governed by the geometry of the surface, as opposed to the more normal situation, where it is the lattice that determines the bulk electron wave functions. It would be interesting to know the transition point between these two regimes. Shell structure in systems larger than atoms and nuclei is furthermore interesting because it offers an opportunity to pursue this phenomenon towards the limit of very large single-particle action quantum numbers, where one should be able to establish a correspondence between classical and quantal motion. Here, closed classical orbits of triangular and square shapes are expected to play a special role.

This subject is pursued in the theoretical study by Nishioka, Hansen, and Mottelson.[9] It applies and extends ideas originally developed by Balian and Bloch,[11] and further by Bohr and Mottelson,[12] to the concrete case of electrons moving in a spherical Woods-Saxon potential with parameters appropriate to metallic sodium. In particular, the volume of the binding field is proportional to the number of constituents N in the cluster. Adding the single-particle energy eigenvalues of this potential leads to a sum $E(N)$, where the main trend is a (negative) volume term, proportional to the number of electrons N, and a (positive) surface term, proportional to $N^{2/3}$. Superimposed on this is an oscillating term, $E_{\text{shell}}(N)$. This quantity[9] is presented in Fig. 1, where it is plotted as a function of the linear dimensions of the cluster, i.e., $\sim N^{1/3}$. The downward cusps represent shell closings, occurring at magic numbers. Our experimental results corroborate the mean-field, independent-particle assumptions and substantiate a prominent feature of this calculation, namely, the approximately equidistant spacing of shells, when expressed in terms of the linear dimensions.

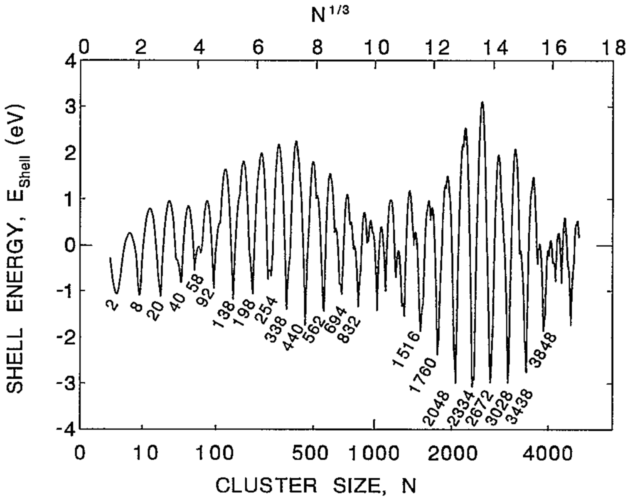

FIG. 1. The periodically varying contribution from valence electrons to the binding energy of a spherical sodium cluster. Magic numbers are indicated. Based on Ref. 9.

The experiments were performed with beams of free flying clusters produced by adiabatic expansion from a hot oven into vacuum. In the oven, argon or krypton gas at stagnation pressures of $(4-8)\times10^5$ Pa is seeded with saturated sodium vapor at 700–800 °C, i.e., partial sodium pressures of $(1-4)\times10^4$ Pa. The diameter of the cylindrical expansion nozzle is 0.07 mm and its length about 0.15 mm. With the aid of skimmers and a differential pumping stage, the sodium cluster beam is introduced into a 3-m-long flight line. Ionization of the clusters is achieved by crossing the beam with a 2-mm-diam ray of ultraviolet light from a 1-kW xenon lamp. The photon energy is centered at 3.9 eV, with a bandwidth (FWHM) of 1.0 eV. This ensures an ionization probability that varies smoothly with size, and at the same time negligible heating of the ionized species.[13] After ionization the clusters are analyzed by time-of-flight mass spectrometry to obtain the abundance variations as a function of size N. The flight time prior to analysis is typically 1 ms. The time-of-flight spectrometer consists of a 5–10-kV acceleration stage, deflection plates that sweep the ionized dc beam across a narrow slit at about 3 kHz picking out narrow bunches with a well-defined starting time for the flight-time measurement, a reflectron to compensate for small velocity variations, and a channeltron ion detector. The arrival times are recorded with a multihit time-to-digital converter and passed to a computer that records the mass spectrum. The mass resolution is typically $\Delta M/M=1200$. After background subtraction each mass peak is integrated to give the total mass abundance I_N.

The top panels in Fig. 2 show the measured abundance distributions I_N. On the left-hand side are results obtained with argon carrier gas; to the right, results with krypton gas. In both cases, the spectra have a bell-shaped envelope modulated by a sawtoothlike fine structure. The envelopes reflect the global kinetics of cluster growth during the high-pressure phases of the expansion, while the fine structure is interpreted[1,14] as being due to shell structure (Fig. 1). We believe that the cluster condensation processes are likely to produce large clusters at near boiling temperatures, and that the sawtooth struc-

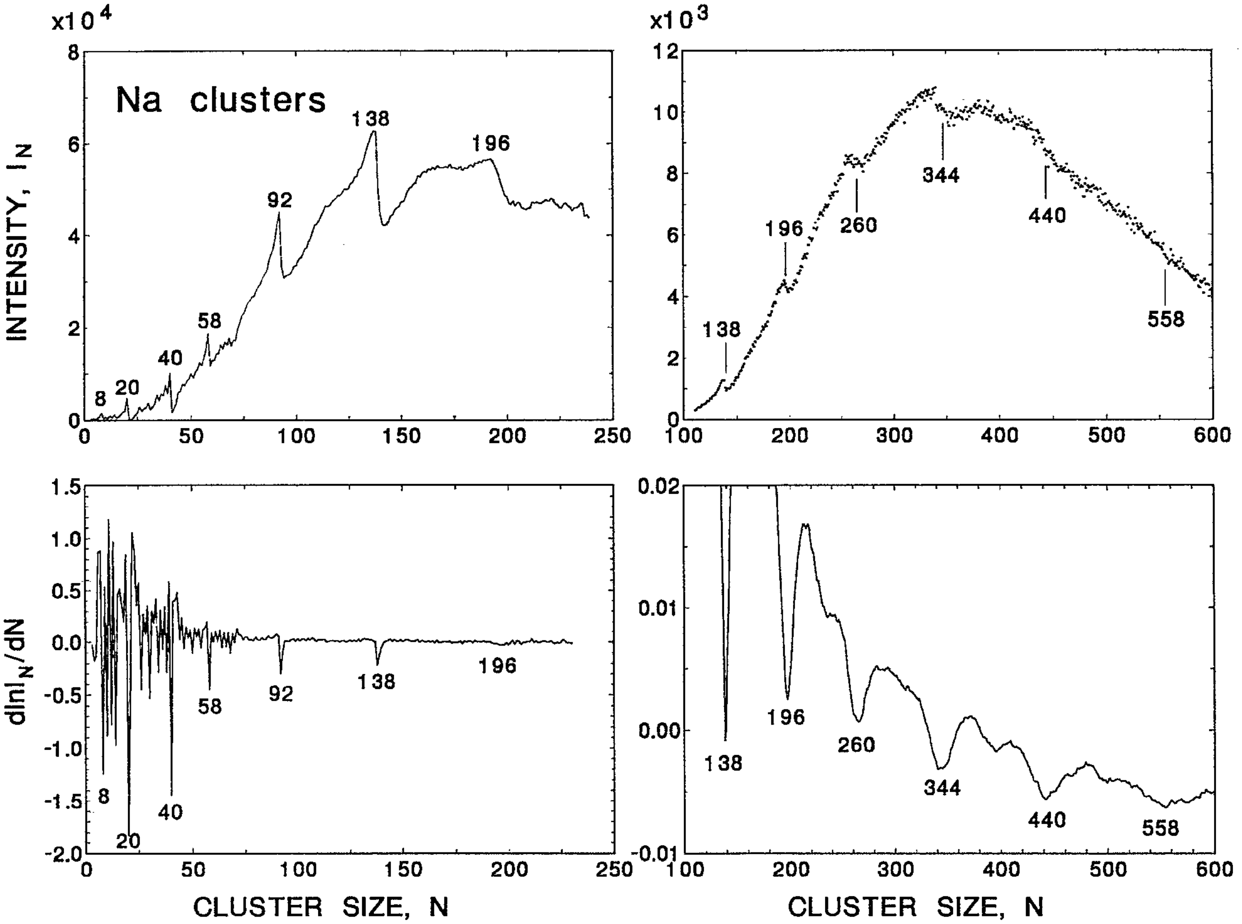

FIG. 2. Top panels: Abundance distributions for sodium clusters produced by adiabatic expansion and measured by time-of-flight mass spectrometry. Bottom panels: Logarithmic derivative of results in top panels. Bottom left, Eq. (1); bottom right, Eq. (2).

tures emerge as a result of subsequent evaporation and cooling in flight from isolated clusters.[15] A given cooling time defines a definite temperature.[15,16] In our case, 1 ms, it is estimated to be 300–400 K.

The sawtooth steps become gradually more rounded as one proceeds towards higher magic numbers (see, e.g., the step near $N=196$). With an increasing number of shells, confined to an energy interval about equal to the Fermi energy —3.24 eV for Na—the gaps at the closed shells will diminish. At finite temperatures electrons can be excited across the gaps, and this tends to smear out the shell structure. Quantitative interpretations of the abundance spectra will require consideration of the thermodynamics of the electronic degrees of freedom, in addition to the ionic degrees of freedom, in estimating the free energies of monomer evaporation. Work along this line is in progress.[17]

The local features of the abundance spectra can be displayed more clearly by taking the logarithmic derivative of the I_N values:

$$d\ln I_N/dN = 2(I_{N+1}-I_N)/(I_{N+1}+I_N)\,. \tag{1}$$

The lower-left panel in Fig. 2 is a plot of this quantity. It eliminates the influence of the global shape. On the other hand, the above-mentioned smearing at higher shells tends to reduce the value of the logarithmic derivative strongly. This is compounded by the general decrease in relative magnitude of the sawtooth steps with increasing N. As a result, statistical uncertainties begin to obscure the shell effects. In the lower-right-hand panel we have plotted a generalized logarithmic derivative,

$$\left(\frac{d\ln I_N}{dN}\right)_W = \frac{\sum_{k=0}^{\infty}[2(I_{N+1+k}-I_{N-k})/(I_{N+1+k}+I_{N-k})]\exp(-k^2/W^2)}{\sum_{k=0}^{\infty}(2k+1)\exp(-k^2/W^2)}\,, \tag{2}$$

with $W=6$ for size 100 increasing linearly to $W=36$ for size 600. Averaging over mass intervals W comparable to the smearing makes the shell dips stand out clearly again. The magic numbers determined experimentally in this way are indicated in Fig. 2 and in Table I. By comparison with Fig. 1 it is readily seen that the experimental shells also scale with the cube root of the cluster size, i.e., with the linear dimensions.

Any *spherical* binding field will have $2(2l+1)$ degenerate levels for each eigenvalue of l. The average spacing of these subshells scales with $N^{2/3}$. The $N^{1/3}$ periodicity, on the other hand, involves a bunching of several subshells with different l values. The precise values of the magic numbers will depend on the detailed shape of the radial potential. In Table I we compare experimentally determined shell closing with theoretical model predictions. The comparison shows that both experimentally and theoretically the positions of shell closings may vary from case to case, but the general $N^{1/3}$ scaling prevails.

This $N^{1/3}$ periodicity is characteristic of a constant-

TABLE I. Magic numbers describing spherical shell closures in metal clusters. LDA denotes local-density approximation.

	Experiment				Theory (Na)	
Shell n	Ag [a]	Au [a]	Cs [b]	Na [c]	Woods-Saxon [d]	Jellium LDA [e]
0	2	2	2	2	2	2
1	8	8	8	8	8	8
2	20	20	18/20	20	20	18/20
3	40	34	34/40	40	40	34/40
4	58	58	58	58	58	58
5	92	···	92	92	92	92
6	138	···	138	138	138	138
7	(198)	···	198 ± 2	196	198	186/196
8			263 ± 5	260 ± 4	254/268	254
9			341 ± 5	344 ± 4	338	338
10			443 ± 5	440 ± 2	440	440
11			557 ± 5	558 ± 8	562	556
12			700 ± 15		694	676
13			840 ± 15		832	832
14			1040 ± 15		1012	

[a] Reference 4.
[b] References 3 and 18 and T. P. Martin (private communication).
[c] This work.
[d] Reference 9.
[e] Reference 17.

density, weak-field medium confined by a more or less steeply rising spherical surface potential,[9] but it is not unique. A classical packing model can also give rise to closed, shell-like configurations with magic numbers that scale with $N^{1/3}$, as shown, for example, by Miehle *et al.* with Xe clusters.[19] The quantal origin of the presently observed shells, Fig. 2, is first of all suggested by the close agreement with the calculations in Fig. 1. In addition, the following simple considerations support a quantal interpretation. If the sodium droplets all have the same density, their radii are equal to $R = r_{\text{WS}} N^{1/3}$, where r_{WS} is the Wigner-Seitz radius.[20] Inserting the six highest magic numbers N_0 from Fig. 2 shows that there is an increment in radius of $\Delta R = (0.61 \pm 0.02) r_{\text{WS}}$ each time a new shell is added. Such a small increment is hardly compatible with a packing model, where each shell represents an atomic layer. Instead one may compare the Fermi wavelength of electrons in simple metals, $\lambda_F = (32\pi^2/9)^{1/3} r_{\text{WS}} = 3.28 r_{\text{WS}}$, with the increment in the length ΔL of a peripheral circular orbit, $2\pi\Delta R = (3.83 \pm 0.12) r_{\text{WR}}$. This agreement already supports a quantal origin of the observed shell structure. As a further step one may compare[9] with a triangular orbit, $\Delta L = 3\sqrt{3}\Delta R = (3.17 \pm 0.10) r_{\text{WS}}$, or with a square orbit $\Delta L = 4\sqrt{2}\Delta R = (3.45 \pm 0.01) r_{\text{WS}}$. The two values bracket the Fermi wavelength. In semiclassical terms[9] one may thus visualize a shell in terms of the increase in surface radius required to give room for an extra node in stationary waves of approximately triangular or square shapes.

Summarizing, we have shown experimentally that the mean-field, independent-particle model used to describe atoms and nuclei can be extended to sodium metal clusters containing many hundreds of conduction electrons. Each spherical shell comprises several l values, and a new shell closing appears whenever the radius of the cluster has been incremented by a characteristic length, equal to about 0.6 times the Wigner-Seitz radius.

There is no reason to believe that the present experiments with up to 600 electrons in a cluster have reached an upper limit for the occurrence of quantal shell structure. The perspective of extending experiments to clusters with several thousand electrons appears to be open.[21] One interesting possibility is the study of large-scale modulations of the shell structure (supershells[9]) as shown in Fig. 1.

Special thanks are due to W. D. Knight for guiding the authors into the field of experimental cluster research during a sabattical stay at the Niels Bohr Institute. Theoretical discussions with M. Brack, B. R. Mottelson, and H. Nishioka are gratefully acknowledged. We also thank D. Radford for developing our peak fitting program. This work has been supported by The Carlsberg Foundation, The Danish Research Academy, The Danish National Science Research Council, Julie Damm's Fund, Novo's Fund, SARC Fund, and Thomas B. Thriges Fund. The authors are grateful to W. A. de Heer and W. D. Knight for detailed advice on the construction of the cluster machine.

---

[a] Present address: Physics Department, University of New Hampshire, Durham, NH 03834.

[1] W. D. Knight, K. Clemenger, W. A. de Heer, W. A. Saunders, M. Y. Chou, and M. L. Cohen, Phys. Rev. Lett. **52**, 2141 (1984).

[2] K. Clemenger, Ph.D. thesis, University of California, Berkeley, 1985 (unpublished).

[3] T. Bergmann and T. P. Martin, J. Chem. Phys. **90**, 2848 (1989).

[4] I. Katakuse, T. Ichihara, Y. Fujita, T. Matsuo, T. Sakurai, and H. Matsuda, Int. J. Mass Spectrom. Ion Processes **67**, 229 (1985).

[5] W. Ekardt, Phys. Rev. B **29**, 1558 (1984).

[6] O. E. Beck, Solid State Commun. **49**, 381 (1984).

[7] M. Y. Chou and M. L. Cohen, Phys. Lett. A **133**, 420 (1986).

[8] M. G. Mayer and J. H. D. Jensen, *Elementary Theory of Nuclear Shell Structure* (Wiley, New York, 1955).

[9] H. Nishioka, K. Hansen, and B. R. Mottelson, Phys. Rev. B (to be published).

[10] S. Bjørnholm, Contemp. Phys. (to be published).

[11] R. Balian and C. Bloch, Ann. Phys. (N.Y.) **69**, 76 (1971).

[12] A. Bohr and B. R. Mottelson, *Nuclear Structure II* (Benjamin, London, 1975).

[13] W. A. de Heer, Ph.D. thesis, University of California, Berkeley, 1985 (unpublished).

[14] W. A. de Heer, W. D. Knight, M. Y. Chou, and M. L. Cohen, Solid State Phys. **40**, 93 (1987).

[15] C. E. Klots, J. Chem. Phys. **92**, 5864 (1988).

[16] C. Brechignac, Ph. Cahuzac, J. Leygnier, and J. Weiner, J. Chem. Phys. **90**, 1492 (1989).

[17] M. Brack, O. Genzken, and K. Hansen (to be published).

[18] T. P. Martin, T. Bergmann, H. Göhlich, and T. Lange, Phys. Rev. Lett. **65**, 748 (1990).

[19] W. Miehle, O. Kandler, T. Leisner, and O. Echt, J. Chem. Phys. **91**, 5940 (1989).

[20] N. W. Ashcroft and N. D. Mermin, *Solid State Physics* (Saunders College, Philadelphia, 1976).

[21] T. P. Martin has recently reported on measurements of Na clusters up to several thousand (private communication).

[C]

Z. Phys. D – Atoms, Molecules and Clusters 21, 65–81 (1991)

Atoms, Molecules
Zeitschrift für Physik D and Clusters

Thermal properties of the valence electrons in alkali metal clusters*

M. Brack[1], **O. Genzken**[1], **and K. Hansen**[2]

[1] Institute for Theoretical Physics, University of Regensburg, W-8400 Regensburg, Federal Republic of Germany
[2] The Niels Bohr Institute, Blegdamsvej 17, DK-2100 Copenhagen, Denmark

Received 16 January 1991; final version 2 April 1991

Abstract. The finite-temperature density functional approach is applied for the first time to calculate thermal properties of the valence electron system in metal clusters using the spherical jellium model. Both the canonical and the grand canonical formalism are applied and their differences are discussed. We study the temperature dependence of the total free energy $F(N)$ (including a contribution from the ionic jellium background) for spherical neutral clusters containing N atoms. We investigate, in particular, its first and second differences, $\Delta_1 F = F(N-1) - F(N)$ and $\Delta_2 F = F(N+1) + F(N-1) - 2F(N)$, and discuss their possible relevance for the understanding of the mass abundance spectra observed in cluster production experiments. We show that the typical enhancement of magic spherical-shell clusters with $N = 8$, 20, 34, 40, 58, 92, 138, 186, 254, 338, 398, 440, 508, 612..., most of which are well established experimentally, is decreasing rather fast with increasing temperature T and cluster size N. We also present electronic entropies and specific heats of spherical neutral clusters. The Koopmans theorem and related approximations for calculating $\Delta_1 F$ and $\Delta_2 F$ at $T > 0$ are discussed.

PACS: 36.40.+d; 31.20.Sy; 05.30.−d; 65.50.+m

1. Introduction

Metal clusters offer on opportunity for studying interesting size and shell effects that are typical of finite Fermion systems. In particular, an enhanced stability of clusters with the 'magic' numbers of atoms[1] $N = 8, 20, 40, 58, 92$ has been observed by many groups (see [1] for recent reviews of expermential results). This stability can be explained in terms of a *shell model* for the valence electrons which move in an external field created by the ions. One of the most striking indications of the validity of the shell model is the coincidence of the steps in the first differences $\Delta_1 E(N)$, or the peaks in the second differences $\Delta_2 E(N)$, of the total energy $E(N)$ of neutral clusters

$$\begin{aligned} \Delta_1 E(N) &= E(N-1) - E(N), \\ \Delta_2 E(N) &= E(N+1) + E(N-1) - 2E(N), \end{aligned} \tag{1}$$

with similar features observed experimentally in mass abundance spectra and their logarithmic derivatives, at magic numbers corresponding to spherical closed shells. Steps are also observed in the electronic ionization potentials at the same magic numbers, confirming the assumption that the shell structure in the total energy is dominated by the valence electrons.

Microscopic calculations of self-consistent potentials for the electrons, taking into account their mutual Coulomb interaction, have been performed in the so-called jellium background model [2] within the Kohn-Sham density functional formalism [3]. However, these calculations – and many others since – have been performed for the ground state at zero temperature, $T = 0$. On the other hand, in most experiments the clusters are produced at temperatures up to several hundred Kelvin [1], and one has to raise the question to what extent the temperature averaging of the single-particle structure might affect these results. At first sight, one would expect that a temperature of a few hundred Kelvin (i.e., a few tens of millielectronvolt) should be negligible in view of the typical major shell spacings of $\simeq 0.5 - 1$ eV of the electron levels in the smaller clusters. However, as we shall see, the first and second differences of the total *free energy* $F(N)$ with respect to the atomic number N are very sensitive to temperature due to the high degeneracy of the electronic single-particle level spectrum around the magic shell closures. Bulk properties, such as total binding en-

---

* Work partially supported by the Danish Natural Science Research Council and by Deutsche Forschungsgemeinschaft

[1] We shall limit ourselves here to neutral clusters of monovalent atoms

ergies and frequencies of collective dipole excitations of the electrons, are much less affected by temperature.

In this paper we shall present detailed selfconsistent microscopic calculations of the electronic structure of spherical metal clusters at finite temperatures. Some first results of our calculations were presented at a recent conference [4]. Our formalism is based on the $T > 0$ extension of the Kohn-Sham method [5] which was originally formulated for *grand canonical* ensembles where the particle number is conserved only on the average. For calculations of thermal properties of a *macroscopic* object, the choice of ensemble is merely a matter of convenience. This is, however, no longer true in small systems where the properties under study, in particular properties affected strongly by shell structure, can change significantly within the range of a typical particle number fluctuation. For such systems a *canonical* description is a priori more appropriate, and the grand canonical description cannot be expected to lead to the same results.

The subsystem of valence electrons in metallic clusters represent, in fact, an ideal example of a canonical ensemble. Due to the large difference between the energy of the vibrational quanta of the positive ions and the Fermi energy, only a very minute, but finite, amount of the total thermal energy of a typical cluster will be carried by the electrons. The valence electrons will effectively be embedded in a heat bath, even for a system of free clusters. Consequently, the canonical partition function is expected to give a much better description of the thermal properties of the electronic system than either the microcanonical or the grand canonical partition functions. Since the density functional formalism also applies to canonical ensembles (see Evans [5]), we shall study here both the canonical and the grand canonical approach and compare their results systematically and carefully.

The explicit treatment of the thermal properties of the positive ionic cores is largely irrelevant for the discussion here, because all properties are assumed to change smoothly with the number of ions present in the cluster, such that the observed shell-like deviations from a smooth behaviour must be attributed to the valence electrons. This is consistent with the very idea behind the jellium model approximation which we are using: the geometrical structure of the positive ions is ignored and replaced by a uniform charge background ('jellium'). A finite temperature should only render this assumption more correct: the ensemble averaging over a slow thermal motion of the ions is likely to be equivalent to an averaging over their geometrical configurations. Thus, in the jellium model, the total (free) energy of a cluster (and quantities derived from it) only contains contributions of the ions in an *averaged* form. In this crude model, it would make little sense to introduce an explicit temperature dependence of the jellium density. The essential point is to include the thermal motion of the ions in terms of a *heat bath* with $T > 0$.

Besides providing a heat bath for the electrons, the finite temperature of the ionic cores has one more consequence: namely to render the cluster unstable. Any cluster with a total excitation energy exceeding the energy needed to evaporate one atom (or, in principle, a particle of any kind) will – given sufficient time – decay. Although the mass abundance spectra display peaks near the shell closings, it is therefore not clear that measuring these spectra corresponds to a sampling of an equilibrium ensemble. Since production and sampling of the spectra experimentally is separated by at least some microseconds, sufficient time is available for substantial changes of the original abundances through evaporation. This process will also tend to increase the number of closed-shell clusters due to the strong dependence of the evaporation rate on the dissociation energy. Therefore, peaks in the observed abundance spectra can be associated with shell closures even without invoking thermal equilibrium. The pronounced asymmetry of the mass spectra around magic shell closings (see, e.g., [1]) may, in fact, be taken as an indication of a significant amount of evaporation *after* production and *before* mass selection.

A semi – quantitiative comparison of observed abundance spectra with preliminary results of our calculations has been quite encouraging [6]. A more detailed comparison would necessitate the inclusion of deformation effects for clusters in the regions between the filled spherical shells. Nevertheless, we believe it to be instructive to study the properties of the electronic subsystem of individual spherical metal clusters in a thermal equilibrium situation as functions of size and temperature. Models for local chemical equilibrium or for evaporation from an initially hot ensembly may be subsequently developed. There, the free energy $F(N)$ and its first and second differences will be needed as an important input.

In Sect. 2 we present the density functional formalism for $T > 0$ in the spherical jellium model. In Sect. 3 we compare the grand canonical and the canonical results for some crucial quantities and further discuss useful approximations. Section 4 is devoted to a discussion of the Koopmans theorem and related approximations which might be used to calculate $\Delta_1 F$ and $\Delta_2 F$ in a purely non-interacting particle picture. In Sect. 5, we present some typical results over a large range of cluster sizes and temperatures.

2. Kohn-Sham formalism for the jellium model at finite temperature

2.1. Energy functional and variational equations

We employ the spherical jellium model [2] in which the charges of the ions (i.e. atoms minus valence electrons) are uniformly spread out over the volume of a sphere of radius $R_I = r_s N^{1/3}$, where N is the number of ions, $r_s = \left(\frac{4\pi}{3}\rho_I\right)^{-1/3}$ is the Wigner-Seitz radius characterizing the metal, and ρ_I its density. As we have discussed in the introduction, it would not make much sense to introduce any explicit temperature dependence of the jellium density. We therefore keep the value of r_s fixed for all temperatures.

The jellium sphere creates an external attractive potential $V_I(r)$ for the electrons. According to Mermin [5] and Evans [5], the Helmholtz free energy F of the cluster is a functional of the local density $\rho(r)$ of the electrons:

$$F = F[\rho] = U[\rho] - TS[\rho]. \tag{2}$$

U is the total internal energy, S the entropy and T the temperature[2]. Following the Kohn-Sham procedure [3], we introduce a non-interacting free kinetic energy $G_s[\rho]$

$$G_s[\rho] = E_s^{\text{kin}}[\rho] - TS_s[\rho], \tag{3}$$

where E_s^{kin} and S_s are, in the standard notation, the kinetic energy and entropy, respectively, of a *non-interacting* system of electrons having the density $\rho(r)$. The total free energy of a cluster is then

$$\begin{aligned} F[\rho] = G_s[\rho] + \int \Big\{ & V_I(r)\,\rho(r) \\ & + \tfrac{1}{2}\,\rho(r) \left[e^2 \int \frac{\rho(r')}{|\mathbf{r}-\mathbf{r}'|}\, \mathrm{d}^3 r' \right] \\ & + \mathscr{F}_{xc}[\rho] \Big\}\, \mathrm{d}^3 r + E_I. \end{aligned} \tag{4}$$

Hereby $V_I(r)$ and E_I are the potential and the electrostatic energy, respectively, of the ionic jellium background; the second term under the integral is the Hartree Coulomb energy of the electrons, and $\mathscr{F}_{xc}[\rho]$ is the exchange and correlation free energy density functional. We stress again here that F contains the energy of the ions only in a very crude schematic way through the jellium background density; this contribution E_I varies smoothly with N and any shell structure effects in $F(N)$ will be due to the electrons. Similarly, the entropy associated with the ionic motion is assumed to be a smooth function of N; its contribution to $F(N)$ is disregarded in the following.

Next, we write [3, 5] the local density $\rho(r)$ of the electrons in terms of auxiliary single-particle wavefunctions φ_i and finite-temperature occupation numbers n_i as

$$\rho(r) = \sum_i |\varphi_i(\mathbf{r})|^2 n_i, \qquad \int \rho(r)\, \mathrm{d}^3 r = \sum_i n_i = N, \tag{5}$$

and the non-interacting kinetic energy as

$$E_s^{\text{kin}}[\rho] = \frac{\hbar^2}{2m} \int \sum_i |\nabla \varphi_i(\mathbf{r})|^2 n_i\, \mathrm{d}^3 r. \tag{6}$$

In all sums over i, we shall count the degenerate single-particle states separately, so that $0 \leqq n_i \leqq 1$. In principle, these sums include also an integration over the positive energy states in the particle continuum. In practice, however, we shall limit our temperatures such that the n_i become negligible in the continuum, in order that a static equilibrium approach be justified at all.

Varying the free energy (4) with respect to the single-particle wavefunctions $\varphi_i^*(\mathbf{r})$ leads to the usual Kohn-Sham (KS) equations

$$\{\hat{T} + V_{\text{tot}}(r)\}\, \varphi_i(\mathbf{r}) = \varepsilon_i \varphi_i(\mathbf{r}). \tag{7}$$

Note that the entropy part of G_s in (3) does not contribute to (7), since the non-interacting entropy S_s does not depend explicitly on the wavefunctions (see Sect. 2.2). In (7), $\hat{T}$ is the kinetic energy operator and the local potential V_{tot} is a sum of three terms:

$$V_{\text{tot}}(r) = V_I(r) + V_H[\rho(r)] + V_{xc}[\rho(r)], \tag{8}$$

whereof V_I is the jellium potential already mentioned, $V_H[\rho]$ is the Hartree potential of the electrons, given in the square brackets in (4) above, and the last term is due to the exchange and correlation contributions:

$$V_{xc}[\rho\,(/r)] = \frac{\delta}{\delta\rho(r)}\, \mathscr{F}_{xc}[\rho]. \tag{9}$$

A word has to be said about the choice of the exchange-correlation free energy Ω_{xc} which depends, in principle, *explicitly* on the temperature (not only through ρ):

$$\Omega_{xc}[\rho, T] = \int \mathscr{F}_{xc}[\rho(r), T]\, \mathrm{d}^3 r. \tag{10}$$

Gupta and Rajagopal [5] have calculated Ω_{xc} for uniform electron plasmas and presented it as a function of the reduced temperature $t = T/T_F$. Ω_{xc} was shwon to approach zero with increasing t, but only for $t \gtrsim 0.1$ does a noticeable temperature dependence set in. The Fermi temperature T_F itself depends on the density of the system like $T_F \sim \rho^{2/3}$. Using these results within the local density approximation (LDA), one therefore has a different reduced temperature t at each point where the density $\rho(r)$ is varying. For the typical bulk electron densities of alkali metals ($\rho_I \simeq 10^{22} - 10^{23}\,\text{cm}^{-3}$), with which we are concerned here, T_F is [5] of the order of $10^4 - 10^5$ K, so that the temperature dependence of Ω_{xc} is practically negligible in the interiour of the clusters at temperatures below 2000 K. Only in the extreme surface, where ρ has decreased by two to three orders of magnitude, will the temperature variation of Ω_{xc} come into effect. But the contribution at low density to the total electronic free energy is small, and it seems therefore perfectly well justified to replace $\mathscr{F}_{xc}[\rho(r), T]$ in (4) by the $T=0$ energy density functional $\mathscr{E}_{xc}[\rho]$.

In conclusion, the temperature effects in alkali metal clusters can be expected to come only from the occupation numbers n_i, which will be determined in the following, and from the corresponding changes in the densities (5) and the mean field (8). In our numerical calculations, we used for $\mathscr{E}_{xc}[\rho]$ the LDA functional of Gunnarsson and Lundqvist [7].

In an exact treatment of the Coulomb exchange, the total potential $V_{\text{tot}}(r)$ would fall off asymptotically like $1/r$ at large distances. The spectrum ε_i would therefore contain an infinite number of bound Rydberg states which could lead the sums over the single-particle states i to diverge. Due to the use of the LDA functional, however, the asymptotic fall-off of V_{tot} is faster than $1/r$ and there is only a finite number of bound states [2], so that this

---

[2] We put the Boltzman constant $k \equiv 1$ and measure the temperature alternatively in degrees Kelvin (K) or in energy units: 1 Ry = 13.606 eV = $15.789 \cdot 10^4$ K

is a functional of the local density $\rho(r)$ of the electrons:

$$F = F[\rho] = U[\rho] - TS[\rho]. \tag{2}$$

U is the total internal energy, S the entropy and T the temperature[2]. Following the Kohn-Sham procedure [3], we introduce a non-interacting free kinetic energy $G_s[\rho]$

$$G_s[\rho] = E_s^{\mathrm{kin}}[\rho] - TS_s[\rho], \tag{3}$$

where E_s^{kin} and S_s are, in the standard notation, the kinetic energy and entropy, respectively, of a *non-interacting* system of electrons having the density $\rho(r)$. The total free energy of a cluster is then

$$F[\rho] = G_s[\rho] + \int \Big\{ V_I(r)\,\rho(r) + \tfrac{1}{2}\,\rho(r) \left[e^2 \int \frac{\rho(r')}{|\mathbf{r}-\mathbf{r}'|}\,\mathrm{d}^3 r' \right] + \mathscr{F}_{xc}[\rho] \Big\}\,\mathrm{d}^3 r + E_I. \tag{4}$$

Hereby $V_I(r)$ and E_I are the potential and the electrostatic energy, respectively, of the ionic jellium background; the second term under the integral is the Hartree Coulomb energy of the electrons, and $\mathscr{F}_{xc}[\rho]$ is the exchange and correlation free energy density functional. We stress again here that F contains the energy of the ions only in a very crude schematic way through the jellium background density; this contribution E_I varies smoothly with N and any shell structure effects in $F(N)$ will be due to the electrons. Similarly, the entropy associated with the ionic motion is assumed to be a smooth function of N; its contribution to $F(N)$ is disregarded in the following.

Next, we write [3, 5] the local density $\rho(r)$ of the electrons in terms of auxiliary single-particle wavefunctions φ_i and finite-temperature occupation numbers n_i as

$$\rho(r) = \sum_i |\varphi_i(\mathbf{r})|^2 n_i, \qquad \int \rho(r)\,\mathrm{d}^3 r = \sum_i n_i = N, \tag{5}$$

and the non-interacting kinetic energy as

$$E_s^{\mathrm{kin}}[\rho] = \frac{\hbar^2}{2m} \int \sum_i |\nabla \varphi_i(\mathbf{r})|^2 n_i\,\mathrm{d}^3 r. \tag{6}$$

In all sums over i, we shall count the degenerate single-particle states separately, so that $0 \leqq n_i \leqq 1$. In principle, these sums include also an integration over the positive energy states in the particle continuum. In practice, however, we shall limit our temperatures such that the n_i become negligible in the continuum, in order that a static equilibrium approach be justified at all.

Varying the free energy (4) with respect to the single-particle wavefunctions $\varphi_i^*(\mathbf{r})$ leads to the usual Kohn-Sham (KS) equations

$$\{\hat{T} + V_{\mathrm{tot}}(r)\}\,\varphi_i(\mathbf{r}) = \varepsilon_i \varphi_i(\mathbf{r}). \tag{7}$$

Note that the entropy part of G_s in (3) does not contribute to (7), since the non-interacting entropy S_s does not depend explicitly on the wavefunctions (see Sect. 2.2). In (7), $\hat{T}$ is the kinetic energy operator and the local potential V_{tot} is a sum of three terms:

$$V_{\mathrm{tot}}(r) = V_I(r) + V_H[\rho(r)] + V_{xc}[\rho(r)], \tag{8}$$

whereof V_I is the jellium potential already mentioned, $V_H[\rho]$ is the Hartree potential of the electrons, given in the square brackets in (4) above, and the last term is due to the exchange and correlation contributions:

$$V_{xc}[\rho(/r)] = \frac{\delta}{\delta\rho(r)}\,\mathscr{F}_{xc}[\rho]. \tag{9}$$

A word has to be said about the choice of the exchange-correlation free energy Ω_{xc} which depends, in principle, *explicitly* on the temperature (not only through ρ):

$$\Omega_{xc}[\rho, T] = \int \mathscr{F}_{xc}[\rho(r), T]\,\mathrm{d}^3 r. \tag{10}$$

Gupta and Rajagopal [5] have calculated Ω_{xc} for uniform electron plasmas and presented it as a function of the reduced temperature $t = T/T_F$. Ω_{xc} was shwon to approach zero with increasing t, but only for $t \gtrsim 0.1$ does a noticeable temperature dependence set in. The Fermi temperature T_F itself depends on the density of the system like $T_F \sim \rho^{2/3}$. Using these results within the local density approximation (LDA), one therefore has a different reduced temperature t at each point where the density $\rho(r)$ is varying. For the typical bulk electron densities of alkali metals ($\rho_I \simeq 10^{22} - 10^{23}\,\mathrm{cm}^{-3}$), with which we are concerned here, T_F is [5] of the order of $10^4 - 10^5$ K, so that the temperature dependence of Ω_{xc} is practically negligible in the interiour of the clusters at temperatures below 2000 K. Only in the extreme surface, where ρ has decreased by two to three orders of magnitude, will the temperature variation of Ω_{xc} come into effect. But the contribution at low density to the total electronic free energy is small, and it seems therefore perfectly well justified to replace $\mathscr{F}_{xc}[\rho(r), T]$ in (4) by the $T=0$ energy density functional $\mathscr{E}_{xc}[\rho]$.

In conclusion, the temperature effects in alkali metal clusters can be expected to come only from the occupation numbers n_i, which will be determined in the following, and from the corresponding changes in the densities (5) and the mean field (8). In our numerical calculations, we used for $\mathscr{E}_{xc}[\rho]$ the LDA functional of Gunnarsson and Lundqvist [7].

In an exact treatment of the Coulomb exchange, the total potential $V_{\mathrm{tot}}(r)$ would fall off asymptotically like $1/r$ at large distances. The spectrum ε_i would therefore contain an infinite number of bound Rydberg states which could lead the sums over the single-particle states i to diverge. Due to the use of the LDA functional, however, the asymptotic fall-off of V_{tot} is faster than $1/r$ and there is only a finite number of bound states [2], so that this

---

[2] We put the Boltzman constant $k \equiv 1$ and measure the temperature alternatively in degrees Kelvin (K) or in energy units: $1\,\mathrm{Ry} = 13.606\,\mathrm{eV} = 15.789 \cdot 10^4$ K

divergence problem is regularized automatically in the local density approximation.

We have solved (7) iteratively for spherical clusters on a finite mesh in r-space. The explicit form of the occupation numbers n_i in terms of the single-particle spectrum ε_i, which have to be included at each iteration, depends on the choice of the statistical ensemble and will be discussed in the following subsection. For partially filled spherical shells we made the usual [2] 'filling approximation' which amounts to an averaging of the occupied states over their polar angles (θ, ϕ), such that the density ρ and the total potential V_{tot} stay spherical.

2.2. *Entropy and occupation numbers*

We shall now discuss the calculation of the entropy and the occupation numbers at finite temperature T. As shown above, we need only know these quantities for a system of non-interacting Fermions in a local potential $V_{\text{tot}}(r)$, with eigenenergies ε_i according to (7), at each given temperature. We shall, therefore, in the following omit the subscript s of the entropy S_s. We call $U_s = \sum_i \varepsilon_i n_i$ the total internal energy of this system, such that $F_s = U_s - TS$ is its free energy. The energies F_s and U_s should not be confused with those of the interacting system, i.e., $F[\rho]$ and $U[\rho]$ in (2) and (4), which have entirely different values.

a) Grand canonical ensemble: We start with the grand canonical ensemble which is fairly standard and easy to calculate. The entropy for this ensemble is given explicitly in terms of the occupation numbers as [8]

$$S[n_i] = \sum_i s(n_i) = -\sum_i \{n_i \log n_i + (1-n_i)\log(1-n_i)\}. \tag{11}$$

Minimizing the free energy – non-interacting or interacting does not matter, as long as (7) is used – with respect to the n_i, using a constraint on the particle number N

$$\sum_i n_i = N \tag{12}$$

with the help of a Lagrange multiplier μ

$$\frac{\delta}{\delta n_i}\left\{F - \mu \sum_j n_j\right\} = 0, \tag{13}$$

i.e., minimizing the grand potential $\Omega = F - \mu N$, leads to the Fermi occupation numbers

$$n_i = \{1 + \exp[(\varepsilon_i - \mu)/T]\}^{-1}. \tag{14}$$

In the KS calculations, the chemical potential μ must be determined at each iteration such as to fulfil (12) and (14). The entropy S, (11), need only be calculated at the end, after convergence of the KS iterations.

It should be remembered that N in (12) is only an *average* particle number in the grand canonical ensemble. The variance of the particle number N is given by

$$\sigma_N^2 = \sum_i n_i(1-n_i) = -T \sum_i \frac{\partial n_i}{\partial \varepsilon_i}. \tag{15}$$

Even for moderate temperatures σ_N is easily of order unity for the clusters considered in this paper. Therefore we have to investigate the canonical ensemble where N is fixed exactly from the beginning.

b) Canonical ensemble: In order to calculate entropy and occupation numbers for a canonical ensemble, we cannot avoid evaluating the partition function $Z_N(\beta)$ which is given by [8]

$$Z_N(\beta) = \sum_\alpha e^{-\beta E_\alpha(N)}; \tag{16}$$

$\beta = 1/T$ is the inverse temperature. The sum runs over all partitions α, i.e. all possibilities to distribute N particles over the single-particle levels ε_i, with energies $E_\alpha(N)$:

$$E_\alpha(N) = \sum_i p_i^\alpha \varepsilon_i, \quad p_i^\alpha = 0 \text{ or } 1, \quad \sum_i p_i^\alpha = N. \tag{17}$$

From $Z_N(\beta)$ we get U_s, F_s and S by the canonical relations

$$F_s = -\log Z_N/\beta, \qquad U_s = -\frac{1}{Z_N}\frac{\partial}{\partial\beta} Z_N, \qquad S = \beta(U_s - F_s). \tag{18}$$

To define the occupation numbers n_i, we start from the basic probability P_α for the system to have the energy E_α at the temperature $1/\beta$:

$$P_\alpha = e^{-\beta E_\alpha(N)}/Z_N(\beta); \quad \sum_\alpha P_\alpha = 1. \tag{19}$$

In terms of the P_α, we can write the internal energy U_s and the entropy S as

$$U_s = \langle E_\alpha \rangle = \sum_\alpha P_\alpha E_\alpha, \tag{20}$$

$$S = -\langle \log P_\alpha \rangle = -\sum_\alpha P_\alpha \log P_\alpha. \tag{21}$$

The n_i now are defined as the ensemble averages of the microscopic occupations p_i^α:

$$n_i = \langle p_i^\alpha \rangle = \sum_\alpha P_\alpha p_i^\alpha. \tag{22}$$

Combining (17), (19), (20) and exchanging sums, we see that

$$\sum_i \varepsilon_i n_i = U_s; \quad \sum_i n_i = N. \tag{23}$$

In practice, the evaluation of Z_N and the n_i cannot be done by summing explicitly over all partitions α in (16) and (22), because there are far too many of them for

$N \gtrsim 10$. An economic way of calculating these quantities exactly, nevertheless, is described in the Appendix. Still, the numerical treatment of the canonical ensemble, in particular the evaluation of the n_i, is far more time consuming than for the grand canonical case. We have therefore developed a way to avoid the iterative determination of the canonical n_i in the KS calculations, which shall be presented and tested in Sect. 3.2 below.

3. Numerical tests and approximations

3.1. *Comparison of the two ensembles*

As some of the most sensitive quantities to details of level structure and to the choice of the statistical ensemble, we investigate the first and second differences of the total interacting free energy F, (4), of a neutral cluster with respect to the number N of atoms:

$$\Delta_1 F(N) = F(N-1) - F(N), \tag{24a}$$

$$\begin{aligned} \Delta_2 F(N) &= \Delta_1 F(N) - \Delta_1 F(N+1) \\ &= F(N+1) + F(N-1) - 2F(N). \end{aligned} \tag{24b}$$

We recall that the energy of the ions is included only in the jellium approximation at $T=0$; therefore the entropy part in these quantities is coming exclusively from the valence electrons.

The first difference $\Delta_1 F(N)$ is related to the dissociation free energy D_N of one neutral atom by

$$D_N = \Delta_1 F(N) + F(1), \tag{25a}$$

where $F(1)$ is the free energy of a single atom. This latter quantity, $F(1)$, is certainly not correctly described in the jellium model; nevertheless, (25a) turns out to be a good estimate of the experimental dissociation energy (see Sect. 5.1). In any case, since $F(1)$ is a constant, we may consider the factor $\exp\{-\beta \Delta_1 F(N)\}$ to be a measure for the stability of the cluster N against *evaporation* of a monomer:

$$\mathrm{Na}_N \rightarrow \mathrm{Na}_{N-1} + \mathrm{Na}_1 .$$

(See the beginning of Sect. 5 for a further discussion on the relation of $\Delta_1 F$ and $\Delta_2 F$ to mass abundances in cluster beams.)

On the other hand, in a *chemical equilibrium* of three adjacent sodium clusters,

$$\mathrm{Na}_{N-1} + \mathrm{Na}_{N+1} \leftrightharpoons 2\,\mathrm{Na}_N ,$$

the law of mass action expresses that $\Delta_2 F$ and cluster concentration (or probability) c_N are related approximately through

$$\begin{aligned} \Delta_2 F(N) &\simeq -T \Delta_2 \log c_N \\ &= T \log \left[\frac{c_N^2}{c_{N-1} c_{N+1}} \right], \end{aligned} \tag{25b}$$

$F(N)$ being the total free energy of a cluster at unit probability for a given volume and temperature. The relation (25b) would be exact if the rotational, translational and vibrational degrees of freedom of the ions were included. Treating those degrees of freedom classically and assuming that the cluster is a sphere with a volume proportional to its mass, their contribution to the free energy is a smooth function of cluster size. More specifically [1], this part of the free energy is the sum of a volume and a logarithmic term in cluster size, and differentiating twice leaves an error of order N^{-2}; hence its omission from $\Delta_2 F(N)$ is inconsequential.

In Figs. 1–3 we show $\Delta_1 F$ and $\Delta_2 F$ as functions of temperature for a series of neutral Na clusters. The solid lines are obtained for the canonical ensemble and the short-dashed lines are obtained for the grand canonical ensemble. For both ensembles, the KS equations (7) have been solved iteratively including the corresponding occupation numbers n_i, until convergence (i.e., selfconsistency of the field V_{tot}) was reached. We see that there are significant differences between the results obtained with the two ensembles, in particular in the physically interesting region around temperatures of a few hundred up to about 1000 degrees. The error introduced by the particle number non-conservation in the grand canonical treatment differs from case to case, depending sensitively on the shell structure in the single-particle spectrum ε_i near the Fermi energy. In all cases, the error decreases for $T \gtrsim 1000$ K and becomes very small for $T \gtrsim 2000$ K.

The linear behaviour of $\Delta_1 F(T)$ and $\Delta_2 F(T)$ near $T=0$, with slopes that are clearly different for the two ensembles, can easily be understood in terms of the degeneracies of the last occupied levels ε_i. Indeed, for $T \lesssim 200$ K, the smaller clusters can be considered to be perfectly cold: the occupation numbers of all completely filled levels ε_i are identically one. If there are ν particles in the last level ε_0 and the degeneracy of this level (including spin factor 2) is g, then the exact microscopic

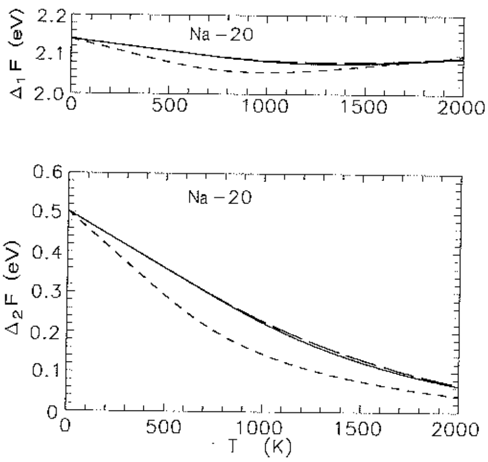

Fig. 1. First and second differences $\Delta_1 F$ and $\Delta_2 F$ (24), of total free energy of the sodium cluster with $N=20$ versus temperature. *Solid lines:* selfconsistent canonical results. *Short-dashed lines:* selfconsistent grand canonical results. *Long-dashed lines:* result of approximation (32), i.e. using one canonical iteration at the end of a grand canonical selfconsistent calculation

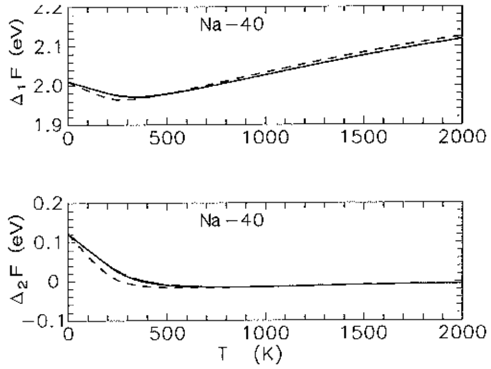

Fig. 2. As Fig. 1, for $N = 40$

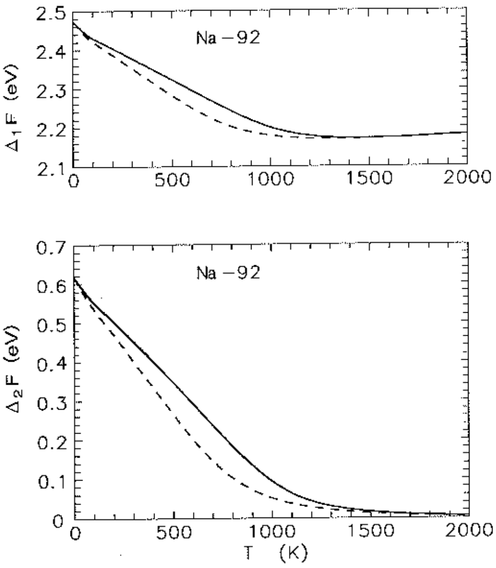

Fig. 3. As Fig. 1, for $N = 92$

probability P_α and the occupation number n_0 of this state are given by

$$P_\alpha = \binom{g}{\nu}^{-1} = \frac{\nu!\,(g-\nu)!}{g!}; \qquad n_0 = \frac{\nu}{g}. \tag{26}$$

The canonical entropy of the corresponding cluster in the limit $T = 0$ is then, with (21),

$$\begin{aligned} S_0^{\mathrm{can}} &= \log \binom{g}{\nu} \\ &= \log g! - \log \nu! - \log (g-\nu)!\,. \end{aligned} \tag{27}$$

(This value is exactly reproduced in our numerical calculation for the canonical ensemble from (16), (18) in the limit $T = 0$.) Since the internal energy $U(T)$ has a zero slope at $T = 0$, the slopes of $\Delta_1 F$ and $\Delta_2 F$ are thus identical to minus the first and second differences $\Delta_1 S$ and $\Delta_2 S$, respectively, of the entropy at $T = 0$.

For the grand canonical ensemble, now, one obtains from (26) and (11) a different value of the entropy, namely

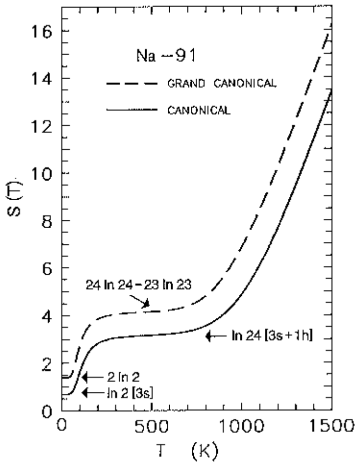

Fig. 4. Entropy of the Na_{91} cluster versus temperature. *Solid line:* canonical result, *dashed line:* grand canonical result. The finite values at $T = 0$ come from one electron in the $3s$ level (degeneracy $g = 2$). The plateau values for $300 \lesssim T \lesssim 600$ K are the $T = 0$ entropies of an electron in a 24-fold degenerate level, corresponding to the combined $3s + 1h$ levels of this cluster (see text)

$$\begin{aligned} S_0^{\mathrm{g.c.}} &= s(n_0) \\ &= g \log g - \nu \log \nu - (g-\nu) \log (g-\nu) \end{aligned} \tag{28}$$

which, incidentally, corresponds to using Stirling's approximation to the factorials in the correct expression (27). In the case of $\nu = 1$ particle in an s level (angular momentum zero, spin degeneracy $g = 2$), the error in (28) with respect to the canonical entropy (27) is a factor of two.

This is illustrated in Fig. 4 where we show the entropy of the Na_{91} cluster as a function of temperature, evaluated both for the canonical and the grand canonical ensemble. The highest occupied level in this cluster at $T = 0$ is the $3s$ level: we clearly recognize the two limiting values $S_0^{\mathrm{can}} = \log 2$ and $S_0^{\mathrm{g.c.}} = 2 \log 2$ at the left of the figure. In the temperature region $300 \lesssim T \lesssim 600$ K, the entropies in Fig. 4 exhibit plateaux at the values $S^{\mathrm{can}} = \log 24$ and $S^{\mathrm{g.c.}} = 24 \log 24 - 23 \log 23$, respectively. This is due to the fact that the $3s$ level is nearly degenerate with the 1h level ($g = 22$) which lies lower in energy by only $0.033\ \mathrm{eV} \simeq 400$ K. Therefore, at temperatures around $T \simeq 500$ K, these two levels appear as one level with a total degeneracy of $g = 2 + 22 = 24$, whereas all the other levels of the spectrum are far enough away to have occupation numbers equal to 1 or 0 and thus do not contribute to the entropy. This rapidly changing increase of the entropy at small temperatures is another manifestation of electronic shell structure. Only above several thousand degrees K, the shell effects are averaged out and S takes on its expected linear temperature dependence (see Sect. 5.2).

We have thus found that the differences in the slopes of the curves in Figs. 1–3 at small T reflect the wrong entropies obtained in the grand canonical treatment. Note that the error, near $T = 0$, does not lie in the Fermi occupation number given by (14) which also leads to the

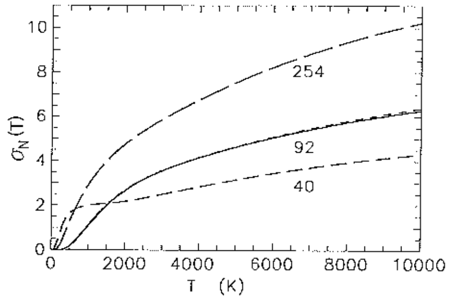

Fig. 5. Root of particle number variance σ_N (15), versus temperature for the clusters with $N=40$, 92, and 254 in the grand canonical treatment. *Solid line:* exact selfconsistent result. *Dashed lines:* using the approximation of Sect. 3.3, in which the spectra $\varepsilon_i^{(0)}$ of the cold clusters ($T=0$) are used

correct numerical value of n_0 (26) at small temperatures (although the exact $T=0$ limit does not exist for $\varepsilon_0=\mu$).

In Fig. 5 the variance σ_N, (15), of the particle number, obtained in the grand canonical ensemble for three cluster sizes is plotted versus temperature up to $T=10\,000$ K. For $N=92$, the solid line is the fully selfconsistent result. The dashed lines show σ_N obtained in the approximation where the cold spectrum $\varepsilon_i^{(0)}$ of the selfconsistent solution at $T=0$ is used; an approximation which is seen here to work very well for σ_N. (See, however, the discussion and results in Sect. 3.3 below). From these results it is not surprising that errors enter into the differences $\Delta_1 F(N)$ and $\Delta_2 F(N)$, since they hinge precisely upon an exact knowledge of the particle number N.

For $T \gtrsim 3000$ K, all three curves in Fig. 5 can be parametrized approximately by $\sigma_N^2/N \simeq cT$ with $c=0.045\cdot 10^{-3}\,\mathrm{K}^{-1}=7.1\,\mathrm{Ry}^{-1}$. This linear T dependence is easily derived from the rhs of (15), if shell effects are neglected and the average single-particle level density $\tilde{g}(\varepsilon)$ is kept constant to its value at the Fermi energy:

$$\sigma_N^2 \sim \int_{-\infty}^{\infty} \tilde{g}(\varepsilon)\, n_\varepsilon (1-n_\varepsilon)\, \mathrm{d}\varepsilon$$

$$\simeq -T\tilde{g}(\varepsilon_F) \int_{-\infty}^{\infty} \frac{\partial n}{\partial \varepsilon}\, \mathrm{d}\varepsilon = T\tilde{g}(\varepsilon_F) = \frac{6}{\pi^2}\, aNT,$$

where a is the level density parameter discussed in Sect. 5.2. The numerical value $a=11.6\,\mathrm{Ry}^{-1}$ found there from fitting entropies to (46) is in quantitative agreement with $c=\frac{6}{\pi^2}\,a$, indeed.

Summarizing this subsection, we can state that the *canonical* treatment of the clusters under investigation here is mandatory in order to obtain quantitatively correct results, especially for the entropy. The spread in particle number in the grand canonical treatment is, in particular, too large to obtain exact values for the quantities $\Delta_1 F$ and $\Delta_2 F$ at the physically interesting temperatures below $T \simeq 1000$ K. Another quantity that is sensitive to a canonical treatment is the specific heat; it will be discussed in Sect. 5.3.

3.2. Approximately selfconsistent treatment of the canonical ensemble

The iterative inclusion of the canonical occupation numbers n_i (see the Appendix) in the KS calculations is rather time consuming for large clusters and high temperatures. We have therefore developed an approximate scheme which we will show here to be completely sufficient for all practical purposes. It permits one to obtain the canonical results with only negligibly more computing time than that required for the grand canonical calculation.

Our idea is to assume that the main error in the grand canonical calculation does not lie in the determination of the occupation numbers n_i, (14), but in (11) for the entropy. In the limit $T=0$, we have just shown in Sect. 3.1 above that this is, indeed, exactly the case. Now, in the iterative solution of the KS equations (7), only the occupation numbers n_i are needed for the density (5) and the entropy never enters. Thus, the temperature dependence of the selfconsistent mean field V_{tot} in a grand canonical KS calculation is as good as the occupation numbers n_i are. We therefore propose to perform the KS iterations with the grand canonical occupation numbers (14) until convergence is reached, and then to correct the total free energy *perturbatively* by introducing the canonical ensemble in a last step.

To do so, let us denote the exact canonical occupation numbers (2) by n_i as before; the grand canonical ones, (14), (which become slightly wrong at $T>0$) by $\tilde{n}_i$, and their difference by δn_i:

$$\delta n_i = n_i - \tilde{n}_i\,. \tag{29}$$

It is now straightforward, using the underlying variational principle which leads to the KS equations (7), to show that *to first order in the differences* δn_i, the error introduced in the total, grand canonical *interacting* free energy $F^{\mathrm{g.c.}}=F[\rho,\tilde{n}_i]$ (4) is equal to

$$\delta_1 F_s = F_s^{\mathrm{can}} - F_s^{\mathrm{g.c.}}[\tilde{n}_i] \tag{30}$$

in terms of the *non-interacting* free energies, evaluated for the two ensembles indicated by the superscripts, in terms of the level spectrum ε_i of the grand canonical ensemble. Adding the correction $\delta_1 F$ (30) to $F^{\mathrm{g.c.}}$ will therefore give the selfconsistent *canonical* free energy $F^{\mathrm{can}}=F[\rho,n_i]$ up to errors of second and higher order in δn_i:

$$F^{\mathrm{can}} = F^{\mathrm{g.c.}} + \delta_1 F_s + \mathcal{O}[(\delta n_i)^2]\,, \tag{31}$$

so that we can use the approximation

$$\begin{aligned} F^{\mathrm{can}} &\simeq F^{\mathrm{g.c.}}[\rho,\tilde{n}_i] + \delta_1 F_s \\ &= U^{\mathrm{g.c.}}[\rho,\tilde{n}_i] - \sum_i \varepsilon_i \tilde{n}_i + F_s^{\mathrm{can}}\,. \end{aligned} \tag{32}$$

Note that the entropy $S[\tilde{n}_i]$ (11), which is the major cause for the error in the grand canonical ensemble, cancels on the rhs of (32) and is replaced by the canonical one (in F_s^{can}). Note also, that in the approximation (32) the canonical occupation numbers n_i are not needed, since F_s^{can} is evaluated according to (18) directly from the canonical partition function. Therefore, the partition function (16) has to be calculated only once at the end of the KS iterations, which takes only little extra computing time (see the Appendix) and thus makes our procedure a very efficient one.

This perturbative correction of the total energy of an interacting system, due to small differences in occupation numbers, has been applied many times in different fields of physics. It is the starting point of Landau's Fermi liquid theory [9] in terms of quasi-particles; in nuclear physics, it gives the basis of Strutinsky's shell-correction method [10] in the framework of Hartree-Fock (HF) theory (see also [11]), and in solid state theory a 'force theorem' has been derived along similar lines [12]. Finally, the Koopmans theorem which we shall discuss in Sect. 4 is also closely related to this line of arguments.

In Figs. 1–3, we have included the results obtained in the approximation (32) by the long-dashed lines. They are in all cases seen to reproduce the exact canonical results with a very small and practically negligible error. This result can be understood by looking at the single-particle levels ε_i, which are almost identical for the two ensembles. In fact, also the mean field V_{tot} is practically the same in both cases; this was the starting assumption for the derivation of the approximation (32).

Thus we have shown that the choice of ensemble is not essential for obtaining the selfconsistent mean fields and densities, and that for all practical purposes a perturbative treatment at the end of a grand canonical Kohn-Sham iterative scheme is sufficient to describe the canonical ensemble.

3.3. Importance of the selfconsistent temperature dependence of the mean field

The question may be raised to which extent the temperature dependence of the self-consistent mean field V_{tot}, (8), is important in our calculations. In Fig. 6 we show the density $\rho(r)$ and the potential $V_{\mathrm{tot}}(r)$ of the same cluster, obtained at the three temperatures $T=0$, 1000 and 2000 K for the canonical ensemble. (The corresponding curves for the grand canonical ensemble would hardly be distinguishable on the scale of the figure.) We should like to mention that in HF calculations for hot nuclei, the dependence of the mean fields on temperature has been found earlier [13, 14] to be very weak.

In consequence, one may use arguments as those presented in Sect. 3.2 above to treat the finite temperature effects perturbatively at the end of a KS calculation at $T=0$. In fact, since the temperature dependence of the mean field only enters through the occupation numbers n_i, one may include the $T>0$ effects up to first order in $\delta n_i^T = n_i(T) - n_i(0)$ by adding the correction

$$\delta_T F_s = F_s(T, \varepsilon_i^{(0)}) - \sum_{i=1}^{N} \varepsilon_i^{(0)} \tag{33}$$

to the total ground state energy for $T=0$, leading to the approximation

$$F[\rho, n_i] \simeq E[\rho, T=0] + \delta_T F_s; \tag{34}$$

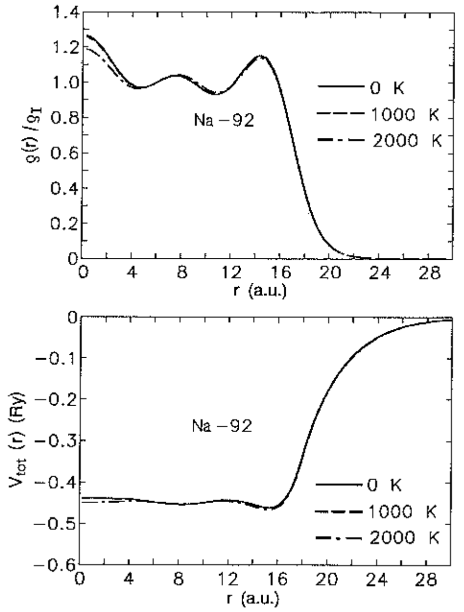

Fig. 6. Electron density $\rho(r)$, in units of jellium density ρ_I (upper part), and total mean field $V_{\mathrm{tot}}(r)$ (lower part) of the Na_{92} cluster at three different temperatures, at $T>0$ evaluated for the canonical ensemble

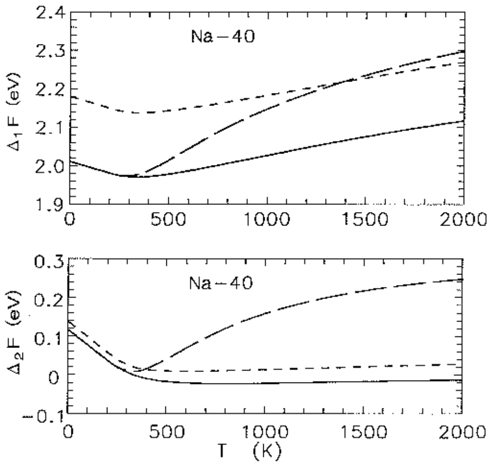

Fig. 7. Same as Fig. 2 for the canonical ensemble, but *long-dashed lines:* using the approximation (34) in terms of the cold specrum $\varepsilon_i^{(0)}$, and *short-dashed lines:* using the Koopmans approximation (43) discussed in Sect. 4. The solid lines are the exact selfconsistent results and identical to those in Fig. 2

hereby, the 'cold spectrum' $\varepsilon_i^{(0)}$ is used in (33). Equations (33), (34) may be used for either of the two ensembles discussed above. (In the nuclear HF calculations, done for grand canonical ensembles, this led to a fairly reasonable approximation of entropies and excitation energies [11]).

In Figs. 7, 8 we test the approximation (34) by comparing the results for $\Delta_1 F$ and $\Delta_2 F$, obtained from the $T=0$ spectrum $\varepsilon_i^{(0)}$ (long-dashed curves), to those of the fully selfconsistent canonical calculation (solid curves, identical to those in Figs. 2, 3). For well-pronounced spherical magic shell situations, such as $N=92$, this ap-

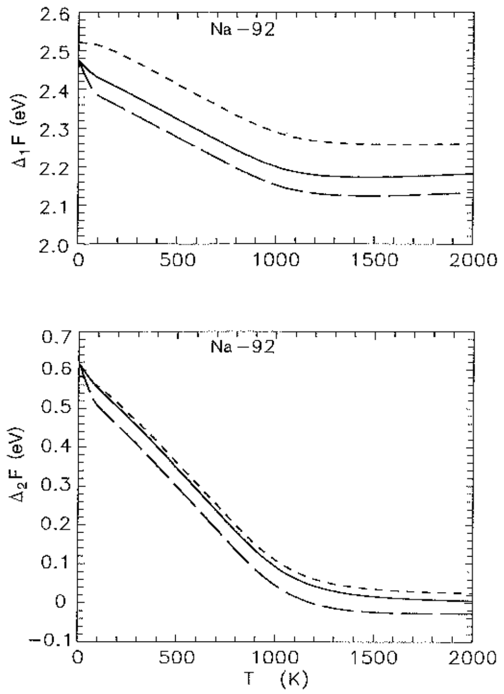

Fig. 8. As Fig. 7, for $N = 92$

proximation is seen to work very well. However, in the case $N = 40$, where there is only a weak gap in the spectrum ε_i, the temperature dependence of $\Delta_1 F$ and $\Delta_2 F$ obtained by (34) is not perfect. It therefore seems important to include the finite temperature selfconsistently in order to retreive correctly the details of shell structure in these quantities. In Sect. 4 we shall investigate the Koopmans theorem for $T > 0$ and find a somewhat better perturbative description of the temperature dependence of $\Delta_1 F$ and $\Delta_2 F$.

4. Discussion of the Koopmans theorem at $T > 0$

In this paper we put a great deal of emphasis on the quantities $\Delta_1 F(N)$ and $\Delta_2 F(N)$ which are closely related to separation energies of a neutral atom. At zero temperature, experience with the well-known Koopmans theorem in atomic, solid state [15] and nuclear physics [16] tells us that electron or nucleon separation energies can be well approximated by the Kohn-Sham (or Hartree-Fock) energy of the highest occupied single-particle level [17]. For the electronic ionization potential of a cluster with N atoms at $T = 0$, Koopmans' theorem reads [18]

$$\mathrm{IP}(N) = -\varepsilon_{\mathrm{ho}} + \frac{e^2}{2R_I}, \tag{35}$$

where $\varepsilon_{\mathrm{ho}}$ is the KS energy of the highest occupied level and the second term in (35) comes from the total electrostatic energy including the jellium self energy. Now, we can always rewrite $\Delta_1 F$ (24a) as

$$\begin{aligned}\Delta_1 F(N) &= F(N-1) - F(N)\\ &= \mathrm{IA}(N-1) + \mathrm{IP}(N),\end{aligned} \tag{36}$$

where we have extended the definition of the ionization potential to finite temperatures by

$$\mathrm{IP}(N) = F(N, -1) - F(N, 0) \tag{37}$$

in terms of the *free* energy $F(N, z)$ of a cluster with N atoms and z excess electrons. In (36), IA (N) is the ion affinity of a neutral cluster with N atoms. This quantity is not expected to exhibit significant shell effects upon variation of N – at least in the present jellium model. In our approximation (see Sect. 2.1) it also is independent of temperature. In order to estimate IA (N), we can therefore start from a semiclassical liquid-drop-model type expansion [19, 20] of the average energy $\tilde{E}$ (at $T = 0$) of a cluster with N atoms and z excess electrons:

$$\begin{aligned}\tilde{E}(N, z) &= E^{(0)}_{\mathrm{Coul}}(N, z)\\ &\quad - z\Delta\phi_0 + e_b(N+z) + \dots\end{aligned} \tag{38}$$

Here $E^{(0)}_{\mathrm{Coul}}$ is the classical Coulomb energy of the cluster, corresponding to a square density distribution of the electrons. $\Delta\phi_0$ is the outer part of the Coulomb barrier of an infinite plane metal surface (i.e., its electrostatic potential taken between an infinite distance outside the metal and the jellium edge; see, e.g., [21]), e_b is the electronic bulk energy (i.e., the energy per electron in the bulk metal), and the dots in (38) indicate surface energy and higher order terms which go at most like $N^{2/3}$ or $(N+z)^{2/3}$. (See [19] for the details of this expansion.) From (38), we find the leading order terms for the ion affinity

$$\begin{aligned}\mathrm{IA}(N) &= \tilde{E}(N, 0) - \tilde{E}(N+1, -1)\\ &\simeq -\Delta\phi_0 - \frac{e^2}{2R_I},\end{aligned} \tag{39}$$

the last term on the rhs of (38) coming from the classical Coulomb energy. Using (35) and (38) in (36), the terms $\frac{e^2}{2R_I}$ cancel to leading order and we obtain the 'Koopmans approximation' for $\Delta_1 F(N)$ at $T = 0$:

$$\Delta_1 E(N) \simeq -\varepsilon_{\mathrm{ho}} - \Delta\phi_0 . \tag{40}$$

The second difference then becomes straightforwardly

$$\Delta_2 E(N) \simeq \varepsilon_{\mathrm{lu}} - \varepsilon_{\mathrm{ho}}, \tag{41}$$

where $\varepsilon_{\mathrm{lu}}$ is the lowest unoccupied level in the cluster N (or, to avoid confusion in case of degenerate levels: the highest occupied level in the cluster $N+1$; if a degenerate level is not completely filled in the cluster N, $\varepsilon_{\mathrm{lu}}$ and $\varepsilon_{\mathrm{ho}}$ will be identical and $\Delta_2 E$ becomes zero). Note that the electrostatic correction $\Delta\phi_0$ and herewith all explicit contributions of the ions cancel in $\Delta_2 E$ to leading order.

Table 1. Test of approximations to first and second differences $\Delta_1 E$ and $\Delta_2 E$, respectively, of total energies at $T=0$ for various cluster sizes (N). a: Exact values, (1), evaluated from the selfconsistent interacting ground-state energy. b: Koopmans approximation, (40, 41). c: Using (43) in the limit $T=0$ with *different* spectra ε_i for the different values of N

Cluster size	$\Delta_1 E$(eV)			$\Delta_2 E$(eV)		
	a	b	c	a	b	c
18	2.525	2.596	3.365	0.326	0.348	−0.429
19	2.199	2.241	3.794	0.060	0.000	0.055
20	2.139	2.199	3.738	0.504	0.515	0.490
21	1.635	1.784	3.248	−0.096	0.000	−0.003
34	2.448	2.511	3.368	0.419	0.438	−0.564
39	2.017	2.165	3.964	0.006	0.000	0.017
40	2.011	2.181	3.947	0.122	0.143	0.796
92	2.474	2.521	4.150	0.617	0.586	0.085
106	1.949	2.151	4.023	−0.183	−0.173	1.018
254	2.354	2.458	3.866	0.272	0.271	−0.539
338	2.322	2.444	3.816	0.315	0.315	−0.622
339	2.008	2.131	4.439	0.001	0.000	−0.004
340	2.006	2.133	4.442	0.001	0.000	−0.004
450	2.113	2.239	2.878	−0.002	0.000	−0.005
508	2.265	2.376	4.266	0.068	0.068	0.572
832	2.243	2.388	3.619	0.046	0.047	0.912

For later reference, we add here also the expression obtained from (38) for the average part (without shell effects) of the electronic ionization potential at $T=0$:

$$\widetilde{\mathrm{IP}}(N)=\tilde{E}(N,-1)-\tilde{E}(N,0) \simeq \Delta\phi_0 - e_b + \frac{e^2}{2R_I}. \tag{42}$$

(We have omitted here, as well as in (38), some minor contributions stemming from the missing surface energy terms in (38) which change the coefficient of $1/R_I$ somewhat; in $\widetilde{\mathrm{IP}}$ the coefficient e.g. for Na clusters ($r_s=3.96$ a.u.) becomes [19] ~0.4 instead of 1/2.) The first two terms on the rhs of (42) constitute a valid expression [21] for the work function of the bulk metal, $W=\Delta\phi_0 - e_b$, which was shown in extended Thomas-Fermi variational calculations [19, 20] to be reached asymptotically by the ionization potentials of spherical clusters in the limit $N\to\infty$.

We show in Table 1 the results obtained in the 'Koopmans approximation' for $\Delta_1 E$ and $\Delta_2 E$, (40, 41), in columns b. They are shown to reproduce the exact selfconsistent results (columns a) very well, within less than 0.15 eV for $\Delta_1 F$ and even much better for $\Delta_2 F$, at all clusters sizes. The error in $\Delta_1 F$ is furthermore approximately constant for the larger clusters and could be reduced by renormalizing the value of $\Delta\phi_0$. We have used the theoretical value for the infinite plane metal surface [19]: $\Delta\phi_0=0.63$ eV for Na with $r_s=3.96$ a.u. Note that the omission of this term in (40) would lead to very poor results for $\Delta_1 F$.

By a straightforward extension of the derivation [17, 18] of the Koopmans theorem and the above considerations leading to (40) and (41), we find for $T>0$

$$\begin{aligned} \Delta_1 F(N) &\simeq \Delta_1 F_s(N) - \Delta\phi_0, \\ \Delta_2 F(N) &\simeq \Delta_2 F_s(N). \end{aligned} \tag{43}$$

This consists in replacing the interacting free energy F by the non-interacting one, F_s, and adding the electrostatic correction $\Delta\phi_0$ (which may, in principle, depend on the temperature) to the first difference $\Delta_1 F$. However, in taking the differences of $F_s(N)$, one must make sure to keep a fixed spectrum ε_i, i.e., *not to use different spectra* ε_i *for the neighbouring clusters* N *and* $N\pm 1$! Otherwise (43) would not reduce to (40, 41) in the limit $T\to 0$, since the sum of all fully occupied levels at $T=0$ no longer would cancel. (We shall test below what this would lead to.)

The extension of the 'Koopmans approximation' to $T>0$ therefore consists in using the non-interacting free energy $F_s(N)$, but taking the differences with respect to N in (43) for the *fixed spectrum* ε_i *of the cluster with* N *atoms.* Since the practical interest of the Koopmans theorem is to avoid selfconsistent iterations beyond the evaluation of the ground-state solution, we have tested this approximation using the spectrum $\varepsilon_i^{(0)}$ of the *cold* cluster at $T=0$, i.e. treating the $T>0$ effects only perturbatively as in Sect. 3.3. Here we have also kept $\Delta\phi_0$ constant at its $T=0$ value. The results are shown by the short-dashed curves in Figs. 7, 8. The quality of this approximation at $T=0$, already demonstrated in columns a and b of Table 1, appears to persist more or less up to $T=2000$ K in all cases. It is, in particular, better than that of the approximation studied in Sect. 3.3 (and shown by the long-dashed curves), where the fully interacting ground-state energy was used.

The necessity of using the fixed spectrum ε_i of the cluster N shall be demonstrated by showing what happens otherwise. Using (43) with the different selfconsistent spectra $\varepsilon_i^{(0)}$ obtained for each value of N leads to results which differ from those of the approximation (34) discussed in Sect. 3.3 only by a constant independent of T, namely the difference between the interacting ground-state energy $E[\rho, T=0]$ and the sum of the lowest occupied levels $\varepsilon_i^{(0)}$ (plus the constant $\Delta\phi_0$ in the case of $\Delta_1 F$). It is thus sufficient to give the results at $T=0$; their temperature dependence is identical to that of the long-dashed curves in Figs. 7, 8. The results for $\Delta_1 E$ and $\Delta_2 E$ are included in Table 1 in the columns c. Their values are seen to be much worse than those obtained in the Koopmans approximation and not sufficient to reproduce even qualitatively the shell effects contained in these quantities.

This may be surprising, because at first sight one might expect to improve the approximation by including a certain amount of selfconsistency in letting the spectra ε_i adjust themselves to the particle size. The situation is, however, exactly the reverse. Using the non-interacting energy expression with N dependent spectra would be an inconsistent ad hoc prescription, whereas Koopmans' theorem, which is derived [17] consistently from a change of occupation numbers with fixed wave functions and ε_i, has a solid variational basis.

We emphasize this point in view of practical applications of the Koopmans approximation. Indeed, our results seem to encourage its use in connection with parametrized phenomenological potentials, such as the Nilsson model potential of [1] or a Woods-Saxon potential fitted to selfconsistent Kohn-Sham results [22], whose parameters depend explicitly on the cluster size N. But the correct use of the expressions (43) with a *fixed spectrum* should then be borne in mind.

5. Thermal properties and stability of hot metal clusters

A good estimate of the electronic free energies is a key to understanding cluster concentrations in equilibrium. It is also equally important for the understanding of the process of *evaporation* of neutral atoms from clusters at finite temperatures. Evaporation is usually described by statistical theories where level density considerations play a major role. To date, only the phonon degrees of freedom have been included [23, 24], parametrizing the electronic influence by a single number D. If it can be assumed that the transition state of the evaporation process is identical with the fully dissociated final state, D is equal to the free separation energy D_N defined in (25a). In ordinary chemical reactions, D_N can be evaluated at $T=0$ because the electronic subsystem remains in its adiabatic non-degenerate ground state and does not contribute to the total entropy. In general, however, the free separation energies *are* temperature dependent. For the case of sodium clusters, we have demonstrated this dependence in Sect. 3, linking it (for temperatures $0 < T \lesssim 500$ K) directly to the high degeneracy of the electronic single-particle levels next to the magic-shell gaps.

Even though not completely understood, the electronic modifications to the evaporative decay constant seem to be of considerable importance. It is likely that the observed shell structure in abundance spectra from an adiabatic expansion source results from evaporation between the time of formation and the time of detection (compare, e.g., the shell structure in the abundance spectra of [1] and [24]). Recent experimental results [25] in the large cluster region $N \simeq 200$–600, obtained by an expansion source, corroborate this hypothesis, displaying the characteristic saw-tooth behaviour of the separation energies in contrast to the much more symmetric shapes expected from quasi-equilibrium. In the observed spectra, the magnitude of the shell structure decreases and the widths of the shell closings increase with cluster size. Both these features are expected to result if the electronic free energy is included in the evaluation of decay constants [26]. The similarity of our curves for $\Delta_1 F(N)$, presented below in Sect. 5.1, to the abundance spectra of [25] is, indeed, striking (see also [6]).

In lack of dynamical evaporation calculations, we content ourselves here by presenting systematic results for neutral clusters in their equilibrium states over a large range of cluster sizes at various temperatures. All calculations were done for Na clusters using the Wigner-Seitz radius $r_s = 3.96$ a.u. for the jellium background. Unless otherwise mentioned, the free energy $F(N)$ was calculated for *canonical* ensembles in the approximation discussed in Sect. 3.2.

5.1. Temperature dependence of $F(N)$, $\Delta_1 F(N)$ and $\Delta_2 F(N)$

We shall first briefly discuss the temperature dependence of the total free energy $F(N)$ of neutral Na clusters. Since the main effect of temperature is to reduce the shell structure, rather than to affect the average properties, we extract the fluctuating part of the total interacting free energy $F(N)$. Like in nuclear physics [10], we define the shell-correction energy $\delta F(N)$ by

$$\delta F(N) = F(N) - \tilde{F}(N). \tag{44}$$

$\tilde{F}(N)$ is the average value of $F(N)$ which, by definition, does not contain any shell effects. It may be obtained either by a numerical energy averaging [10] or by semiclassical methods [11]. Since we only need an approximate determination of $\tilde{F}$ for the present discussion, we simply use here its liquid drop model (LDM) expansion at $T=0$ already discussed in Sect. 4 (cf. (38) for the neutral case $z=0$):

$$\tilde{E}(N) = e_b N + a_s N^{2/3} + a_c N^{1/3} + a_0. \tag{45}$$

In principle, one can obtain the asymptotic values of the LDM parameters a_i from semi-infinite calculations [19, 20], but these are strictly valid only for very large clusters and more terms would be needed in (45) to correctly describe small clusters, too. As a compromise for a fit to clusters with $8 \lesssim N \lesssim 1000$, we take the bulk energy $e_b = -0.1659$ Ry and the asymptotic surface energy [19] $a_s = 0.0400$ Ry as fixed values and adjust the parameters a_c and a_0 by a simple eye fit to the calculated KS results of $F(N)$, yielding $a_c = 0.0787$ Ry and $a_0 = -0.0735$ Ry.

In Fig. 9 we show the shell-correction $\delta F(N)$ versus $N^{1/3}$ at the three temperatures $T = 0$, 400 and 600 K. Note the sharp minima at the magic numbers $N = 8, 20, \ldots$ indicating an increased stability of the corresponding spherical clusters. A figure very similar to ours at $T=0$ was

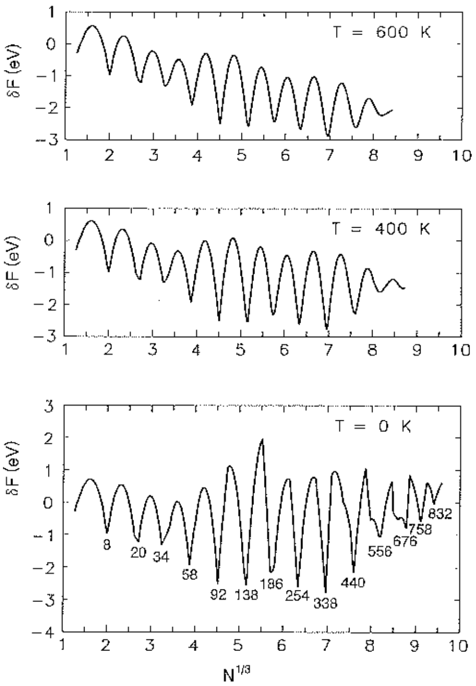

Fig. 9. Shell-correction δF to the free energy, (44), versus particle number at three temperatures. The magic numbers corresponding to closed main shells are indicated for $T=0$ at the bottom

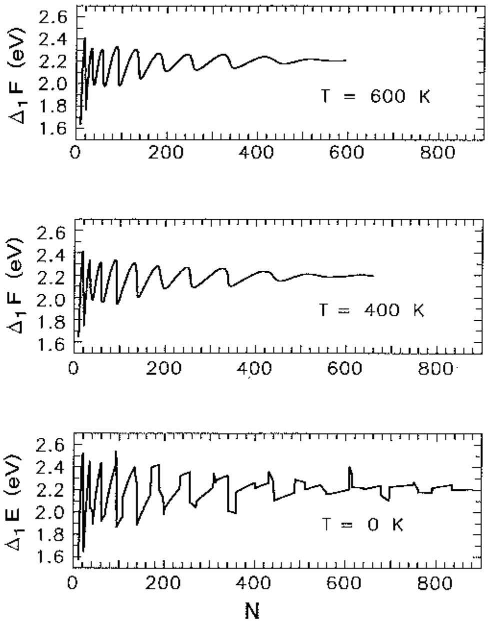

Fig. 10. First differences $\Delta_1 F$ of free energies versus cluster size N at three temperatures, evaluated for canonical ensembles in the approximation (32) in Sect. 3.2 (see text for details)

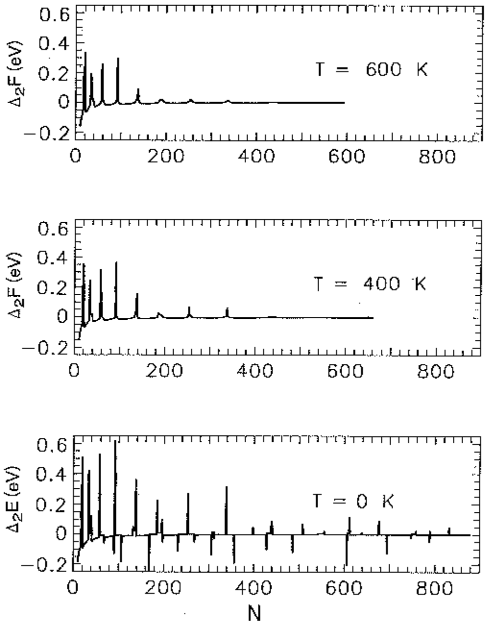

Fig. 11. As Fig. 10, but second differences $\Delta_2 F(N)$

obtained in [22] with a phenomenological Woods-Saxon potential fitted to earlier KS potentials [2]. In the regions between the magic numbers, where $\delta F(N)$ has maxima, the clusters will be deformed like nuclei; therefore our absolute values of the shell-correction are exaggerated here due to the imposed spherical symmetry. The fact that $\delta F(N)$ at $T>0$ has a slight drift towards negative values for larger N indicates that the correct LDM parameters should be temperature dependent. But the important thing to notice here is the decrease of the *amplitude* of δF with increasing temperature for the larger clusters: for $N \sim 400$–600, even at the moderate temperature of 600 K, it is reduced by a factor of at least 2 compared to its value at $T=0$. Also, the minima of δF become less sharp with increasing cluster size and temperature. This effect will be emphasized when investigating the first and second differences of $F(N)$ in the following.

In Figs. 10 and 11 we present the quantities $\Delta_1 F$ and $\Delta_2 F$ as defined in (24a) and (24b), respectively, versus atom number $N \leq 880$ at the same three temperatures. At $T=0$, we observe the familiar [1, 28] saw-tooth like behaviour of $\Delta_1 F(N)$ and positive spikes of $\Delta_2 F(N)$ at the magic numbers. The latter appear at the numbers $N=2$ and 8 (not shown), 18, 20, 34, 40, 58, 92, (132), 138, 186, 196, 254, (306, 312), 338, (398, 438), 440, 508, (542, 556), 612, (638), 676, 758, (788), and 832 (minor shell closures in parentheses). Up to $N=196$, these magic numbers are in agreement with those calculated earlier [2] and with the older experimentally observed ones [1]. In recent experiments [25, 27] there is also evidence for magic shell closures of Na clusters around $N=260$, 344, 440, 558, and, perhaps, a minor shell closure near $N \sim 394$.

The negative spikes seen in $\Delta_2 F$ at $T=0$ are an artefact of the spherical symmetry imposed in our calculations. They appear when two levels lie very close to the Fermi energy. Due to their residual interaction, their positions change place during the filling of the lower state, such that when it is full, the originally higher one (assumed to stay empty) is shifted below the other. This is a typical selfconsistency effect which cannot occur with parametrized phenomenological potentials [1, 22]. It happens in regions where we know that jellium clusters are deformed, like nuclei, once the spherical symmetry is relaxed (see also [28] for selfconsistent jellium model calculations for deformed clusters with $N \leq 40$). In computing our figures, we chose to fill such pairs of levels sequentially (i.e., not allowing for two partially filled shells) in the order which leads to the lowest possible total energy for each particle number N. These negative spikes disappear as soon as a finite temperature is switched on. Due to the mixing of the spherical shells near the Fermi energy by the noninteger occupation numbers, such pairs of close levels are smeared over and appear like one degenerate larger shell; the energy then varies smoothly and monotonously with N in the corresponding region.

The positive spikes in $\Delta_2 F(N)$, on the other hand, are due to large gaps in the spectrum ε_i at the Fermi energy, see (41). They survive the temperature averaging effects, as long as T is considerably smaller than $(\varepsilon_{\mathrm{lu}} - \varepsilon_{\mathrm{ho}})$ of the magic cluster. However, as seen already in Sect. 3, their amplitudes decrease with increasing temperature. This effect, which goes along with a smear-out of the saw-tooth structure of $\Delta_1 F(N)$, is seen in Figs. 10 and 11 to become more important with increasing cluster size. This is so because the spectra ε_i become more compressed with increasing N.

The qualitative picture of our dissociation energies $\Delta_1 F(N)$ at $T=400$ (or 600) K seen in Fig. 10, with relatively sharp saw-teeth for $N \lesssim 50$ and their increasing smear-out and decreasing amplitude with increasing cluster size N, has an astonishing resemblance to the *relative* variations of the mass abundances of the recent experiments [25] around their average values. The global trend of the abundances cannot be compared because they depend largely on the dynamics of the ions, which is not included in our approach, and on the experimental conditions (pressure of the carrier gas, geometry of the nozzle, etc.). However, if one assumes that the relative variations are essentially due to the electronic shell effects in the free energy $F(N)$ – which is strongly supported already by the good agreement of the observed and calculated magic numbers in general –, this resemblance shows us that *the finite entropy of the electronic system does play an important role and can, indeed, be observed!*

From our analysis in Sect. 3.1 it becomes clear that it is essentially the entropy part $-TS$ of the electronic free energy that is responsible for the thermal smearing effects in $\Delta_1 F(N)$ and $\Delta_2 F(N)$. Detailed dynamical calculations including evaporation will, hopefully, make it possible to investigate more quantitatively in which way these two quantities determine the observed mass abundance spectra.

Our values of $\Delta_1 F$ reach an average value of ~ 2.2 eV for large N. Indeed, according to (36), (38) in Sect. 4, or also (45) above, their average value at $T=0$ should be $-e_b = 2.26$ eV for Na clusters. This value is larger than the average experimental dissociation energy $D_N \simeq 1$ eV of a neutral atom. The difference is the binding energy of the neutral atom, $E(1)$, according to (25a). We cannot, of course, expect the jellium model to be correct for a single atom. Nevertheless, (25a) evaluated within the jellium model leads to an acceptable value of the average D_N. The total energy for $N=1$ obtained in our Kohn-Sham calculation at $T=0$ is $E(\mathrm{Na}_1) = -1.06$ eV; adding this constant to $-e_b$ gives, indeed, a very reasonable average dissociation energy of $D_N = 1.2$ eV. Thus, the main error in the total jellium binding energy, stemming from the neglect of the core electrons, cancels on the rhs of (25a) for the dissociation energy. Note from Fig. 10 that the *average* value of $\Delta_1 F$ hardly depends on the temperature in the range considered here.

5.2. Entropy and specific heat of the valence electrons

In Fig. 4 in Sect. 3.1, we have already presented the temperature dependence of the total entropy of a finite cluster. At temperatures large enough to average out the shell effects, but still much smaller than the Fermi energy ($E_F \sim 2\,\mathrm{eV} \sim 23\,000$ K), one expects the entropy S to be linear in T, i.e.

$$S \sim 2aNT, \qquad (46)$$

where a is the level density parameter. For an infinite and homogeneous noninteracting Fermi gas, a is given by [8]

$$a_\infty = \frac{\pi^2}{6}\left(\frac{2}{3\pi^2}\right)^{1/3}\left(\frac{2m}{\hbar^2}\right) r_s^2 = 0.670\, r_s^2\,[\mathrm{Ry}^{-1}]. \qquad (47)$$

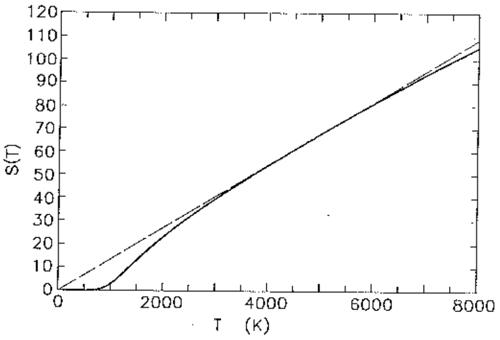

Fig. 12. Canonical entropy S of the cluster Na_{92} versus temperature. The dashed line corresponds to the linear expression on the rhs of (46) with $a = 11.6\,\mathrm{Ry}^{-1}$. The deviation of this straight line below $T \simeq 3000$ K is due to the shell effect (See text for deviation at large T)

With $r_s = 3.96$ a.u. according to Na, this gives $a_\infty = 10.5\,\mathrm{Ry}^{-1}$.

In Fig. 12, we show the canonical entropy versus T, obtained for the Na_{92} cluster, up to very high temperatures. For $T \gtrsim 3000$ K it grows, indeed, linearly. (The slight deviation from a straight line above $T \sim 6000$ degrees is due to the fact that the number of states ε_i included in the calculation was not sufficient; this is thus just a numerical truncation effect.) Fitting the slope in Fig. 12, we find $a = 11.6\,\mathrm{Ry}^{-1}$, in good agreement with the above Fermi gas value. The difference of about 10% is due to finite size corrections (e.g., a surface term in a which would be proportional to $N^{-1/3}$). Note that the value of a is identical for the grand canonical and the canonical ensemble; this has been confirmed in our results for various cluster sizes.

The temperature $T \simeq 3000$ K, at which the entropy in Fig. 12 reaches its homogeneous Fermi gas value (46), represents the critical temperature necessary to completely smear out the shell effects. In heavy nuclei, this critical temperature was found [13] to be ~ 3 MeV, which is about a third of a typical major shell spacing of the nucleonic single-particle levels. The situation is thus very similar here: $2500\,\mathrm{K} \simeq 0.2$ eV is about one third of the shell spacing at the Fermi level of the magic Na_{92} cluster (see Table 1). This is in good qualitative agreement with the result of a schematic analysis [29] in terms of a harmonic oscillator spectrum with level spacing $\hbar\omega$, for which the temperature dependence of the shell-correction energy of a closed-shell nucleus is found to be

$$\delta F(T) = \delta F(0) \cdot \frac{t}{\operatorname{Sinh} t}; \qquad t = \frac{2\pi^2 T}{\hbar\omega}.$$

Due to the factor $2\pi^2$ in the dimensionless temperature variable t, a temperature $T \simeq \hbar\omega/3$ is, indeed, sufficient here to suppress the $T=0$ value of the shell-correction by a factor of about 100!

In Fig. 13. we plot the entropy S/TN versus $N^{1/3}$ at the two temperatures $T = 400$ and 600 K. Dramatic shell effects are seen which essentially are due to the degeneracy of the spherical shells. As already observed in Sect. 3.1, up to temperatures of a few hundred degrees most smaller

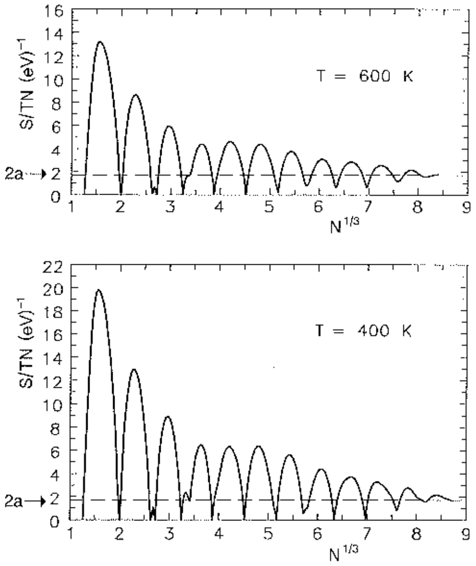

Fig. 13. Canonical entropy per particle, divided by T, at two temperatures, versus $N^{1/3}$. Note the decreasing amplitude of the shell oscillations with increasing temperature and particle number. The horizontal dashed lines indicate twice the level density parameter a according to (46)

clusters are essentially cold in the sense that their entropy still has its $T=0$ value S_0, which is given by (27) in terms of the occupancy of the highest (partially) filled shell. (The case $N=91$ shown in Fig. 4 is rather an exception due to the accidental near-degeneracy of two levels at the Fermi energy.) The oscillations in Fig. 13 therefore essentially represent the logarithms of the binomial coefficients in (27) for each region between two neighbouring filled shells (for which $S_0=0$). Only for larger temperatures and for larger sizes, a smearing of the entropy takes place; it is this effect which is responsible for the smear-out of the differences $\Delta_1 F$ and $\Delta_2 F$ observed in Figs. 10 and 11. Note that the linear behaviour of S, (46), is reached also in the large-N limit (at fixed T) with exactly the same value of the level density parameter a, as indicated by the horizontal dashed line in Fig. 13.

As a by-product of our calculations, we shall finally present some results for the electronic specific heat of metal clusters. The specific heat c_v (here: heat capacity per electron) is defined as [8]

$$c_v=\frac{1}{\mathrm{N}}\frac{\partial U_s}{\partial T}=\frac{T}{N}\frac{\partial S}{\partial T}. \tag{48}$$

To keep the volume constant amounts here to work at fixed particle number N. For the canonical ensemble, we can rewrite this in terms of the partition function as

$$c_v=\frac{1}{N}\beta^2\left\{\frac{1}{Z_N}\frac{\partial^2}{\partial\beta^2}Z_N-U_s^2\right\}. \tag{49}$$

For the grand canonical ensemble, it is easiest to use the second expression in (48), taking the derivative $\partial S/\partial T$ at a constant chemical potential μ. Note that in our present jellium model calculations, c_v is a purely electronic quantity since we have not included any ionic contribution to the entropy.

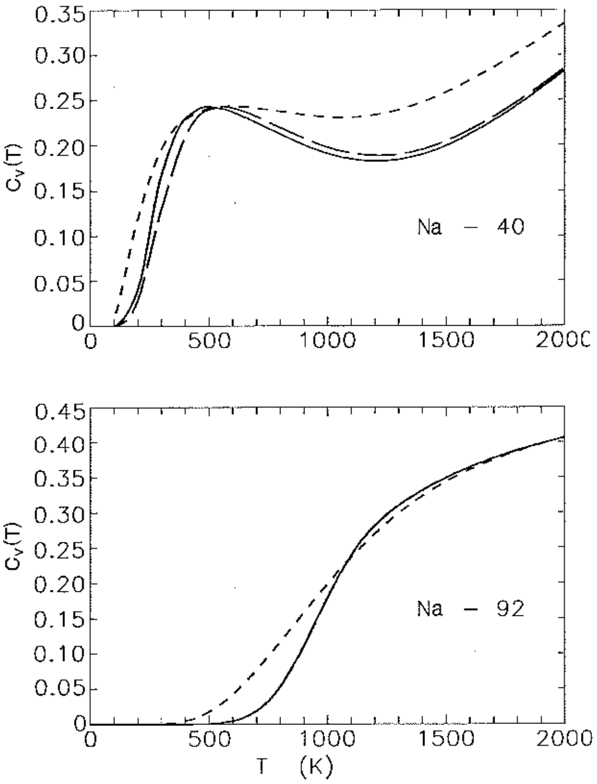

Fig. 14. Electronic part of the specific heat of the clusters Na_{40} and Na_{92} versus temperature. *Solid lines:* canonical results, *short-dashed lines:* grand canonical results, *long-dashed lines* (for Na_{92} hardly distinguishable from solid line!): canonical results in the approximation (32) discussed in Sect. 3.2

In Fig. 14 we show the electronic specific heat of the sodium clusters with $N=40$ and 92, plotted versus temperature. As in Figs. 1–3, the solid lines show the canonical and the short-dashed lines the grand canonical results. They are seen to be quite different in Na_{40} even for $T \sim 2000$ K. The long-dashed curves are obtained in the perturbative treatment discussed in Sect. 3.2, which amounts to evaluating c_v canonically in terms of the spectrum ε_i obtained in the grand canonical KS calculation. This approximation is again seen to be satisfactory at all temperatures. Note the strong shell effects in the form of oscillations around the average (linear) increase with T, which are, of course, just a consequence of the shell structure in the entropy already discussed.

6. Summary and conclusions

We have presented microscopic density functional calculations of Kohn-Sham type for a canonical ensemble of metal clusters at finite temperatures, employing the jellium model for the description of the ionic background. The electronic shell effects, known from earlier calculations at $T=0$, are demonstrated to be smeared out by the finite temperature.

We have, in particular, investigated the first and second differences, $\Delta_1 F$ and $\Delta_2 F$, of the free energy with respect to the number of atoms N. The quantity $\Delta_1 F$ is likely to be related to the stability of clusters against evaporation of an atom and may thus be correlated with the observable mass abundance spectra. The shell fluctuations in these quantities are exclusively due to the valence electrons, the ionic background only giving smoothly varying contributions. A striking similarity of these shell fluctuations in our calculated curves $\Delta_1 F(N)$ around $T \sim 400$–600 K with the oscillations in recently measured [25] mass abundance spectra is found [6]. The smearing of the saw-tooth like structures and the reduction of their amplitude, which is clearly observable for the larger clusters with $N \gtrsim 200$, are coming from the *finite entropy of the valence electrons* and its variation with temperature and cluster size.

The larger the clusters, the smaller are the shell spacings of the electron orbits and the larger is therefore the smearing effect of temperature. For temperatures $T \sim 400$–600 K, the smallest sizes with $N \lesssim 50$ are still cold as far as their valence electrons are concerned, such that the sharp saw-tooth structure in the dissociation energies or the peaks in their differences $\Delta_2 F$ still persist. However, for large clusters with $N \gtrsim 600$, very little shell structure is left at these temperatures. One might therefore question the practical feasability of observing the 'supershells', predicted [22] from $T=0$ considerations, using abundance measurements from adiabatic expansion sources of the type used in [25]. Spectroscopic techniques (see, e.g. [27]) which are directly sensitive to the position of the electronic single-particle levels ε_i might be more favourable to this purpose. As we have found, these positions do not depend visibly on temperature.

The critical temperature which is sufficient to completely average out the shell effects has found to be ~ 3000 K in a Na cluster with $N \sim 100$. Like in the case of nuclei, this is only about one third of the major shell spacing in the single-particle levels responsible for the shell effects. On the other hand, the total mean field of this cluster (and thus the positions of the single-particle energies) remain practically unaffected even up to temperatures of $T \gtrsim 2000$ deg. This means that all the averaging effects of temperature are brought about through the occupancies of the single-particle states alone. This statement, of course, only holds as long as the deformation of the mean field is kept constant, as in the present spherical calculations. Otherwise, the attenuation of the shell effects, which are responsible for deformed ground-state shapes in regions between the magic numbers, can lead to considerable variations of the mean fields accompanied by shape transitions (cf., again, the case of nuclei [11, 13]), which we expect here to take place at temperatures $1000\,\mathrm{K} \lesssim T \lesssim 3000$ K.

As a consequence of the temperature independence of the mean spherical field, we have found that the Koopmans theorem can be exploited to extract finite-temperature results from the single-spectra of the cold clusters, obtained selfconsistently at $T=0$, in a quite reasonable approximation. Similarly, we have seen that if a selfconsistent Kohn-Sham calculation is wanted at finite temperature, the numerically much simpler grand canonical treatment is sufficient to yield the selfconistent mean field, from which the canonical calculation of the free energy, entropy and other thermodynamical quantities can be obtained perturbatively in a single iteration. Either of these two approximations might prove useful in future large-scale applications of the present method.

Like the mean field, we found also the average bulk energy e_b to be nearly independent of temperature. Let us just briefly mention here that, using a local-current approximation to the random phase approximation (RPA) recently developed [30], we have also investigated the temperature dependence of the static dipole polarisabilities α_s and the frequencies of dipole plasmons of alkali clusters. We found both quantities to remain constant within a few percent up to $T \gtrsim 2000$ K. This is not so surprising in the light of the above results and knowing [1] that α_s is roughly proportional to the volume of the cluster and thus a tpyical bulk quantity. Its deviation from the classical bulk value in smaller clusters, as well as the red-shift of the surface plasmon, is due to finite-size effects and therefore rather a surface than a bulk effect. Nevertheless, also this surface effect has by and large a smooth N dependence, depending very little on local shell structure in the electron spectrum ε_i and thus on temperature averaging effects.

We finally recall that we have imposed spherical symmetry in our calculations. Consequently, the role of shell effects is, to some extent, exaggerated in the present results. Nevertheless, we believe that the temperature smearing effects described here *at and near the magic main shell closures* are realistic, since the corresponding clusters are believed to be truly spherical and to stay so also when deformational degrees of freedom are taken into account. A closer examination of this aspect is in progress.

We are grateful to S. Bjørnholm for his continuing interest and support, for a careful reading of the manuscript and many valuable comments. We also thank J. Borggreen, B. Mottelson, H. Nishioka and J. Pedersen for stimulating discussions. Two of us (M.B. and O.G.) acknowledge the Hospitality of the Niels Bohr Institute during several visits. The assistance of G. Fuchs at the Rechenzentrum of the Regensburg University in accelerating the canonical ensemble code was a great help for handling the 'fat' clusters.

Appendix

A. Calculation of canonical partition function and occupation numbers

We want to calculate the partition function $Z_N(\beta)$ for distributing N particles over M levels with energy ε_i – which we count such that each of the ε_i is singly degenerate – at the temperature $T=1/\beta$. Let us display the dependence on the number M of levels explicitly (although it should numerically not depend on M!):

$$Z_N(\beta) = Z(N, M; \beta) = \sum_{\alpha=1}^{I_{NM}} \mathrm{e}^{-\beta E_\alpha(N)} \tag{A1}$$

with $E_\alpha(N)$ given by the sum of occupied levels ε_i for each partition α:

$$E_\alpha(N)=\sum_{i=1}^{M} p_i^\alpha \varepsilon_i \quad \text{with} \quad p_i^\alpha=0 \text{ or } 1;$$

$$\sum_{i=1}^{M} p_i^\alpha=N. \tag{A2}$$

The number I_{NM} of partitions is equal to a binomial coefficient

$$I_{NM}=\binom{M}{N} \tag{A3}$$

and is usually huge. As a typical example, let us take the spherical cluster with $N=92$ electrons: to have a good convergence of S at temperatures up to ~ 2000 K, we use 42 spherical levels; counting separately their degeneracies gives $M=338$ states and one finds $I_{NM}\sim 10^{86}$.

It is thus impossible, even on a large computer, to sum over the partitions α explicitly, except in very small clusters ($N\lesssim 10$). In order to calculate, nevertheless, the canonical partition function (A1) and the derived thermodynamical quantities exactly, we use the following recurrence relation (which simply expresses the fact that the last level added is either occupied or unoccupied)

$$\begin{aligned} Z(N,M;\beta)&=Z(N,M-1;\beta)\\ &\quad+\exp(-\beta\varepsilon_M)\,Z(N-1,M-1;\beta)\\ &\quad(N\geqq 1, M\geqq N) \end{aligned} \tag{A4}$$

with the extra conditions

$$\begin{aligned} &Z(0,M;\beta)\equiv 1, \quad \forall M\geqq 0;\\ &Z(N,N-1;\beta)\equiv 0, \quad \forall N\geqq 1. \end{aligned} \tag{A5}$$

Starting with $N=1$ particle, (A4) gives the one-particle partition function

$$Z(1,M;\beta)=\sum_{m=1}^{M} e^{-\beta\varepsilon_m}. \tag{A6}$$

By adding successively more particles, one sees easily by induction that (A4) leads, indeed, to the correct N-particle partition function $Z(N,M;\beta)$ obeying (A1) and (A2). For that, one thus has to perform the algebraic manipulation in (A4) – two multiplications, one exponentiation and one addition – only a number of $\tilde{I}_{NM}$ times, which is given by

$$\tilde{I}_{NM}=N(M-N). \tag{A7}$$

In the above example with $N=92$ and $M=338$, this gives $\tilde{I}_{NM}=22\,632$ instead of the $I_{NM}\sim 10^{86}$ exponentiations, multiplications and additions necessary to get $Z(N,M;\beta)$ from (A1).

To get the derivatives of Z with respect to β, needed for U, S and c_v in (18) and (49), we use the correspondingly derived forms of the recurrence relation (A4).

The evaluation of the occupation numbers n_i in (22) is done similarly using the above recurrence scheme, by recalculating $Z(N,M;\beta)$ for each level ε_i in the situation where this level is kept empty (i.e. ε_i is removed from the spectrum), dividing by the total Z and subtracting the result from 1. This calculation has to be done as many times as there are different (degenerate) levels ε_i (42 in the above example). It takes, of course, much more computing time than in the grand canonical ensembles, but is still manageable for N up to a few hundred and T up to $\sim 10\,000$ K.

To check the numerical convergence we have ensured that all thermodynamical quantities derived from Z and the n_i did not depend on the number M of states included in the calculations. Furthermore, the fraction N_{cont} of electrons occupying the continuum region ($E>0$) was found to be smaller than 0.1 up to $T\simeq 6000$ K, and well below unity even for $T\simeq 10\,000$ K. We can therefore be assured that for the physically interesting temperatures experienced by metal clusters, the electronic continuum effects play a completely negligible role.

References

1. Knight, W.D., Heer, W.A. de, Clemenger, K.: Solid State Commun. **53**, 445 (1985); Heer, W.A. de, Knight, W.D., Chou, M.Y., Cohen, M.L.: Solid State Phys. **40**, 93 (1987)
2. Ekardt, W.: Phys. Rev. B**29**, 1558 (1984); Beck, D.E.: Phys. Rev. B**30**, 6935 (1984)
3. Kohn, W., Sham, L.J.: Phys. Rev. **140**, 1133A (1965)
4. Brack, M., Genzken, O., Hansen, K.: Z. Phys. D – Atoms, Molecules and Clusters **19**, 51 (1991)
5. Mermin, N.D.: Phys. Rev. **137**, 1441A (1965); Gupta, U., Rajagopal, A.K.: Phys. Rep. **87**, 259 (1982); Evans, R.: Adv. Phys. **28**, 143 (1979)
6. Bjørnholm, S., Borggreen, J., Echt,. O., Hansen, K., Pedersen, J., Rasmussen, H.D.: Z. Phys. D – Atoms, Molecules and Clusters **19**, 47 (1991)
7. Gunnarsson, O., Lundqvist, B.I.: Phys. Rev. B**13**, 4274 (1976)
8. See any textbook on Statistical Mechanics. We liked particularly well the presentation of P. Morse: Thermal Physics, Chs. 16ff. New York: Benjamin 1965
9. Landau, L.: Sov. Phys. JETP **3**, 920 (1957)
10. Strutinsky, V.M.: Nucl. Phys. A**122**, 1 (1968)
11. Brack, M., Quentin, P.: Nucl. Phys. A**361**, 35 (1981)
12. Mackintosh, A.R., Andersen, O.K.: In: Electrons at the Fermi Surface, Springford, M. (ed.). Cambridge: Cambridge University Press 1980
13. Brack, M., Quentin, P.: Phys. Lett. **52B**, 159 (1974); Phys. Scr. A**10**, 163 (1974)
14. Bonche, P., Levit, S., Vautherin, D.: Nucl. Phys. A**436**, 265 (1985)
15. Perdew, J.P.: In: Density Functional Methods in Physics, p. 309. Dreizler, R.M., Providência, J. da (eds.) New York: Plenum Press 1985
16. Bassichis, W.H., Strayer, M.R.: Ann. Phys. (N.Y.) **66**, 457 (1971)

17. Janak, J.F.: Phys. Rev. B**18**, 7165 (1978)
18. Perdew, J.P.: In: Condensed Matter Theories, Vol. 4, p. 149. Keller, J. (ed.). New York: Plenum Press 1989
19. Seidl, M., Spina, M.E., Brack, M.: Z. Phys. D - Atoms, Molecules and Clusters **19**, 101 (1991); see also Seidl, M., Meiwes-Broer, K.H., Brack, M.: J. Chem. Phys. 1991 (in press)
20. Spina, M.E., Seidl, M., Brack, M.: In: Symposium on atomic and surface physics - SASP '90, Märk, T.D., Howorka, F. (eds.), Innsbruck University, Austria, 1990, p. 426; see also: Brack, M.: Phys. Rev. B**39**, 3533 (1989)
21. Mahan, G.D., Schaich, W.L.: Phys. Rev. B**10**, 2647 (1974)
22. Nishioka, H., Hansen, K., Mottelson, B.R.: Phys. Rev. B**42**, 9377 (1990)
23. Engelking, P.C.: J. Chem. Phys. **87**, 936 (1987)
24. Bréchignac, C., Cahuzac, Ph., Leygnier, J., Weiner, J.: J. Chem. Phys. **90**, 1492 (1989)
25. Bjørnholm, S., Borggreen, J., Echt, O., Hansen, K., Pedersen, J., Rasmussen, H.D.: Phys. Rev. Lett. **65**, 1627 (1990)
26. Hansen K., et al.: (in preparation)
27. Martin, T.P., Bergmann, T., Göhlich, H., Lange, T.: Z. Phys. D - Atoms, Molecules and Clusters **19**, 25 (1991) and submitted to Chem. Phys. Lett
28. Ekardt, W., Penzar, Z.: Phys. Rev. B**38**, 4273 (1988)
29. Bohr, A., Mottelson, B.: Nuclear Structure II, p. 607ff. New York: Benjamin 1975
30. Reinhard, P.G., Brack, M., Genzken, O.: Phys. Rev. A**41**, 5568 (1990)

Note added in proof. Sodium clusters with N up to ~ 3000 have now been produced experimentally in an expansion source [Pedersen, J., Bjørnholm, S., Hansen, K., Martin, T.P., Rasmussen, H.D.: Preprint NBI-91-22. Nature (submitted for publication)] and the 'supershell' structure predicted in [22] has been clearly put into evidence - against the pessimism expressed in our summary (Sect. 6). We have extended our Kohn-Sham calculations and find a good qualitative agreement with the observed structure. If we multiply the calculated $\Delta_2 F$ with a factor $N^{1/2}\exp(cN^{1/3})$, as it was done with the logarithmic differences $\Delta_1 \ln I_N$ of the experimental mass yields by Pedersen et al., we find, indeed, that the second supershell starting at $N \gtrsim 850$ becomes visible even at $T \sim 500-600$ degrees Kelvin with an increasing amplitude of the shell oscillations [Genzken, O., Brack, M. (to be published)].

[D]

Z. Phys. D – Atoms, Molecules and Clusters 19, 47–50 (1991)

Atoms, Molecules
Zeitschrift für Physik D and Clusters

The influence of shells, electron thermodynamics, and evaporation on the abundance spectra of large sodium metal clusters

S. Bjørnholm, J. Borggreen, O. Echt*, K. Hansen, J. Pedersen, and H.D. Rasmussen

The Niels Bohr Institute, University of Copenhagen, DK-4000 Roskilde, Denmark

Received 10 September 1990

Abstract. Measurements of the mass abundance spectra of sodium clusters containing up to 600 atoms are presented. The clusters are produced in a seeded supersonic expansion of Ar or Kr gas, and the spectra are obtained by a time-of-flight technique. The sawtooth features in the spectra are interpreted as evidence of a regular spherical shell structure with magic numbers, N_0, scaling approximately with the cube root of the number of sodium atoms. Altogether twelve shell closings are observed, $N_0 = 2$, 8, 20, 40, 58, 92, 138, 196, 260, 344, 440 and 558. There is also a pronounced odd-even staggering all the way up to $N=70$. The experimentally observed intensity changes for the clusters around the magic numbers are discussed in terms of the electronic free energy, $F(N)$, calculated at finite temperature, and the second differences of the free energy $\Delta_2 F(N) = F(N-1) - 2F(N) + F(N+1)$. The processes behind the non-uniform abundance distributions, and the thermodynamics of finite electron systems with non-uniform level spacings are discussed on this basis.

PACS: 36.40; 35.20.Wg; 03.65.-w

Introduction

This contribution addresses questions related to the existence of periodically varying properties of clusters of simple metals, initially discovered by W.D. Knight et al. [1] (with Na- and K-clusters) and by I. Katakuse et al. [2] (with Cu, Ag, and Au-clusters).

We have measured abundance spectra of sodium clusters, generated by seeded adiabatic expansion, up to cluster sizes N corresponding to 600 atoms. The results obtained, are in qualitative agreement with the shell structure predicted theoretically by Nishioka et al. [3, 4] and by Brack et al. [5, 6] as presented at this conference.

A more quantitative comparison of the first difference of the logarithm of the experimental intensities $\Delta_1 \ln I_N = \ln(I_{N+1}/I_N)$ with the calculated [5] second difference of Helmholtz' free energy, $F = E - TS$, including electronic contributions, shows striking similarities. Based on these similarities, a picture of the processes behind the production of the experimentally observed, non-uniform abundance distributions is conjectured. It involves the following assumptions:

(i) Insufficient removal of the heat of condensation during expansion leads to a broad and initially structureless distribution of large clusters at near-boiling temperatures.
(ii) During flight for about one millisecond, the cluster distribution forms an evaporative ensemble [7, 8], cooling to 400–500 K by monomer evaporation, as shown by Bréchignac et al. [9].
(iii) Within size intervals corresponding to at least one major shell, the cooling will occur in secular equilibrium all the time; i.e. the turnover, or the product of decay constant and abundance, will be the same irrespective of size.
(iv) The decay constant can be cast in the form $k_N = \nu A \exp(\Delta_1 F(N-1)/kT)$ with $\nu \simeq 10^{13}\,\mathrm{s}^{-1}$, A the number of atoms in the surface, and $\Delta_1 F(N-1)$ the first difference of the Helmholtz free energy [10].
(v) The transition state for monomer evaporation can be identified with the final, fully dissociated state; i.e. the effective activation energy $-\Delta_1 F(N-1)$ for evaporation can be obtained from calculations of the free energy of the clusters in their equilibrium state [5, 6].
(vi) The 'true' shell gaps in the electron eigenvalue spectra are smaller than calculated theoretically for spherical droplets. A single phenomenological scaling parameter can account for this in a crude way.

The magnitude of the shell-structure modulations of the abundance spectra are measurable although they become quite weak for large clusters. The above assumptions are helpful, if not necessary, as steps towards a more complete understanding of the experimental mass spectra.

---

* *Present address*: Physics Department, University of New Hampshire, Durham, NH 03834, USA

In addition to shell modulations, the abundance spectra also exhibit pronounced odd-even alternations in the size intervals between major shells. This aspect is discussed in B.R. Mottelson's contribution to this conference [11].

Experimental procedure and results

The experiments were performed with beams of free flying clusters produced by adiabatic expansion from a hot oven into vacuum. In the oven, argon or krypton gas at stagnation pressures of (4–8)·10^5 Pa is seeded with saturated sodium vapor at 700–800°C, i.e. partial sodium pressures of (1 – 4)·10^4 Pa. The diameter of the cylindrical expansion nozzle is 0.07 mm and its length about 0.15 mm. With the aid of skimmers and a differential pumping stage, the sodium cluster beam is introduced into a 3 m long flight line. Ionization of the clusters is achieved with ultraviolet light from a 1 kW xenon lamp. The photon energy is centered at 3.9 eV, with a band width (FWHM) of 1.0 eV. This ensures an ionization probability that varies smoothly with size, and at the same time negligible heating of the ionized species [12, 13]. After ionization the clusters are analysed by time-of-flight mass spectrometry to obtain the abundance variations as a function of size, N. The time-of-flight spectrometer consists of a 5–10 kV acceleration stage, deflection plates that sweep the ionized d.c. beam across a narrow slit at about 3 kHz picking out narrow bunches with a well defined starting time for the flight time measurements, a reflectron to compensate for small velocity variations, and a channeltron ion detector. The arrival times are recorded with a multi-hit time-to-digital converter and passed to a computer that records the mass spectrum. The mass resolution is typically $M/\Delta M = 1200$. After background subtraction each mass peak is integrated to give the total mass abundance I_N.

The top panels in Fig. 1 show the measured abundance distributions, I_N. On the left hand side are results obtained with argon carrier gas, to the right results with krypton gas. In both cases, the spectra have a bell-shaped envelope modulated by a saw-tooth like fine structure. The envelopes reflect the global kinetics of cluster growth during the high-pressure phases of the expansion, while the saw-tooth structures are believed to emerge as a result of subsequent evaporation–and cooling–in flight from isolated clusters [7–9].

The local features of the abundance spectra can be displayed more clearly by taking the logarithmic difference of the I_N-values:

$$\Delta_1 \ln I_N = \ln(I_{N+1}/I_N) \approx 2(I_{N+1} - I_N)/(I_{N+1} + I_N) \qquad (1)$$

The lower left panel in Fig. 1 is a plot of this quantity. It eliminates the influence of the global shape. On the other hand, the smearing of the saw-teeth occurring at higher shells tends to reduce the value of the logarithmic difference strongly. This is compounded by the general decrease in relative magnitude of the saw-tooth steps with increasing N. As a result, statistical uncertainties begin to obscure the shell effects. On the lower right hand panel we have plotted a generalized logarithmic difference,

$$(\Delta_1 \ln I_N)_{K_0} = \frac{\sum\limits_{K=0}^{K_0} \dfrac{2(I_{N+1+K} - I_{N-K})(2K+1)}{(I_{N+1+K} + I_{N-K})}}{\sum\limits_{K=0}^{K_0} (2K+1)^2} \qquad (2)$$

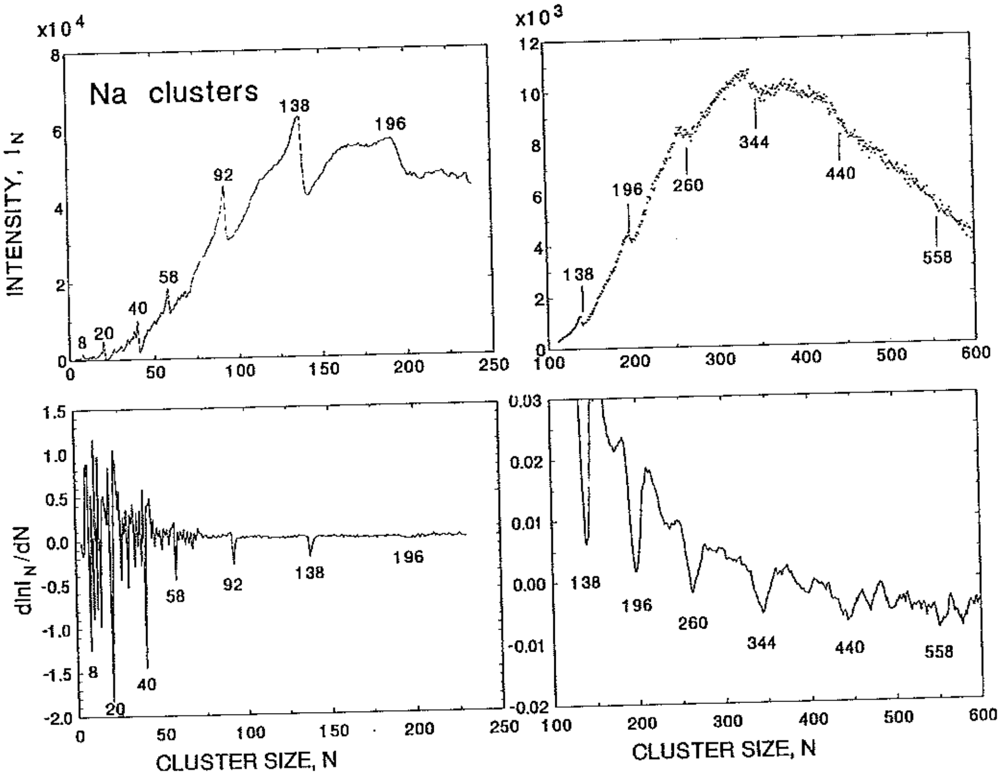

Fig. 1. Top panels: Abundance distributions for sodium clusters produced by adiabatic expansion and measured by time-of-flight mass spectrometry: left: carrier gas Ar; right: carrier gas Kr. Bottom panels: Logarithmic differences of results in top panels. Bottom left: Eq. (1), bottom right: Eq. (2) with $K_0 = 8$. (The last magic number, 558, requires a higher K_0-value to stand out unambiguously)

with $K_0 = 8$. Averaging over mass intervals $2K_0 + 1$, comparable to the smearing, makes the shell dips stand out clearly again.

Discussion

The magic numbers determined experimentally are indicated in Fig. 1 and discussed in [14] in relation to the theoretical study of shells in large quantum systems [3, 4]. Similarly the odd-even staggering, visible in the top left panel of Fig. 1, is discussed in [11].

The two top panels in Fig. 2 present the experimental data once more in the form of the first logarithmic difference $\Delta_1 \ln I_N$, given by (1) or (2), this time multiplied by $kT = 0.043$ eV, corresponding to an estimated [9] final temperature of about 500 K. In addition, the data for the heavier mass interval (right panel) has been linearized by subtracting a smooth curve drawn through the mid-shell segments of the data Fig. 1 (lower right panel).

These experimental quantities are compared to the results of theoretical calculations of the negative of the second difference of the free energy $-\Delta_2 F(N)$, displayed in the two lower panels.

$$\Delta_2 F(N) = F(N-1) - 2F(N) + F(N+1). \quad (3)$$

The second differences are obtained from free energies, calculated for electrons in an external spherical potential of the Woods-Saxon type [3, 4], with $kT = 0.043$ eV. The method used is described in [5, 6]. However, prior to the calculation of $F(N)$, the eigen-energies have been arbitrarily scaled down by a factor 2.5. This reduction accounts in a crude, phenomenological way for the reduction in magnitude of the empirical shell gaps [15, 16], compared to the calculated ones.

The energy scales in Fig. 2 are the same for the experimental and the theoretical results. Furthermore it should be noted that the units on the right hand panels (large clusters) are one hundred times smaller than on the left hand panels (small clusters). In other words, the amplitude of the logarithmic difference $\Delta_1 \ln I_N$ (top panels) varies by more than a factor of hundred in going from shell no. $3 (N_0 = 20)$ to shell no. $9 (N_0 = 260)$. At the same time, the dips at the magic numbers become more and more broad. As can be seen, the calculation (lower panels) simulates the experiment over this very large dynamic range quite well, and also the qualitative changes in the shell dips. The calculation is therefore likely to contain the essential elements of a more complete theory, designed to describe the experimental abundance distributions in detail. The key elements are those listed *(i)–(vi)* in the introduction.

Most important is the conjecture of hotly formed clusters *(i)*, decaying as an evaporative ensemble of isolated clusters *(ii)*, as opposed to (local) chemical equilibrium established by collisions. The assumption of secular equilibrium *(iii)* and the specific form of the decay constant *(iv)* provides the link between $kT\Delta_1 \ln I_N$ and $\Delta_2 F(N)$. A constant turnover *(iii)* implies that for all N

$$I_N k_N = \text{const.} \quad (4)$$

hence, with $k_N = \nu A \exp(\Delta_1 F(N-1)/kT)$

$$\ln I_N = -\ln k_N = -\Delta_1 F(N-1)/kT \quad (5)$$

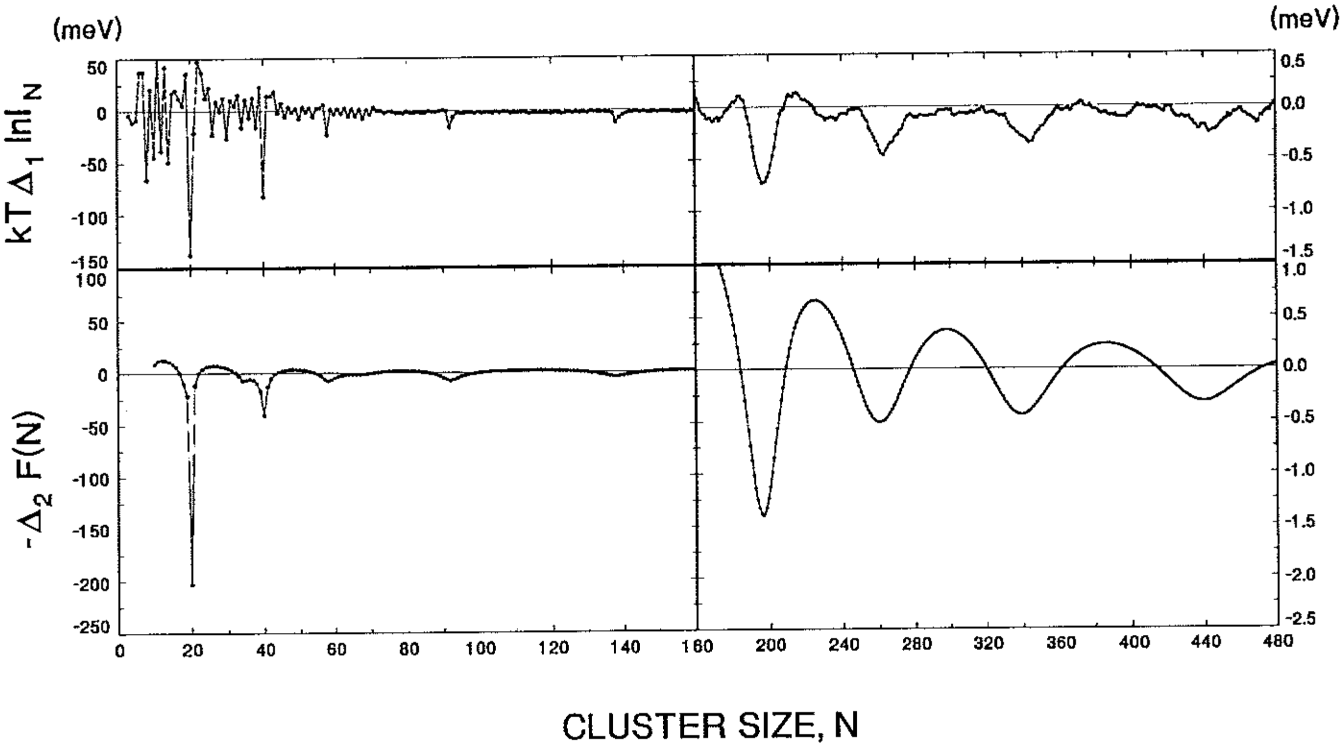

Fig. 2. Top panels: First logarithmic derivative of measured abundances, Fig. 1, multiplied by kT, corresponding to 500 K. Bottom panels: Theoretically calculated second differences of the (electronic) free energy, Eq. (3); Refs. [5, 6]

apart from additive constants or smoothly varying quantities. These are eliminated by forming differences

$$kT\Delta_1 \ln I_N = -\Delta_1 F(N) + \\ + \Delta_1 F(N-1) \equiv -\Delta_2 F(N) \qquad (6)$$

To be meaningful, a comparison of the measured $kT\Delta_1 \ln I_N$ values with the free energy differences $-\Delta_2 F(N)$, calculated for the individual spherical equilibrium states, requires that the free energy of transition state is identical with that of the final state *(v)*. Finally, a compression of the single particle energy scale *(vi)* by a factor of about 2.5 is required to match observations and calculations as shown in Fig. 2. This phenomenological factor mocks up all the perturbations, in the form of deformations [17], thermal shape oscillations, pseudopotentials, effective mass effects etc., that conspire to make the shell gaps in the eigenvalue spectrum less pronounced than in the idealized model calculation [3–6].

Conclusion

A closer study of the experimental abundance modulations of sodium cluster distributions across a large size interval reveals that the observable shell effects are strongly influenced by temperature. The valence electrons, in equilibrium with the ions, absorb finite amounts of heat. The amount of heat absorbed and the entropy varies strongly and also periodically with size [5, 6]. The net effect is a strong attenuation of the observable shell effects for large clusters, compared to zero-temperature predictions. It is nevertheless possible to measure the shell effects by mass abundance spectrometry.

Special thanks are due to W.D. Knight for guiding the authors into the field of experimental cluster research during a sabattical stay at the Niels Bohr Institute in 1988. Theoretical discussions with M. Brack, T. Døssing, B. R. Mottelson and H. Nishioka are gratefully acknowledged. We also thank D. Radford for developing our peak fitting program. This work has been supported by The Carlsberg Foundation, The Danish Research Academy, The Danish National Science Research Council, Julie Damm's Fund, Novo's Fund, the SARC-Fund and Thomas B. Thriges Fund.

References

1. Knight, W.D., Clemenger, K., de Heer, W.A., Saunders, W.A., Chou, M.Y., Cohen, M.L.: Phys. Rev. Lett. **52**, 2141 (1984); de Heer, W.A., Knight, W.D., Chou, M.Y., Cohen, M.L.: Solid State Phys. **40**, 93 (1987)
2. Katakuse, I., Ichihara, T., Fujita, Y., Matsuo, T., Sakurai, T., Matsuda, H.: Int. J. Mass Spectrom. Ion Processes **67**, 229 (1985)
3. Nishioka, H., Hansen, K., Mottelson, B. R.: Phys. Rev. B. (to appear)
4. Nishioka, H.: Z. Phys. D – Atoms, Molecules and Clusters (1991) (this issue)
5. Brack, M., Genzken, O., Hansen, K.: Phys. Rev. B. (submitted for publication)
6. Brack, M., Genzken, O., Hansen, K.: Z. Phys. D – Atoms, Molecules and Clusters (1991) (this issue)
7. Klots, C.E.: J. Chem. Phys. **92**, 5864 (1988)
8. Klots, C.E.: Z. Phys. D – Atoms, Molecules and Clusters (1991) (this issue)
9. Brechignac, C., Cahuzac, Ph., Leygnier, J., Weiner, J.: J. Chem. Phys. **90**, 1492 (1989)
10. Døssing, T.: Private communication (to be published)
11. Mottelson, B.R.: Z. Phys. D – Atoms, Molecules and Clusters (1991) (this issue)
12. de Heer, W.A.: Ph.D. Thesis, University of California, Berkely (1985)
13. The authors are grateful to W.A. de Heer and W.D. Knight for detailed advice on the construction of the cluster machine
14. Bjørnholm, S., Borggreen, J., Echt, O., Hansen, K., Pedersen, J., Rasmussen, H. D.: Phys. Rev. Lett. **65**, 1627 (1990)
15. Bergmann, T., Martin, T. P.: J. Chem. Phys. **90**, 2848 (1989)
16. Homer, M.L., Persson, J.L., Honea, E.C., Whetten, R.L.: Preprint (1990)
17. Ekardt, W., Penzar, Z.: Phys. Rev. B. **38**, 4273 (1988)